Optical Transients in Atomic Vapours

BENJAMIN SIMON CARTWRIGHT

Optical Transients in Atomic Vapours

Benjamin Cartwright

A thesis submitted in fulfilment of the degree of Masters of Science by Research

Department of Physics
Durham University
July 2022

Optical Transients in Atomic Vapours

Benjamin Cartwright

July 2022

Abstract: The propagation of light through atomic vapours gives rise to a variety of interesting effects including self-induced transparency (SIT), optical simultons and the formation of transient trains of light pulses. In this thesis, we investigate such effects using numerical simulations and theoretical techniques. We first study the dynamics of SIT solitons, comparing our numerical results with analytical predictions and previous numerical studies. We then explore the propagation of continuous wave (CW) fields, focusing on the transient dynamics that occur during and shortly after the fields are turned on. We show that a CW field breaks up into a train of pulses as it propagates into a medium, but that these oscillations are dampened in the presence of homogeneous broadening. In the absence of homogeneous broadening, we observe that the pulses become increasingly separated as the field moves deeper into the medium, in contrast to what was concluded in previous studies. We also present original results in which transient pulse trains are seen to form from two CW fields propagating through a medium of three-level V-type resonators and discuss the mechanisms behind their formation.

Contents

List of Figures

Declaration

I confirm that no part of the material offered has previously been submitted by myself for a degree in this or any other University. Where material has been generated through joint work, the work of others has been indicated.

Benjamin Cartwright

Durham, March 31, 2022

Acknowledgements

Thanks to Robert Potvliege and Steven Wrathmall for excellent guidance and supervision during the time of my study. Thanks to Ifan Hughes and Clare Higgins for insightful information about electromagnetically-induced transparency in V-systems. Thanks to everyone else in QLM for being so welcoming and making my time in Durham a wonderful experience. I will miss the Monday football games, Wednesday cake clubs, Thursday running sessions and Friday pub trips...

Chapter 1

Introduction

The interaction of light with matter is a rich and fascinating area of research. It underpins a wide range of physical phenomena and is central to many applications including lasers [1], sensors [2], metrology [3] and quantum technologies [4]. In this work, we will use theoretical techniques and computer simulations to study the interaction between light and the atomic gas contained in thermal vapour cells. However, as will be explained, much of the physics that we will uncover applies to a wide range of light-matter systems, not only the specific case of thermal vapour experiments. In this chapter, we will introduce some important concepts and then explain the key motivation and objectives of the research.

1.1 Important Concepts

1.1.1 Light Propagation in Thermal Vapours

Thermal vapour cells are a popular test bed for exploring light-matter interactions. They consist of a glass cell containing an atomic vapour (typically an alkali metal) at a warm temperature (typically between room temperature and 250°C) and can be used to confine atoms and light to a range of length scales ranging from the macroscale to the nanoscale [5]. In experiments, lasers are directed at these cells to

probe light-matter physics. Such experiments are considerably less expensive than those involving cold (i.e. close to absolute zero) atoms yet a wide range of optical and quantum mechanical effects can be realised with them. Such effects include electromagnetically induced transparency (EIT) [6, 7], light storage [8] and Rydberg physics [9–11]. They can also be used to explore nonlinear phenomena, such as self induced transparency (SIT) [12, 13]. This requires pulsed input fields typically with peak Rabi frequencies on the order of GHz and widths on the order of ns which are now achievable in vapour cell experiments [14, 15]. In order to model such nonlinear effects, one must consider the propagation of light fields (where at least one is sufficiently strong) through the vapour cells (i.e. investigate how the state of the fields and atoms change with distance into the cell). Typically, propagation effects are not considered when modelling vapour cell experiments because the fields used are often applied for too long a time or have intensities too low for nonlinear propagation effects to become significant. In these cases, the only propagation effects are those of Beer-Lambert absorption and diffraction.

1.1.2 SIT

SIT was first discovered by McHall and Hahn in the late 1960s [12]. It is the effect by which a light field propagating through a medium and resonant with a transition in a two-level system (e.g. an atomic transition) is found to propagate much further into the medium than it usually would due to it having a special temporal and spatial profile. This happens when the field has a sech-squared intensity profile of time and distance and a pulse-area of 2π (the pulse area is determined by the width and peak intensity of the pulse and will be defined in Chapter 2). Such a pulse is called an SIT soliton. However, it is not necessary that the initial field incident upon the medium has this exact profile. In fact, other forms of pulsed input fields (e.g. Gaussian pulses) are found to get reshaped as the light propagates further into the medium until the sech-squared intensity profile is obtained. If the input pulses are sufficiently large, then multiple pulses each with (approximately) sech-squared intensity profiles are

created. In the absence of atomic decay, the transparency is total. However, in the presence of decay, the pulses will lose energy as they propagate and consequently will only travel a finite distance. The transparency is created when the pulses have this special shape since it is such that the first half of the pulse transfers the atomic population entirely from the ground state to the excited state but this energy is then released symmetrically back into the light field due to stimulated emission, forming the second half of the pulse [16]. This process takes a finite amount of time and results in the slow-light effect by which the group velocity of the SIT soliton (i.e. the velocity at which the pulse envelope propagates through the medium) can be significantly lower than the speed of light [17].

1.1.3 EIT

The term electromagnetically induced transparency (EIT) was first coined by Harris et al. in 1990 [18], although related effects such as coherent population trapping (CPT) had been known about for some time previously [19]. It is the effect by which the absorption of a weak probe field can be significantly reduced (even to zero in some cases) due to the application of a strong coupling field [20]. The effect occurs in three-level systems of which there are three types: lambda, ladder and V (these will be defined in the background theory section). In a three-level lambda system, the transparency arises due to the quantum mechanical interference that occurs between different excitation pathways (known as Fano interference) [21]. In ladder systems the transparency is dominated by an effect called Autler-Townes (AT) splitting and the Fano interference plays a much smaller role. AT splitting was discovered by Autler and Townes in 1955 and is an AC Stark effect, by which the oscillating electric field of the light causes a shift in the energy levels of the system [22]. In V-systems, the EIT is almost entirely due to AT splitting [23]. It should be noted that there is not a complete consensus on the definition of EIT. Some researchers attribute only transparency effects that arise as a result of quantum mechanical interference to be EIT [24], whereas others use it to refer generally to transparency

effects that are created on one field due to the application of another field [23]. In this thesis, we assume this latter meaning but will explain the mechanisms behind the EIT effects when they are mentioned.

1.1.4 Simultons and Related Effects

In addition to the well known phenomena of SIT and EIT, there are many closely related effects that can occur with different classes of input fields in two and three level media. Such effects include optical simultons and the formation of transient trains of soliton-like pulses.

Simultons are a phenomenon closely related to SIT. They were first studied theoretically by Konopnicki and Eberly in 1981 [25]. They refer to the effect by which two solitons each resonant on separate transitions of a three-level V-system, are found to co-propagate (i.e. follow the same trajectory) as they move through the medium. Recently, a combined theoretical and experimental study was conducted at Durham university which investigated the formation and propagation of optical quasi-simultons in an atomic vapour [26]. These quasi-simultons are distinct from the simultons of Konopnicki and Eberly in that they can form in the case when the two transitions do not have the same oscillator strength, a condition imposed by Konopnicki and Eberly in order to obtain analytic solutions. Quasi-simultons offer potential applications for optical quantum information processing, due to the strong optical nonlinearities that they may be able to produce [27].

Trains of soliton-like pulses may form when a continuous-wave (CW) field is resonant with a two-level medium, instead of the pulsed input required for SIT. This situation was first studied theoretically by Crisp in 1976 [28] and expanded upon by various later studies [29–32]. These pulse trains are generally only transient phenomena, thwarted by spontaneous decay, and occur in the time period before a CW laser field reaches a steady state equilibrium with the medium. Similar effects can also occur in three-level media, and we will show in Chapter 5 that simulton-like pulse

trains can be created when CW input fields are resonant with a three-level V-system instead of pulsed inputs.

1.2 Motivation and Objectives

There are many similarities between the atom-light effects outlined in the previous section. However, there is much that is unclear about the underlying physics that links them. There are also many details that have not been fully explained in the literature and which therefore require further investigation and clarification. SIT and related nonlinear effects once gathered considerable interest (particularly during the 1970s) but have since declined in popularity and there have been fewer investigations exploring them. EIT is currently more widely studied, though it is rarely connected to the associated nonlinear phenomena. Recently, the prospect of realising quantum information processing with atom-light systems (such as with vapour cell technologies [27]) has made the issue of properly understanding SIT, EIT and their related processes a particularly relevant and important topic to address. The primary motivation for this theoretical study is to explore the connection between these effects, aiming to elucidate and contribute to a body of work that began with the discovery of SIT in the 1960s. We will explore these effects from the perspective of modelling vapour cell experiments since this follows naturally from the previous research conducted here in Durham on optical simultons in atomic vapours [26] and may provide a theoretical framework for future experimental investigations with vapour cells. However, the effects are applicable to a wide range of atom-light systems. For example, SIT has been in observed in Ruby crystals [12] and optical fibers [33] as well as in atomic vapours.

1.3 Thesis Structure

The structure of this thesis is as follows.

- Chapter 2: We derive the Maxwell-Bloch equations which form the theoretical framework commonly used to study the propagation of light through atomic media. We also review some important previous work on self-induced transparency, optical simultons and pulse trains.

- Chapter 3: We explore the propagation of SIT solitons through a medium of two-level resonators in the presence or absence of different broadening mechanisms. We compare our results to analytical predictions and previous numerical studies.

- Chapter 4: We study the propagation of CW fields through a medium of two-level resonators. We compare our findings with analytical models as well as numerical studies and present some key results that appear to contradict to those of a previous study.

- Chapter 5: We consider the propagation of two CW fields through a medium of homogeneously broadened three-level resonators. We present some original results and examine the mechanisms underpinning the effects.

- Chapter 6: We discuss our conclusions and suggest possible future work.

Chapter 2

Background Theory

2.1 Introduction

In order to simulate the propagation of light through atomic vapour cells, we need theoretical models for both the light fields and the ensemble of atoms. In general, both obey the laws of quantum mechanics and should be treated quantum mechanically. However, in this thesis we will only consider light fields that are sufficiently intense such that they contain a very large number of photons and can be described with classical electromagnetism theory. The atomic medium, however, must be described in a quantum mechanical framework. Together, these two models comprise a semi-classical approximation of light-matter interaction [34].

2.2 Light-Matter Interactions

2.2.1 The Atomic System

In this thesis, we will consider the propagation of light through a medium of isotopically pure ^{85}Rb atoms. This system was chosen since it was the one used for the previous research on optical quasisimultons that formed the starting point for this work [26]. However, as was explained in Chapter 1, the physics that will be explored

is not limited to this particular system. We consider transitions between the 5S and

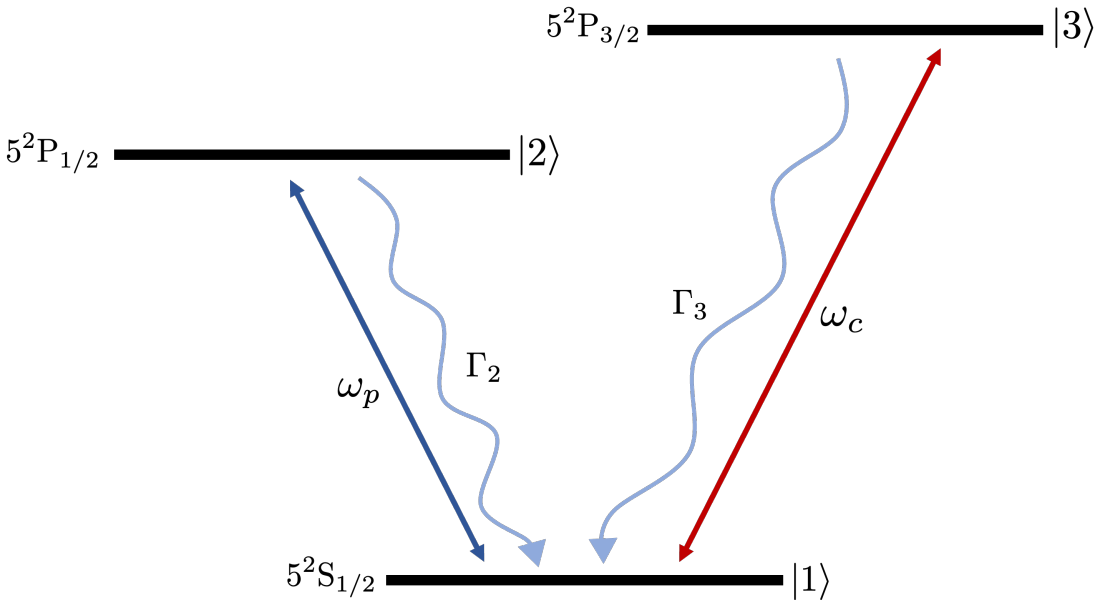

Figure 2.1: 3-state model of ^{85}Rb in which we entirely neglect the hyperfine structure. The probe beam is resonant with $|1\rangle$ and $|2\rangle$ and has angular frequency ω_p. The coupling beam is resonant with $|1\rangle$ and $|3\rangle$ and has angular frequency ω_c. Γ_2 and Γ_3 are the spontaneous decay rates from $|2\rangle$ and $|3\rangle$ respectively. Decay from $|3\rangle$ to $|2\rangle$ is forbidden and there are no decays out of the system.

5P states. ^{85}Rb is an alkali metal and therefore contains only one outer electron. The total electron angular momentum operator is given by

$$\mathbf{J} = \mathbf{L} + \mathbf{S}, \tag{2.2.1}$$

where $\mathbf{L}$ is the electron's orbital angular momentum operator and $\mathbf{S}$ is the electron's spin angular momentum operator. The quantum numbers j, l and s are defined in terms of the eigenvalues of the operators J^2, L^2 and S^2 which represent the magnitude of the angular momentum. For simultaneous eigenstates of J^2, L^2 and S^2, it can be shown that these quantum numbers must satisfy $|l - s| \leq j \leq l + s$ where j must be either an integer or half-integer, l is a positive integer or zero and $s = 1/2$ for a single electron. For the ground state (5S), $l = 0$ and so the only allowed value of j is $j = 1/2$. For the excited state (5P), $l = 1$ and so there are two allowed values of j: $j = 1/2$ or $j = 3/2$. Hence there are three states and we have the system of states shown in Figure 2.1. For each state, there are $2j + 1$ magnetic substates. In

the absence of external magnetic fields, these substates are all degenerate. These magnetic substates, denoted by the quantum number m_j, are eigenvalues of the operator J_z and have eigenvalues $m_j\hbar$. The m_j quantum numbers must vary in integer steps and satisfy $-j \leq m_j \leq j$. Hence we have

$$j = 1/2 : m_j = -1/2, 1/2,$$
$$j = 3/2 : m_j = -3/2, -1/2, 1/2, 3/2.$$

This is known as the fine-structure model [34]. We neglect the hyperfine structure, which takes account of the coupling of **J** with the nuclear angular momentum **I**. We do this to reduce the complexity of the computations to be performed. We will discuss the validity of this assumption later on. As shown in Figure 2.1, states $|2\rangle$ and $|3\rangle$ decay spontaneously to the ground state $|1\rangle$. These decays result in a homogeneous (i.e. the same for all atoms) broadening of the atomic absorption/transmission line [34]. Decay from state $|3\rangle$ to state $|2\rangle$ is forbidden.

2.2.2 The Transitions

We will consider the interaction of two laser fields with the atomic system shown in Figure 2.1. There will be a probe field resonant with the transition between states $|1\rangle$ and $|2\rangle$ (known as the D1 transition) and a coupling field resonant with the transition between states $|1\rangle$ and $|3\rangle$ (known as the D2 transition). We will assume that both fields are polarised along the z-axis and so will only induce π-transitions (where $m_J \rightarrow m'_J = m_J$) [34]. In reality, decays would occur between any of the upper substates to any of the lower substates (e.g. from $m'_J = 1/2 \rightarrow m_J = -1/2$). However, this would lead to an equal population between the ground state substates and so the system can be modelled with no loss of generality by considering that all population is in the $m_J = 1/2$ substate and that transitions occur only between the $m_J = 1/2$ and the $m'_J = 1/2$ substates (with all decays back to the $m_J = 1/2$ substate). It should be stressed that this constitutes a closed system. The electric

dipole operator $\mathbf{d}$ is given by

$$\mathbf{d} = -e\mathbf{r}, \tag{2.2.2}$$

where e is the absolute value of the electric charge and we assume that the mass of the nucleus is infinite so that $\mathbf{r}$ represents the position of the electron relative to its centre. The dipole matrix elements of the transitions are of the form

$$\mathbf{D}_{JJ'} = \langle 5S_J, m_J | \, \mathbf{d} \, | 5P_{J'}, m'_J \rangle = - \langle 5S_J, m_J | \, e\mathbf{r} \, | 5P_{J'}, m'_J \rangle \, . \tag{2.2.3}$$

where J is the total angular momentum quantum number of the ground state and J' is the total angular momentum quantum number of the excited state. For the D1 and D2 transitions considered here, $J = 1/2$, $J' = 1/2$ or $3/2$ and $m_J = m'_J = 1/2$ and so (2.2.3) becomes

$$\mathbf{D}_{1/2J'} = - \langle 5S_{1/2}, m_J = 1/2 | \, e\mathbf{r} \, | 5P_{J'}, m'_J = 1/2 \rangle \, . \tag{2.2.4}$$

Because the light is z-polarised, we need only consider the z-component of $\mathbf{D}_{1/2J'}$ since only this component will contribute to the dot product in (2.2.27). We denote this component by $D_{1/2J'}$ which is given by

$$D_{1/2J'} = - \langle 5S_{1/2}, m_J = 1/2 | \, ez \, | 5P_{J'}, m'_J = 1/2 \rangle \, . \tag{2.2.5}$$

We can express $\mathbf{r}$ in standard components (the spherical basis) as [35]

$$\mathbf{r} = \hat{\mathbf{u}}_{+1} r_{1,+1} + \hat{\mathbf{u}}_0 r_{1,0} + \hat{\mathbf{u}}_{-1} r_{1,-1}, \tag{2.2.6}$$

where the unit vectors in the spherical basis are related to the Cartesian unit vectors by

$$\hat{\mathbf{u}}_{+1} = -\sqrt{\frac{1}{2}}(\hat{\mathbf{x}} + \mathrm{i}\hat{\mathbf{y}}), \tag{2.2.7}$$

$$\hat{\mathbf{u}}_{-1} = +\sqrt{\frac{1}{2}}(\hat{\mathbf{x}} - \mathrm{i}\hat{\mathbf{y}}), \tag{2.2.8}$$

$$\hat{\mathbf{u}}_0 = \hat{\mathbf{z}}, \tag{2.2.9}$$

and we also have that

$$r_{1,0} = z, \tag{2.2.10}$$

$$r_{1,\pm1} = \mp\sqrt{\frac{1}{2}}(x \pm \mathrm{i}y). \tag{2.2.11}$$

This means that (2.2.5) also represents the component of $\mathbf{D}_{1/2J'}$ in the $\hat{\mathbf{u}}_0$ direction in the spherical basis. This means that we can make use of the Wigner-Eckart theorem [36]

$$\langle JM|\, T_{k,p}\, |J', M'\rangle = \langle J'M'kp|JM\rangle \, \langle J|\, |T^{(k)}|\, |J'\rangle\,, \tag{2.2.12}$$

where $T_{k,p}$ is the p-th component of the spherical tensor operator $T^{(k)}$ with rank k and J, M, J' and M' are quantum numbers. The term $\langle J'M'kp|JM\rangle$ is known as the Clebsch-Gordan coefficient and the term $\langle J|\, |T^{(k)}|\, |J'\rangle$ is the reduced matrix element [35]. Hence we can write

$$D_{1/2J'} = -\langle J'\ 1/2\ 1\ 0\ |1/2\ 1/2\rangle \, \langle 5S_{1/2}|\, |e\mathbf{r}|\, |5P_{1/2}\rangle\,. \tag{2.2.13}$$

The Clebsch-Gordan coefficent for each transition can be calculated or located in tables. Changing the notation from $D_{JJ'}$ to D_{ij} where i is the index of the initial state and j is the index of the final state (i.e. $D_{12} = D_{J=1/2,J'=1/2}$ and $D_{13} = D_{J=1/2,J'=3/2}$) we find that

$$D_{12} = -\frac{1}{\sqrt{3}} \langle 5S_{1/2}|\, |e\mathbf{r}|\, |5P_{1/2}\rangle\,, \tag{2.2.14}$$

$$D_{13} = \frac{1}{\sqrt{3}} \langle 5S_{1/2}|\, |e\mathbf{r}|\, |5P_{3/2}\rangle\,. \tag{2.2.15}$$

The reduced matrix elements have been determined to be $\langle 5S_{1/2}|\, |e\mathbf{r}|\, |5P_{1/2}\rangle = 2.5377 \times 10^{-29}$ C m and $\langle 5S_{1/2}|\, |e\mathbf{r}|\, |5P_{3/2}\rangle = 3.58425 \times 10^{-29}$ C m [37].

2.2.3 Other types of Three-level System

The atomic system that we have just described is only one of three types of three-level system. The three types are: lambda, ladder and V. These are shown in

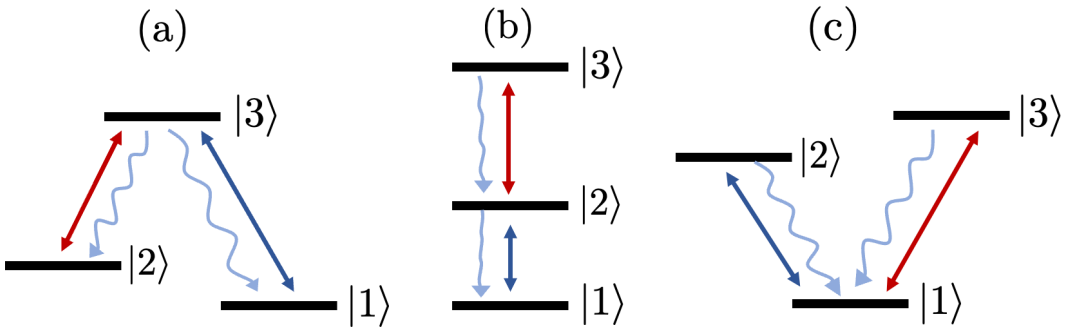

Figure 2.2: The three kinds of three-level system: (a) Lambda system, (b) Ladder system and (c) V-system. The red and blue arrows each represent light fields that interact with the energy levels they are situated between. The wiggly arrows represent spontaneous decays.

Figure 2.2. In a lambda system (Figure 2.2(a)), there is one upper state and two lower states. Light fields couple the lower states to the upper state. Population cannot decay directly between the two lower states (i.e. from $|2\rangle$ to $|1\rangle$). In a ladder system (Figure 2.2(b)), there is a ground state, an intermediate state and an upper state. One field couples the ground state to the intermediate state and a second field couples the intermediate state to the upper state. Population cannot decay directly from the upper state to the ground state (i.e. from $|3\rangle$ to $|1\rangle$). In a V-system, there is one ground state and two upper states. Light fields couple the ground state to each of the upper states. Population cannot decay directly between the two upper states (i.e. from $|3\rangle$ to $|2\rangle$).

2.2.4 The Thermal Vapour

The state of the medium is represented by a density matrix, $\rho(x,t)$. The density matrix contains all of the physically important information about the state of the atomic vapour and is a generalisation of the standard wavefunction of quantum mechanics [38]. Its diagonal terms are called populations and represent the probability that a given state is occupied [39]. Its off-diagonal terms are called coherences and represent the coherence between basis states [39]. The atoms in the vapour

will have a distribution of velocities given by the Maxwell-Boltzmann distribution function [40]

$$f(u_x) = \frac{1}{u_{\text{rms}}\sqrt{\pi}} \exp\Big\{-u_x^2/u_{\text{rms}}^2\Big\}, \tag{2.2.16}$$

where

$$u_{\text{rms}} = \sqrt{2k_B T/M}, \tag{2.2.17}$$

and u_x is the velocity of an atom along the propagation axis x, u_{rms} is the average atomic speed, k_B is Boltzmann's constant, T is the vapour temperature and M the atomic mass. The density matrix $\rho(x,t)$ is an average over all velocities given by

$$\rho(x,t) = \int_{-\infty}^{\infty} f(u_x)\rho(x,t,u_x)\mathrm{d}u_x, \tag{2.2.18}$$

where $\rho(x,t,u_x)$ is the density matrix for the atoms moving with velocity u_x [40]. Atoms moving at different velocities are subjected to different frequencies of light due to the Doppler effect and so this averaging is often called Doppler averaging. This effect results in a broadening of the atomic absorption/transmission line and is an inhomogeneous process as the amount of broadening for different atoms is different since they are all moving at different speeds [34].

2.2.5 Deriving the Hamiltonian

The energy levels of the unperturbed system can be defined in terms of angular frequencies as $E_1 = \hbar\omega_1$, $E_2 = \hbar\omega_2$ and $E_3 = \hbar\omega_3$. Therefore the Hamiltonian of the unperturbed system can be written as

$$\mathcal{H}_0 = \hbar\omega_1 |1\rangle\langle 1| + \hbar\omega_2 |2\rangle\langle 2| + \hbar\omega_3 |3\rangle\langle 3| . \tag{2.2.19}$$

When the fields are switched on, there will be a shift in the energy levels of the system due to the interaction between the fields and the atoms. The change this induces to the system Hamiltonian is described by the interaction Hamiltonian, $\mathcal{H}_I$ [38]. Each ^{85}Rb atom has one outer electron and so the interaction Hamiltonian is given by [34]

$$\mathcal{H}' = e\mathbf{r} \cdot \mathbf{E}, \tag{2.2.20}$$

where e is the absolute value of the electron charge, $\mathbf{r}$ is the position vector of the electron relative to the centre of the nucleus (its mass assumed to be infinite) and $\mathbf{E}$ is the electric field vector. The total Hamiltonian is given by

$$\mathcal{H} = \mathcal{H}_0 + \mathcal{H}_I. \tag{2.2.21}$$

In general, $\mathbf{E} = \mathbf{E}(\mathbf{r}, t)$, however we will be concerned with fields with wavelengths of ~ 800 nm which is much larger than size of the Rb atoms which have radii of ~ 3Å [41]. Therefore we can assume that the fields are constant over the size of the atoms so that $\mathbf{E} = \mathbf{E}(t)$. This is known as the electric dipole approximation [42]. With this approximation, we can write the electric field as

$$\mathbf{E}(t) = \frac{1}{2}\mathcal{E}_\mathrm{p} e^{-i\omega_\mathrm{p} t}\hat{\boldsymbol{\epsilon}}_\mathrm{p} + \frac{1}{2}\mathcal{E}_\mathrm{c} e^{-i\omega_\mathrm{c} t}\hat{\boldsymbol{\epsilon}}_\mathrm{c} + c.c., \tag{2.2.22}$$

where $\mathcal{E}_{\mathrm{p/c}}$ are the constant amplitudes, $\hat{\boldsymbol{\epsilon}}_{\mathrm{p/c}}$ are the polarisation vectors and *c.c.* represents the complex conjugate of the first two terms. Hence the interaction Hamiltonian is

$$\mathcal{H}_I = \frac{1}{2}e\mathbf{r} \cdot \hat{\boldsymbol{\epsilon}}_\mathrm{p}\mathcal{E}_\mathrm{p} e^{-i\omega_\mathrm{p} t} + \frac{1}{2}e\mathbf{r} \cdot \hat{\boldsymbol{\epsilon}}_\mathrm{c}\mathcal{E}_\mathrm{c} e^{-i\omega_\mathrm{c} t} + c.c.\ . \tag{2.2.23}$$

In the basis of the state vectors $|1\rangle$, $|2\rangle$, $|3\rangle$, (2.2.23) becomes

$$\begin{aligned}\mathcal{H}_I = \frac{\hbar\Omega_\mathrm{p}^{12}}{2}e^{-i\omega_\mathrm{p} t}\left|1\right\rangle\left\langle 2\right| + \frac{\hbar\Omega_\mathrm{p}^{21}}{2}e^{-i\omega_\mathrm{p} t}\left|2\right\rangle\left\langle 1\right| \\ + \frac{\hbar\Omega_\mathrm{c}^{13}}{2}e^{-i\omega_\mathrm{c} t}\left|1\right\rangle\left\langle 3\right| + \frac{\hbar\Omega_\mathrm{c}^{31}}{2}e^{-i\omega_\mathrm{c} t}\left|3\right\rangle\left\langle 1\right| + h.c.,\end{aligned} \tag{2.2.24}$$

where

$$\Omega_\mathrm{p}^{mn} = \frac{e\mathcal{E}_\mathrm{p}}{\hbar}\left\langle m\right|\mathbf{r} \cdot \hat{\boldsymbol{\epsilon}}\left|n\right\rangle, \tag{2.2.25}$$

$$\Omega_\mathrm{c}^{mn} = \frac{e\mathcal{E}_\mathrm{c}}{\hbar}\left\langle m\right|\mathbf{r} \cdot \hat{\boldsymbol{\epsilon}}\left|n\right\rangle, \tag{2.2.26}$$

and *h.c.* represents the hermitian conjugate of the preceding terms. From (2.2.25), (2.2.26) and (2.2.2) it can be seen that $\Omega_{\mathrm{p/c}}$ can be written in terms of the electric dipole operator

$$\Omega_{\mathrm{p/c}} = \frac{\mathbf{d}\cdot\mathbf{E}_{\mathrm{p/c}}}{\hbar}. \tag{2.2.27}$$

We note that (2.2.24) does not contain any diagonal terms since all matrix elements of the form $\langle n|\,\mathbf{r}\cdot\hat{\boldsymbol{\epsilon}}\,|n\rangle$ are zero by parity. This must be true since the dipole operator has odd parity and the initial and final states must have the same parity (since they are the same state) and so the total integrand must have odd parity and its integral over all space is zero [43]. The matrix elements $\langle 2|\,\mathbf{r}\cdot\hat{\boldsymbol{\epsilon}}\,|3\rangle$ and $\langle 3|\,\mathbf{r}\cdot\hat{\boldsymbol{\epsilon}}\,|2\rangle$ are also zero since states $|2\rangle$ and $|3\rangle$ must have the same parity given that they must each have the opposite parity to state $|1\rangle$. We now apply the unitary operator $\mathcal{U}$ to the Hamiltonian (known as a rotating frame transformation [44])

$$\mathcal{U} = e^{i\omega_1 t}\,|1\rangle\langle 1| + e^{i(\omega_1+\omega_p)t}\,|2\rangle\langle 2| + e^{i(\omega_1+\omega_c)t}\,|3\rangle\langle 3|\,. \tag{2.2.28}$$

The density matrix and Hamiltonian become [45]

$$\rho' = \mathcal{U}\rho\mathcal{U}^\dagger, \tag{2.2.29}$$

$$\mathcal{H}' = \mathcal{U}\mathcal{H}\mathcal{U}^\dagger - i\hbar\mathcal{U}\partial_t\mathcal{U}^\dagger, \tag{2.2.30}$$

where $\mathcal{H}$ is the total Hamiltonian, $\mathcal{H} = \mathcal{H}_0 + \mathcal{H}_I$, the dagger symbol † represents the Hermitian conjugate, ∂_t is a time derivative and the prime symbol $'$ signifies quantities in the rotating frame. We find that

$$\begin{aligned}\mathcal{H}' = \frac{\hbar}{2}(\Omega_p^{21*} + \Omega_p^{12}e^{-2i\omega_p t})\,|1\rangle\langle 2| + \frac{\hbar}{2}(\Omega_c^{31*} + \Omega_c^{13}e^{-2i\omega_c t})\,|1\rangle\langle 3| + h.c.\\ + \Big[2\omega_2 - 2(\omega_1+\omega_p)\Big]\,|2\rangle\langle 2| + \Big[2\omega_3 - 2(\omega_1+\omega_c)\Big]\,|3\rangle\langle 3|\,,\end{aligned} \tag{2.2.31}$$

where *h.c.* denotes the Hermitian conjugate of the first line. We now make the rotating wave approximation [44]. This approximation neglects the fast-oscillation terms, which in this case are those with frequencies $2\omega_p$ and $2\omega_c$. This approximation is valid so long as the fields are close to the resonance frequency [44]. With this

approximation, (2.2.31) becomes

$$\mathcal{H}' = -\hbar\Delta_p \left|2\right\rangle\left\langle 2\right| - \hbar\Delta_c \left|3\right\rangle\left\langle 3\right| + \left[\frac{\hbar}{2}\Omega_p^{21*}\left|1\right\rangle\left\langle 2\right| + \frac{\hbar}{2}\Omega_c^{31*}\left|1\right\rangle\left\langle 3\right| + h.c.\right], \quad (2.2.32)$$

where $h.c.$ denotes the Hermitian conjugate of the terms within the square brackets.

2.2.6 Deriving the OBEs

We will now derive the optical Bloch equations (OBEs) that describe the time-dependent dynamics of the atomic system being driven by the fields. We start from the Lindblad master equation [46]

$$\frac{\partial\rho'}{\partial t} = -\frac{\mathrm{i}}{\hbar}\left[\mathcal{H}', \rho'\right] + \sum_i \mathcal{L}(\rho', \sigma_i), \quad (2.2.33)$$

where the prime symbols ($\prime$) represent quantities in the rotating reference frame and $\mathcal{L}(\rho', \sigma_i)$ is the Lindblad superoperator given by

$$\mathcal{L}(\rho', \sigma_i) = \frac{1}{2}\sum_i \sigma_i\rho'\sigma_i^\dagger - (\sigma_i^\dagger\sigma_i\rho' + \sigma_i^\dagger\sigma_i\rho'), \quad (2.2.34)$$

where the summation is over the number of decay pathways and the σ_i are collapse operators. For the system shown in Figure 2.1 there are two decay pathways and hence two collapse operators given by

$$\sigma_2 = \sqrt{\Gamma_2}\left|1\right\rangle\left\langle 2\right|, \quad (2.2.35)$$

$$\sigma_3 = \sqrt{\Gamma_3}\left|1\right\rangle\left\langle 3\right|, \quad (2.2.36)$$

where the Γ's are the spontaneous decay rates of the respective levels. Plugging the Hamiltonian (2.2.32) and the Lindblad superoperator with the two collapse operators into the master equation (2.2.33) (and setting $\Omega_p \equiv \Omega_p{}^{21}$, $\Omega_c \equiv \Omega_c{}^{31}$) we can derive the OBEs for the system

$$\partial_t\rho'_{11} = \Gamma_2\rho'_{22} + \Gamma_3\rho'_{33} + \frac{\mathrm{i}}{2}\left[\Omega_\mathrm{p}\rho'_{12} - \Omega_\mathrm{p}^*\rho'_{21} + \Omega_\mathrm{c}\rho'_{13} - \Omega_\mathrm{c}^*\rho'_{31}\right], \quad (2.2.37)$$

$$\partial_t\rho'_{22} = -\Gamma_2\rho'_{22} - \frac{\mathrm{i}}{2}\left[\Omega_p\rho'_{12} - \Omega_\mathrm{p}^*\rho'_{21}\right], \quad (2.2.38)$$

$$\partial_t \rho'_{33} = -\Gamma_3 \rho'_{33} - \frac{\mathrm{i}}{2}\left[\Omega_c \rho'_{13} - \Omega_\mathrm{c}^* \rho'_{31}\right], \tag{2.2.39}$$

$$\partial_t \rho'_{12} = -\frac{\Gamma_2}{2}\rho'_{12} - \mathrm{i}\Delta_\mathrm{p}\rho'_{12} + \frac{\mathrm{i}}{2}\left[\Omega_\mathrm{p}^*(\rho'_{11} - \rho'_{22}) - \Omega_\mathrm{c}^* \rho'_{32}\right], \tag{2.2.40}$$

$$\partial_t \rho'_{13} = -\frac{\Gamma_3}{2}\rho'_{13} - \mathrm{i}\Delta_\mathrm{c}\rho'_{13} + \frac{\mathrm{i}}{2}\left[\Omega_\mathrm{c}^*(\rho'_{11} - \rho'_{33}) - \Omega_\mathrm{p}^* \rho'_{23}\right], \tag{2.2.41}$$

$$\partial_t \rho'_{23} = -\frac{\Gamma_2}{2}\rho'_{23} - \frac{\Gamma_3}{2}\rho'_{23} + \mathrm{i}(\Delta_\mathrm{p} - \Delta_\mathrm{c})\rho'_{23} - \frac{\mathrm{i}}{2}\left[\Omega_\mathrm{p}\rho'_{13} - \Omega_\mathrm{c}^* \rho'_{21}\right], \tag{2.2.42}$$

where Δ_p and Δ_c are the detunings of the probe and coupling lasers, respectively, and the other symbols are defined as previously stated. The density matrix is Hermitian so the off-diagonal elements are related by $\rho'_{ij} = \rho'^{*}_{ji}$ and we do not need separate equations for ρ'_{21}, ρ'_{31} and ρ'_{32}. The populations are also subject to the constraint $\rho'_{11} + \rho'_{22} + \rho'_{33} = 1$ and hence the six OBEs can in fact be reduced to a system of five equations.

2.2.7 Deriving the Propagation Equation

In addition to the optical Bloch equations that describe the state of the atoms, we also need an equation to describe the propagation of light through the atomic vapour. This is called the propagation equation and we will now derive it from first principles.

We first consider the set of Maxwell equations for a medium

$$\boldsymbol{\nabla} \times \mathbf{H} = \mathbf{j} + \frac{\partial \mathbf{D}}{\partial t}, \tag{2.2.43}$$

$$\boldsymbol{\nabla} \times \mathbf{E} = -\frac{\partial \mathbf{B}}{\partial t}, \tag{2.2.44}$$

$$\boldsymbol{\nabla} \cdot \mathbf{D} = \rho, \tag{2.2.45}$$

$$\boldsymbol{\nabla} \cdot \mathbf{B} = 0, \tag{2.2.46}$$

where $\mathbf{E}$ is the electric field, $\mathbf{H}$ is the magnetic field, $\mathbf{D}$ is the electric displacement, $\mathbf{B}$ is the magnetic flux, $\mathbf{j}$ is the free current density and ρ is the free charge density. We also have the relations

$$\mathbf{D} = \varepsilon_0 \mathbf{E} + \mathbf{P}, \tag{2.2.47}$$

$$\mathbf{B} = \mu_0 \mathbf{H} + \mathbf{M}, \tag{2.2.48}$$

where ε_0 is the permittivity of free space, $\mathbf{P}$ is the polarisation density, μ_0 is the permeability of free space and $\mathbf{M}$ is the magnetisation. In this work, we will be considering the propagation of light through vapours of alkali metals. Such a medium is non-magnetic and we will assume that there are no ionised atoms or other free charges or currents. Hence we can set ρ, $\mathbf{j}$ and $\mathbf{M}$ to zero and the set of Maxwell's equations simplifies to

$$\boldsymbol{\nabla} \times \mathbf{B} = \mu_0 \frac{\partial \mathbf{D}}{\partial t}, \tag{2.2.49}$$

$$\boldsymbol{\nabla} \times \mathbf{E} = -\frac{\partial \mathbf{B}}{\partial t}, \tag{2.2.50}$$

$$\boldsymbol{\nabla} \cdot \mathbf{D} = 0, \tag{2.2.51}$$

$$\boldsymbol{\nabla} \cdot \mathbf{B} = 0. \tag{2.2.52}$$

Taking the curl of (2.2.50) and making use of (2.2.49) we find

$$\boldsymbol{\nabla} \times (\boldsymbol{\nabla} \times \mathbf{E}) = \boldsymbol{\nabla} \times \left(-\frac{\partial \mathbf{B}}{\partial t} \right) = -\mu_0 \frac{\partial^2 \mathbf{D}}{\partial t^2}. \tag{2.2.53}$$

Using the vector identity

$$\boldsymbol{\nabla} \times (\boldsymbol{\nabla} \times \mathbf{E}) = \boldsymbol{\nabla}(\boldsymbol{\nabla} \cdot \mathbf{E}) - \nabla^2 \mathbf{E}, \tag{2.2.54}$$

we obtain

$$\boldsymbol{\nabla}(\boldsymbol{\nabla} \cdot \mathbf{E}) - \nabla^2 \mathbf{E} = -\mu_0 \frac{\partial^2 \mathbf{D}}{\partial t^2}. \tag{2.2.55}$$

From (2.2.47) it can be seen that $\boldsymbol{\nabla} \cdot \mathbf{E} = 0$ if $\boldsymbol{\nabla} \cdot \mathbf{P} = 0$. We will assume that the variation of the polarisation density in the plane transverse to propagation is negligible such that $\boldsymbol{\nabla} \cdot \mathbf{P} \approx 0$. Hence we have

$$\nabla^2 \mathbf{E} = \mu_0 \frac{\partial^2 \mathbf{D}}{\partial t^2}. \tag{2.2.56}$$

Substituting in (2.2.47) we obtain

$$\nabla^2 \mathbf{E} - \frac{1}{c^2} \frac{\partial^2 \mathbf{E}}{\partial t^2} = \mu_0 \frac{\partial^2 \mathbf{P}}{\partial t^2}. \tag{2.2.57}$$

In the simulations in this thesis, there will be at most two fields (probe and coupling). We will assume that all fields are polarised along the z-axis and propagate in the x-direction. Therefore we are interested in solutions to (2.2.57) of the form

$$\mathbf{E} = \frac{1}{2}\hat{\mathbf{z}}\mathcal{E}_{\mathrm{p}}e^{-\mathrm{i}\omega_{\mathrm{p}}(t-x/c)} + \frac{1}{2}\hat{\mathbf{z}}\mathcal{E}_{\mathrm{c}}e^{-\mathrm{i}\omega_{\mathrm{c}}(t-x/c)} + c.c., \tag{2.2.58}$$

$$\mathbf{P} = \frac{1}{2}\hat{\mathbf{z}}\mathcal{P}_{\mathrm{p}}e^{-\mathrm{i}\omega_{\mathrm{p}}(t-x/c)} + \frac{1}{2}\hat{\mathbf{z}}\mathcal{P}_{\mathrm{c}}e^{-\mathrm{i}\omega_{\mathrm{c}}(t-x/c)} + c.c., \tag{2.2.59}$$

where $\mathcal{E}_{\mathrm{p/c}}$ and $\mathcal{P}_{\mathrm{p/c}}$ are the electric and polarisation amplitudes of the probe/coupling fields (which are in general complex quantities), $\omega_{\mathrm{p/c}}$ are the carrier wave angular frequencies of the probe/coupling fields and *c.c.* represents the complex conjugate of the preceding terms of the equation. Substituting (2.2.58) and (2.2.59) into (2.2.57) we obtain

$$\left[(\partial_{xx} + 2\mathrm{i}k_\alpha\partial_x - k_\alpha^2) + \partial_{yy} + \partial_{zz} - \frac{1}{c^2}(\partial_{tt} - 2\mathrm{i}\omega_\alpha\partial_t - \omega_\alpha^2)\right]\mathcal{E}_\alpha = \\ = \mu_0(\partial_{tt} - 2\mathrm{i}\omega_\alpha\partial_t - \omega_\alpha^2)\mathcal{P}_\alpha, \tag{2.2.60}$$

where $k_\alpha = \frac{\omega_\alpha}{c}$ is a wavenumber and $\alpha = \mathrm{p/c}$ indicates the probe/coupling field. We will now make an assumption known as the slowly-varying envelope approximation [47]. The slowly-varying envelope approximation assumes that the carrier wave part of $\mathbf{E}$ and $\mathbf{P}$ varies much more rapidly with time and distance than the amplitudes $\mathcal{E}$ and $\mathcal{P}$. We will be considering fields with wavelengths of ~ 800 nm and optical periods of ~ 3 fs. We will consider propagation distances of the order of millimetres and temporal variations of the order of nanoseconds so this approximation is well justified. Specifically, we assume that

$$|\partial_{xx}\mathcal{E}| \ll k|\partial_x\mathcal{E}|, \tag{2.2.61}$$

$$|\partial_{tt}\mathcal{E}| \ll \omega|\partial_t\mathcal{E}|, \tag{2.2.62}$$

$$|\partial_{tt}\mathcal{P}| \ll \omega|\partial_t\mathcal{P}|, \tag{2.2.63}$$

$$|\partial_t\mathcal{P}| \ll \omega|\mathcal{P}|. \tag{2.2.64}$$

We also make use of the vacuum dispersion relation, $\omega = ck$. This relation is valid

since, although the medium is not a vacuum, it is a gas and so has a refractive index very close to 1. With these assumptions, (2.2.60) simplifies to

$$\left[(2\mathrm{i}k_\alpha\partial_x) + \partial_{yy} + \partial_{zz} + \frac{2\mathrm{i}k_\alpha}{c}\partial_t\right]\mathcal{E}_\alpha = -\mu_0\omega_\alpha^2\mathcal{P}_\alpha. \tag{2.2.65}$$

This is the propagation equation. It can be solved to find the electric field amplitude, $\mathcal{E}_\alpha$, given a polarisation amplitude $\mathcal{P}_\alpha$ and the relevant boundary conditions. By making a coordinate transformation using the relations

$$x' = x, \tag{2.2.66}$$

$$t' = t - \frac{x}{c}, \tag{2.2.67}$$

(2.2.65) becomes

$$2\mathrm{i}k_\alpha\frac{\partial\mathcal{E}_\alpha}{\partial x'} + \frac{\partial^2\mathcal{E}_\alpha}{\partial y^2} + \frac{\partial^2\mathcal{E}_\alpha}{\partial z^2} = -\mu_0\omega_\alpha^2\mathcal{P}_\alpha. \tag{2.2.68}$$

This transformation is useful since it reduces the dependence of the differential equation to three variables instead of four. For the simulations in this thesis, we will make the assumption that the fields are plane waves which means that (2.2.68) contains only a derivative with respect to x'. This makes the numerical computations much simpler but is still an accurate model for many experiments in which the Rayleigh lengths are much larger than the propagation distances.

2.2.8 Maxwell-Bloch Model

We now have two models. The optical Bloch equations which describe the state of the atoms exposed to a given set of fields and the propagation equation which describes the state of the fields in a given medium polarisation. However, the two models are connected: the fields change the state of the atomic medium as they travel through it which changes the medium polarisation and the fields themselves are then changed in response to the new polarisation. Therefore, the optical Bloch equations and the propagation equation must be solved self-consistently. Together, they comprise a model called the Maxwell-Bloch model. The connection is through

the medium polarisation, $\mathbf{P}$. The polarisation of a medium is the total electric dipole moment per unit volume [48]. It can be expressed as the expectation value of the dipole operator $\mathbf{d} = -e\mathbf{r}$ multiplied by the number density $\mathcal{N}$ [38]

$$\mathbf{P}(\mathbf{r}, t) = \mathcal{N}\langle \mathbf{d} \rangle. \tag{2.2.69}$$

The expectation value of the dipole operator can be written in the form [49]

$$\langle \mathbf{d} \rangle = \mathrm{Tr}\left[\rho \mathbf{d}\right], \tag{2.2.70}$$

where ρ is the density matrix. Since the light is polarised along the z-axis, all the matrix elements of the dipole operator must be directed along the z-axis and the diagonal elements are all zero as discussed earlier. Hence we must have that

$$\langle \mathbf{d} \rangle = (D_{12}\rho_{21} + D_{21}\rho_{12} + D_{13}\rho_{31} + D_{31}\rho_{13})\hat{\mathbf{z}}. \tag{2.2.71}$$

where D_{12} and D_{13} are the dipole matrix elements defined by (2.2.14) and (2.2.15). The polarisation can also be represented in the form of (2.2.59) and so

$$\begin{aligned} \mathbf{P}(\mathbf{r}, t) &= \mathcal{N}(D_{12}\rho_{21} + D_{13}\rho_{31})\hat{\mathbf{z}} + c.c. \\ &= \frac{1}{2}\mathcal{P}_{\mathrm{p}} e^{-\mathrm{i}\omega_{\mathrm{p}}(t - x/c)}\hat{\mathbf{z}} + \frac{1}{2}\mathcal{P}_{\mathrm{c}} e^{-\mathrm{i}\omega_{\mathrm{c}}(t - x/c)}\hat{\mathbf{z}} + c.c.. \end{aligned} \tag{2.2.72}$$

The density matrix elements in the lab frame are related to those in the rotating frame by $\rho'_{21} = \rho_{21}e^{-\mathrm{i}\omega_p t}$ and $\rho'_{31} = \rho_{31}e^{-\mathrm{i}\omega_c t}$ and hence

$$\mathcal{P}_{\mathrm{p}}(z, t) = 2\mathcal{N}D_{12}\rho'_{21}, \tag{2.2.73}$$

$$\mathcal{P}_{\mathrm{c}}(z, t) = 2\mathcal{N}D_{13}\rho'_{31}. \tag{2.2.74}$$

We can then substitute these expressions into (2.2.68). The propagation of the light through the atomic vapour can be determined by solving the propagation equation (2.2.68) and the optical Bloch equations (2.2.37 - 2.2.42) numerically. For 1D propagation propagation of the probe field, we have an equation of the form

$$\frac{\partial \mathcal{E}_{\mathrm{p}}}{\partial x'} = i\frac{1}{c\epsilon_0}\omega_{\mathrm{p}}\mathcal{N}D_{12}\rho'_{21}. \tag{2.2.75}$$

We can also write the propagation equation in terms of the Rabi frequency rather than the electric field amplitude and using 2.2.25 we obtain

$$\frac{\partial \Omega_{\mathrm{p}}}{\partial x'} = i\mu_{\mathrm{p}}\rho'_{21}, \tag{2.2.76}$$

where μ_{p} is propagation coefficient given by

$$\mu_{\mathrm{p}} = \frac{\omega_{\mathrm{p}}\mathcal{N}}{\hbar\epsilon_0 c} D_{12}^2. \tag{2.2.77}$$

Of course, an analogous equation can be derived for the coupling field.

2.3 SIT Solitons and Simultons

2.3.1 SIT Solitons

Self-Induced Transparency (SIT) is a phenomena first described by McHall and Hahn in the late 1960s [12]. They studied the equations governing the propagation of light pulses through inhomogeneously broadened two-level systems with no decay (homogeneous broadening). They found that the propagation of the pulses had a large dependence on a property called the pulse area, θ. This is defined as [12]

$$\theta(x) = \int_{-\infty}^{\infty} \Omega(x,t)\ dt, \tag{2.3.1}$$

where $\Omega(x,t)$ is the Rabi frequency given by

$$\Omega(x,t) = \frac{D_{12}\mathcal{E}(x,t)}{\hbar}, \tag{2.3.2}$$

and D_{12} is the transition dipole moment for the transition between the two levels. They found that θ obeyed an equation called the area theorem given by [12]

$$\frac{\partial \theta}{\partial x} = -\frac{\alpha}{2}\sin\theta, \tag{2.3.3}$$

where α is the linear absorption coefficient equal to the reciprocal of the Beer's absorption length for the medium. For the case of an atomic vapour in the absence

of inhomogeneous broadening this is given by

$$\alpha = 8\pi^2 \epsilon_0 \mu, \tag{2.3.4}$$

where ϵ_0 is the permittivity of free space and μ is the propagation coefficient defined by (2.2.77). The solution of this equation which satisfies $\theta = \theta_0$ at $x = 0$ is [12]

$$\tan(\theta/2) = \tan(\theta_0/2) \exp[-(\alpha/2)x]. \tag{2.3.5}$$

It can be seen from equation (2.3.5) that as $x \to \infty$, $\tan(\theta/2) \to 0$ and so θ tends to the multiple of 2π closest to θ_0. For example, if $\theta_0 = 1.2\pi$ then the pulse area will tend to 2π. This scenario is shown in Figure 2.3. This means that input pulses with a sufficient width and peak intensity such that they have an initial area larger than π will tend towards a stable shape with constant area as they travel further into the medium. In contrast, pulses with an initial area of less than π will disappear since their area will tend to zero as they travel further into the medium. This case is shown in Figure 2.4. Pulses with an initial area in the range 0.5π to 1.5π are reshaped into a single pulse with an area of 2π and a sech Rabi frequency profile of the form

$$\Omega_{2\pi}(x,t) = \frac{2}{\tau_s} \text{sech}\left(\frac{t - x/v_g}{\tau_s}\right), \tag{2.3.6}$$

where τ_s is the sech-width of the pulse and v_g is its group velocity. τ_s is related to the full-width half-max (τ_w) of the pulse by $\tau_s = 0.379663\tau_w$. The group velocity (i.e. the velocity at which the pulse envelope propagates through the medium), is given by [50]

$$v_g = \frac{2c}{2 + \mu c \tau^2}, \tag{2.3.7}$$

where c is the speed of light, μ is the propagation coefficient as given by (2.2.77) and $\tau = 2/\Omega_0$ where Ω_0 is the peak Rabi frequency of the pulse.

The pulses described by (2.3.6) are known as SIT solitons. Solitons, or solitary waves, are terms used across maths and physics to describe wave packets (pulses) that maintain their shapes as they propagate [51]. The pulse profile given by (2.3.6)

is unique because it is such that the first half of the pulse transfers the atomic population entirely from the ground state to the excited state but the second half of the pulse then causes stimulated emission that transfers the atomic population entirely back to the ground state again [52]. By this mechanism, the soliton preserves its shape as it propagates and it leaves the medium in an entirely unexcited state at it each point it passes through. This process takes a finite amount of time and results in the slow-light effect by which the group velocity of the SIT soliton is significantly lower than the speed of light. For the simulation shown in Figure 2.3, the soliton that forms has a group velocity of 3.2×10^4 m/s which is $\sim 0.01\%$ of the speed of light. However, it is possible to produce solitons with group velocities much lower than this in SIT experiments and speeds as low as 300 m/s have been recently achieved [17].

Input pulses with an area larger than 3π break up into multiple pulses. An example of the propagation of a 4.5π pulse is shown in Figure 2.5. Each of the pulses that form have an area of 2π in the sense that, when the pulses are well separated, an integral of the Rabi frequency over each pulse will give a value of 2π. Once the pulses are well separated, each pulse is well approximated by a sech Rabi frequency profile of the form of (2.3.6). This break up occurs because, as the initial pulse propagates through the medium, both absorption and stimulated emission occur which lead to reshaping of the pulse and result in the formation of N solitons, where N is the integer multiple of 2π closest to the input pulse area [52].

After the initial paper on SIT by McHall and Hahn, the theory was further studied by various other authors. In particular, it was found that the Maxwell-Bloch equations for a 2-level resonator in the presence of inhomogeneous broadening can be solved enitrely analytically by means of the inverse scattering transform [53]. This is a mathematical technique for solving nonlinear partial differential equations first developed by Gardner et al. in the context of solving the Korteweg-deVries equation [54]. The Kortweg-deVries equation describes the behaviour of small amplitude shallow water waves [54]. Indeed the SIT solitons discovered by McHall and Hahn

have been found to be closely related to the soliton solutions of the Kortweg-deVries equation [52, 53, 55].

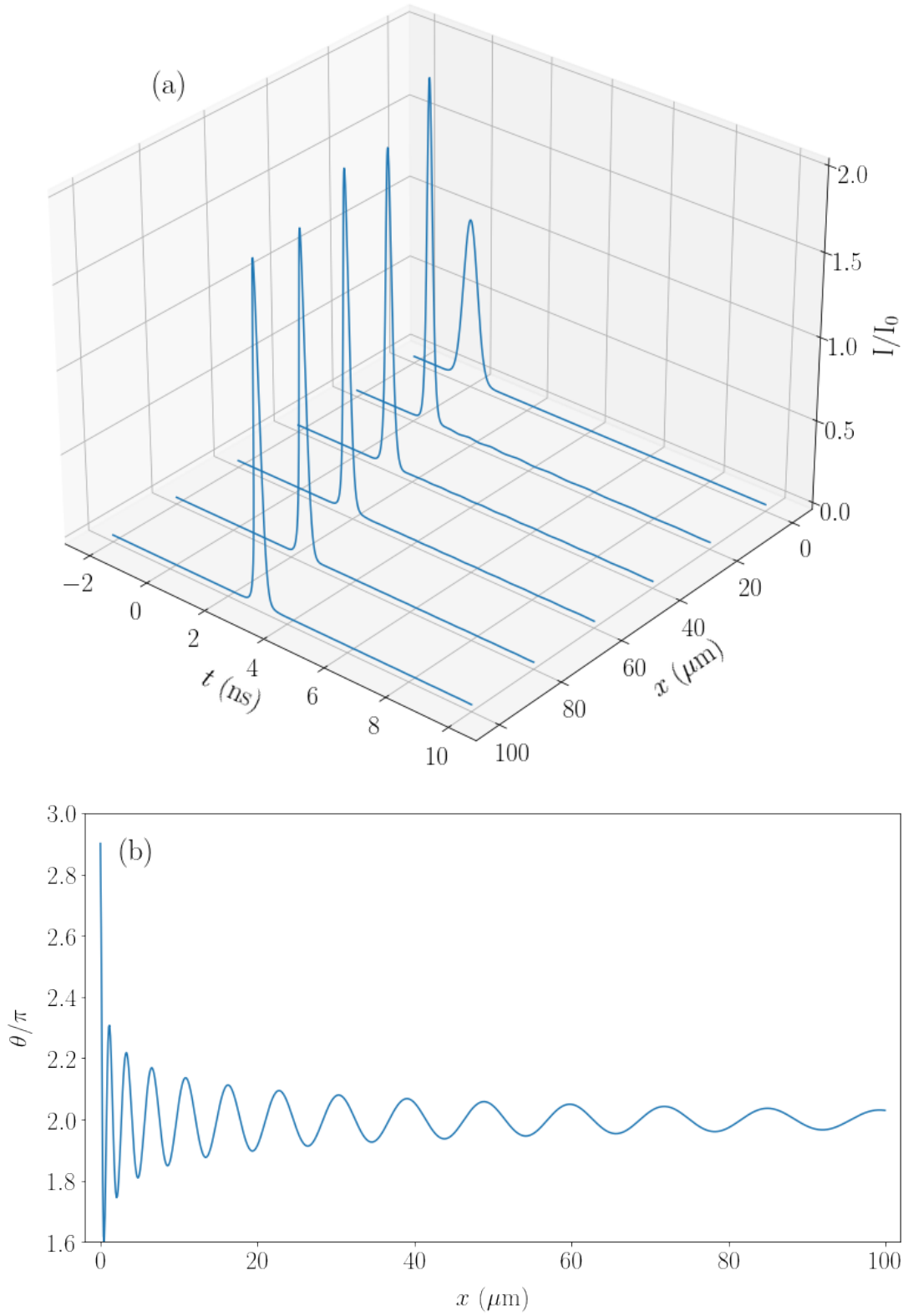

Figure 2.3: (a) The propagation of a pulse with an initially Gaussian profile and an input area of 1.2 π. The intensity is normalised to the peak input intensity, I_0 = 0.39 kW cm^{-2}. (b) The pulse area (as defined by (2.3.1)) divided by π. The field is resonant with the D1 transition in ^{85}Rb and the temperature is 220°C. The simulation does not include homogeneous or inhomogeneous broadening

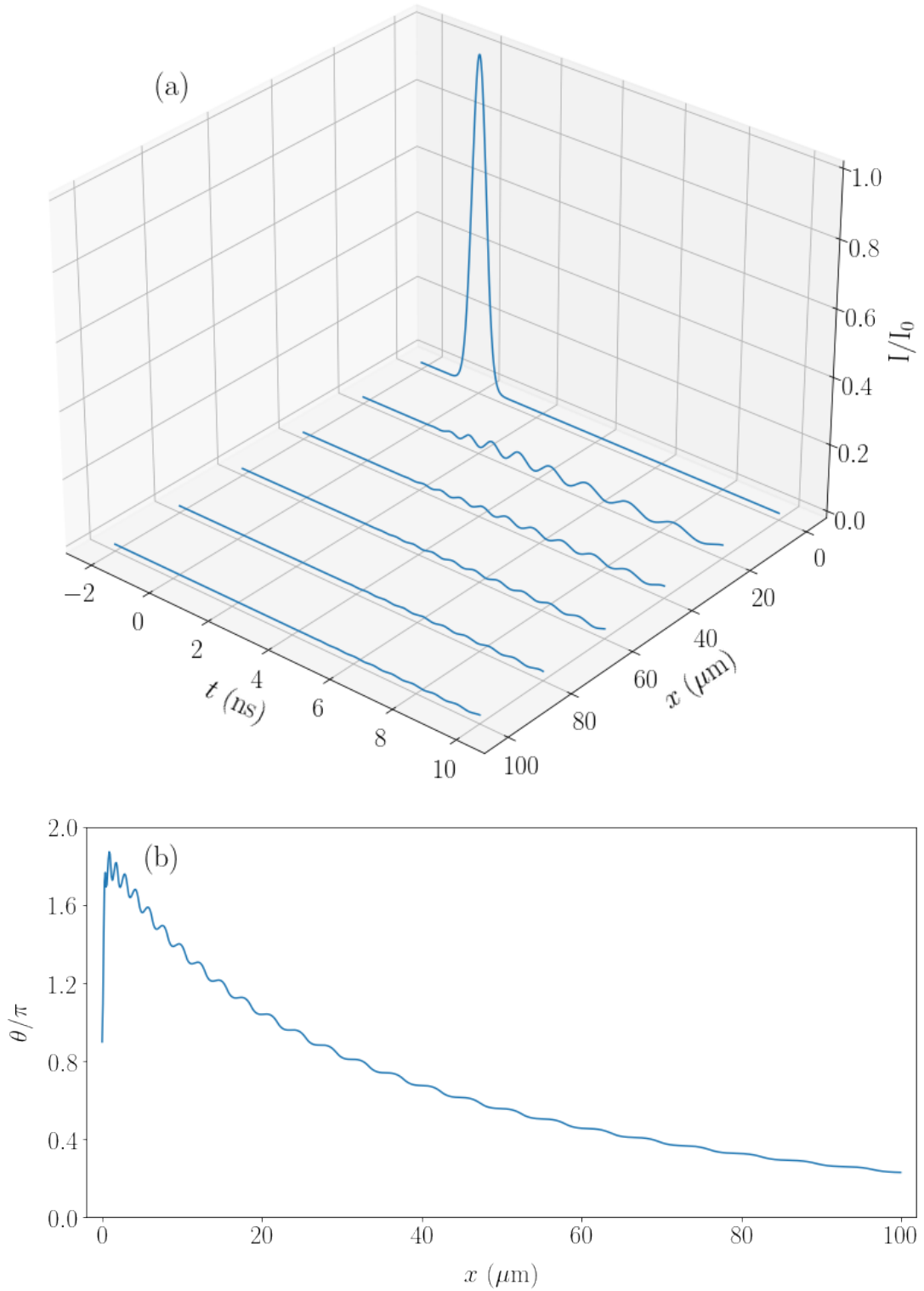

Figure 2.4: (a) The propagation of a pulse with an initially Gaussian profile and an input area of 0.9 π. The intensity is normalised to the peak input intensity, I_0 = 0.038 kW cm^{-2}. (b) The pulse area (as defined by (2.3.1)) divided by π. The field is resonant with the D1 transition in ^{85}Rb and the temperature is 220°C. The simulation does not include homogeneous or inhomogeneous broadening

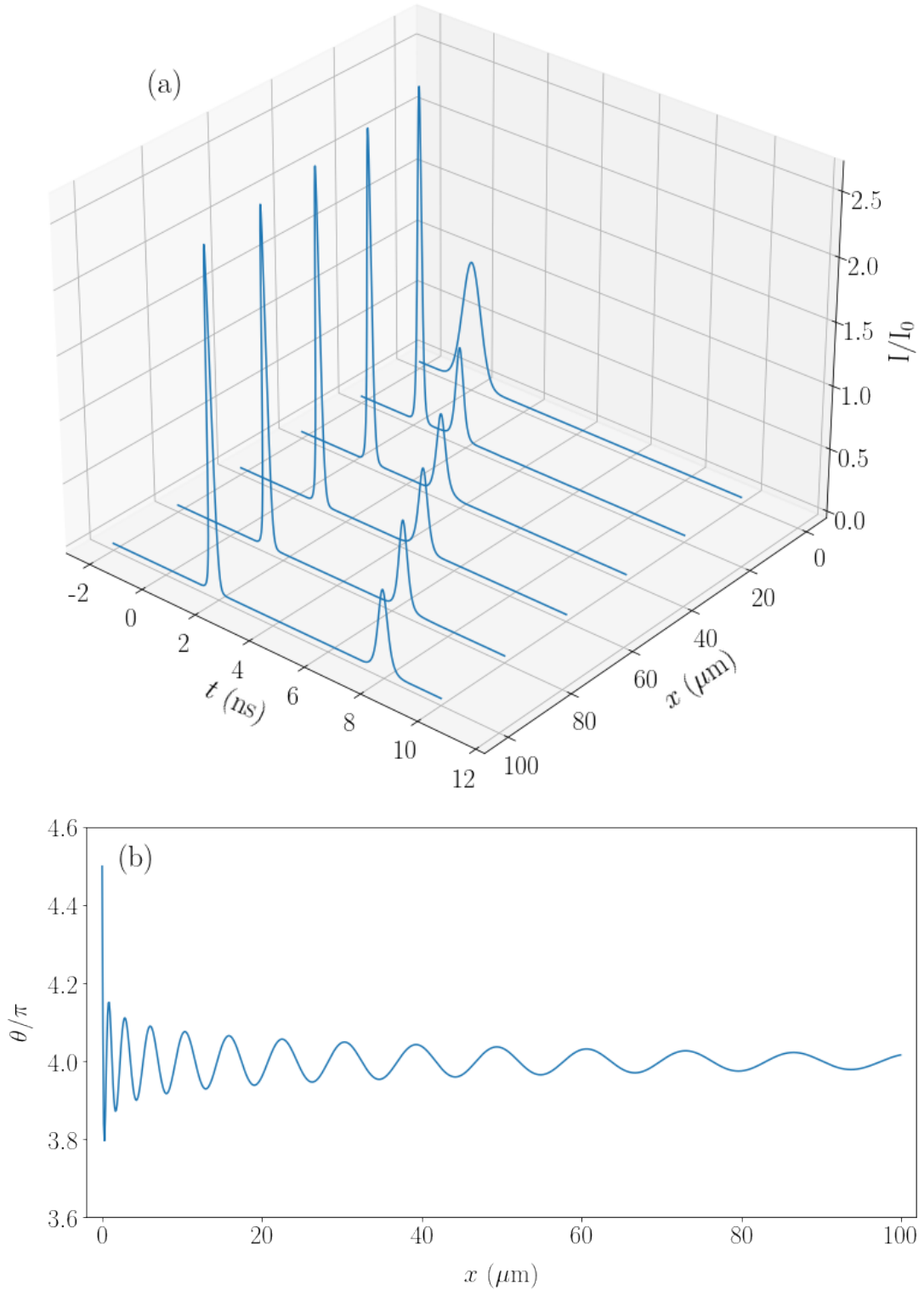

Figure 2.5: (a) The propagation of a pulse with an initially Gaussian profile and an input area of 4.5 π. The intensity is normalised to the peak input intensity, I_0 = 0.47 kW cm^{-2}. (b) The pulse area (as defined by (2.3.1)) divided by π. The field is resonant with the D1 transition in ^{85}Rb and the temperature is 220°C. The simulation does not include homogeneous or inhomogeneous broadening.

2.3.2 Simultons

Related to the phenomenon of SIT is that of simultons. They are a two-field effect and occur in 3-level V-systems. The term simulton was first coined by Konopnicki and Eberly in 1981 to describe the effect by which two solitons, each resonant on separate transitions of a 3-level V-system, are found to follow simultaneous trajectories (co-propagate) as they move through a medium of resonators [25]. They were discvored from the analytic solutions that Konopnicki and Eberly obtained for the 3-level Maxwell-Bloch equations of a V-system with two resonant fields provided that both transitions had the same oscillator strength. The oscilltor strength β is given by [25]

$$\beta = \frac{d_{\mathrm{b}}^2 \omega_{\mathrm{b}}}{d_{\mathrm{a}}^2 \omega_{\mathrm{a}}}, \tag{2.3.8}$$

where $d_{\mathrm{a/b}}$ is the transition dipole moment of transition a/b and $\omega_{\mathrm{a/b}}$ is the resonant angular frequency of transition a/b. This requirement on the oscillator strength was necessary in order to obtain the analytic solutions however it is a difficult condition to fulfill in an experiment. Nevertheless, simultons have been observed in experiments with nonlinear crystals [56]. More recently, a group at Durham university found experimental results that appeared to show the onset of simulton formation in a Rubidium atomic vapour even though (2.3.8) was not satisfied [26]. This was then followed up by a theoretical investigation which showed that in fact simulton-like effects can occur in a three-level V system without the requirement that the transitions have identical oscillator strengths and for situations in which there are spontaneous decays and other broadening processes [26]. These were termed optical quasi-simultons.

Figure 2.6 shows a simulation with identical parameters to one shown in reference [26]. It shows the propagation of two light fields through a medium of ^{85}Rb atoms. Homogeneous broadening is included but inhomogeneous broadening is neglected (though the effect is not restricted to this condition as is explained in reference [26] and we do this only to reduce the computation time). The system is a three-level V-system

identical to that shown in Figure 2.1. The probe field is resonant with the D1 transition and the coupling field is resonant with the D2 transition. The probe field is continuous wave (CW) with a very weak intensity of 10 μW/cm^2. At $t = -2$ ns, the probe is in a steady state with the atomic medium (i.e. it is as though it has been left on for a sufficient time such that the terms with time derivatives in the optical Bloch equations (2.2.37-2.2.42) are all zero). The coupling field is a Gaussian pulse with a peak intensity of 1 kW/cm^2 and a full-width half-max (FWHM) of 0.8 ns, which reaches a peak intensity at $t = 0$ ns. In the absence of the strong coupling pulse, the weak probe field would be absorbed very rapidly in accordance with Beer's law [57]. However, in the presence of the coupling field, a different dynamics occurs. It can be seen in Figure 2.6(a) that the coupling field breaks up into three separate pulses. This is because the Gaussian pulse inputted on the coupling transition has an area of 6.5π and so it breaks up into three soliton-like pulses as it propagates through the medium in accordance with the theory of SIT discussed in the previous subsection. However, in this case homogeneous broadening is included which results in the group velocity of the pulses decreasing with time once the sech-soliton-like pulses have formed. We will investigate the effect of homogeneous broadening on SIT pulses in Chapter 3. It can be seen in Figure 2.6(b) that three pulses also form on the probe transition (though the middle one is very faint) which each co-propagate with a pulse of the coupling field. These pairs of co-propagating pulses are quasi-simultons. Figure 2.7 shows the pulse profiles of the quasi-simultons at a distance of 25 μm into the medium. Each of the pulses have an approximately sech-squared profile. The study in reference [26] also included calculations with the full-hyperfine structure of the D1 and D2 transitions, and quasi-simulton formation was still found to occur even in this more complicated model. In this thesis we restrict our study to the closed three-level V-system shown in Figure 2.1 for simplicity and to allow comparison with other theoretical studies. However it is likely that this model is nevertheless sufficient to capture the essential physics of effects which will persist to some degree in more complex systems, as was found in reference [26].

Ogden et al. [26] attributed the mechanism that underpins the quasi-simulton phenomenon to that of soliton-induced transparency (SOIT). This is a term first coined by Kozlov and Kozlava [58, 59]. SOIT occurs when an SIT soliton on one transition of a three-level V-system is able to induce a transparency to a weak field resonant with the adjacent transition. Kozlov and Kozlova attributed the formation of a sech pulse on the weak field to a kind of pulse-locking effect. This results from the unique property of inhomogeneously broadened SIT pulses by which the strong field coherence term (e.g. ρ_{13} if the SIT pulse is propagating on the 1-3 transition) associated with each of the different velocity classes oscillate in phase with one other [60]. This causes the other coherence's (e.g. ρ_{23} and ρ_{12}) across all velocity classes to also oscillate in phase with the ρ_{13} terms (becoming locked) and hence an SIT pulse is formed on the weak field. The effect is the same in the absence of inhomogeneous broadening except there is only one velocity class in this case.

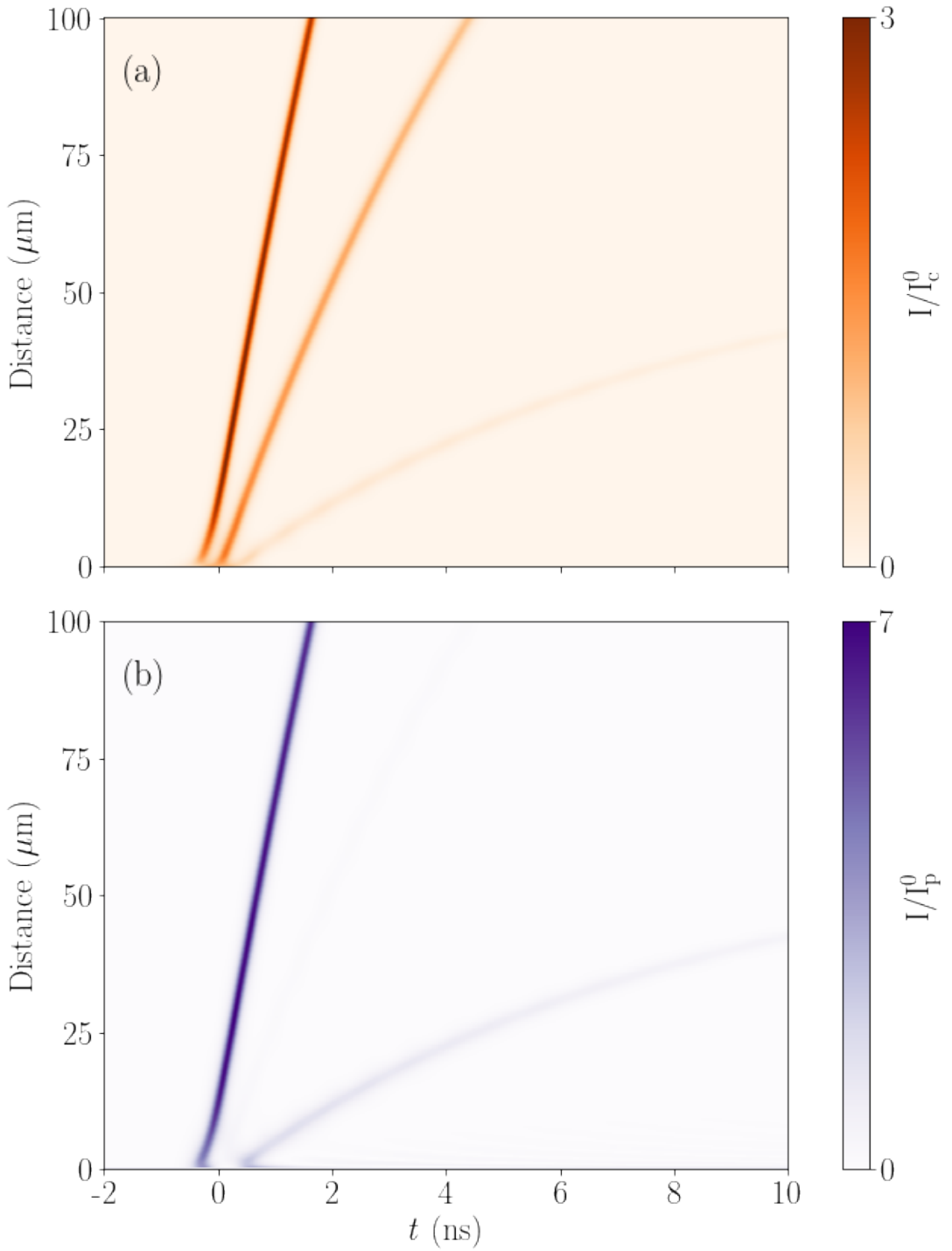

Figure 2.6: The formation of quasi-simultons in a three-level V-model of ^{85}Rb at a temperature of 220°C. The input coupling field is a Gaussian pulse with a full-width half-max of 0.8 ns and a peak intensity $I_c^0 = 1$ kW/cm^2 (the peak occurs at $t = 0$ ns). The input probe field is a CW field with an intensity of $I_p^0 = 10$ μW/cm^2 that has already reached a steady state with the medium at $t = -2$ ns. (a) The coupling field intensity normalised to I_c^0. (b) The probe field intensity normalised to I_p^0.

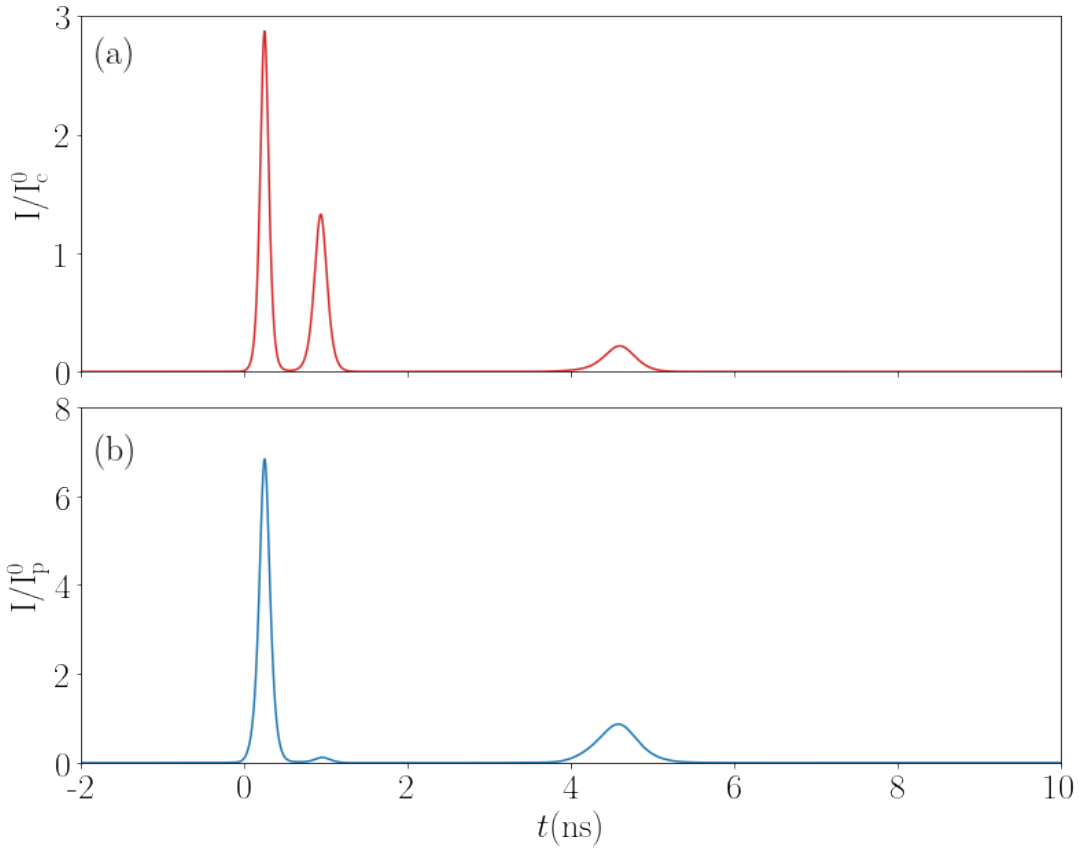

Figure 2.7: The pulse profiles of the quasi-simultons shown in Figure 2.6 at a distance of 25 μm. (a) The coupling field intensity normalised to the peak intensity of the Gaussian input pulse, $I_c^0 = 1$ kW/cm^2. (b) The probe field intensity normalised to the input CW field intensity of the probe field, $I_p^0 = 10$ μW/cm^2.

2.4 The Jacobian Elliptic Functions

We will later explore the physics of pulse train formation in two and three level media. As we will show, such pulse trains can often be approximated by waves described in terms of Jacobian elliptic functions. We will now explain how these functions are defined, their properties and their relation to the sech-solitons considered previously.

The Jacobian elliptic functions are a set of three functions: sn (snoidal), dn (dnoidal) and cn (cnoidal), that are defined as inverses of the incomplete elliptical integral of the first kind, F. This is defined as [61]

$$u(y_1,k) \equiv \int_0^{y_1} \frac{dt}{\sqrt{(1-t^2)(1-k^2t^2)}} = \int_0^{\phi} \frac{d\theta}{\sqrt{1-k^2\sin^2\theta}} = F(\phi,k), \tag{2.4.1}$$

where the parameter k is called the modulus and is defined in the range $0 \leq k \leq 1$. The elliptic functions are then defined by [61]

$$\mathrm{sn}(u,k) = \sin\phi = y_1, \tag{2.4.2}$$

$$\mathrm{cn}(u,k) = \sqrt{1-y_1^2} = \cos\phi, \tag{2.4.3}$$

$$\mathrm{dn}(u,k) = \sqrt{1-k^2y_1^2} = \sqrt{1-k^2\sin^2\phi}\ . \tag{2.4.4}$$

These functions have both a real and an imaginary period and so are described as being doubly-periodic [61]. However, the cases that we will consider involve only real values of u. The functions describe stationary waves which are infinite in extent (i.e. have no start or end). It has been shown that nonlinear optical waves described in terms of these functions can exist, for example in a nonlinear reflection grating [62]. We will focus on the dn function since this will turn out to have the greatest relevance to the physics of pulse train formation from CW input fields.

Figure 2.10 shows the dn function for real values of u in the range -50 to 50 and values of k in the range 0.5 to 1. It can be seen that the period of the dn function increases with k. The period diverges as k approaches unity and the dn function tends toward the sech function. This can be seen clearly in Figure 2.9 which shows the profile of the dn function for values of k very close to unity: the pulses become

more separated and are shaped more like sech pulses as k increases. In the limit $k \to 1$, the dn function becomes a single sech function (or in a way a series of sech functions that are infinitely separated) [63]. It can also be seen from Figure 2.10 that as k increases, the contrast between the maxima and minima increases. We show only values of k in the range 0.5 to 1 to make the figure easier to interpret, however the same trends continue between $k = 0$ and $k = 0.5$. At $k = 0$, the contrast is zero and the function is a constant value of 1.

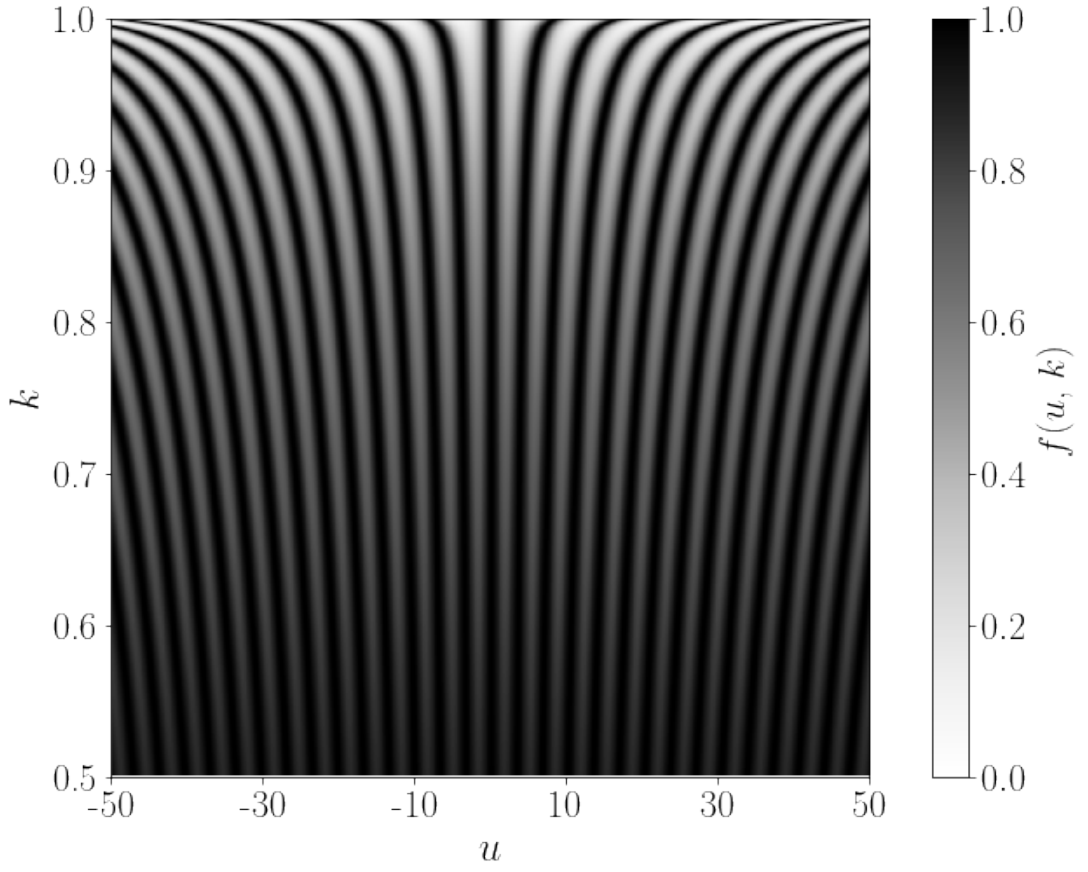

Figure 2.8: The Jacobi dn function for real values of u in the range -50 to 50 and values of k in the range 0.5 to 1.

Figure 2.10 shows the cn function for real values of η in the range -50 to 50 and values of k in the range 0 to 1. In contrast to the dn function, the cn function oscillates between -1 and 1 for all values of k. As k increases, the period increases. In the limit that $k \to 1$, the cn function becomes the sech function as was the case for the dn function [63]. In the limit that $k \to 0$, the cn function becomes the cosine function [63].

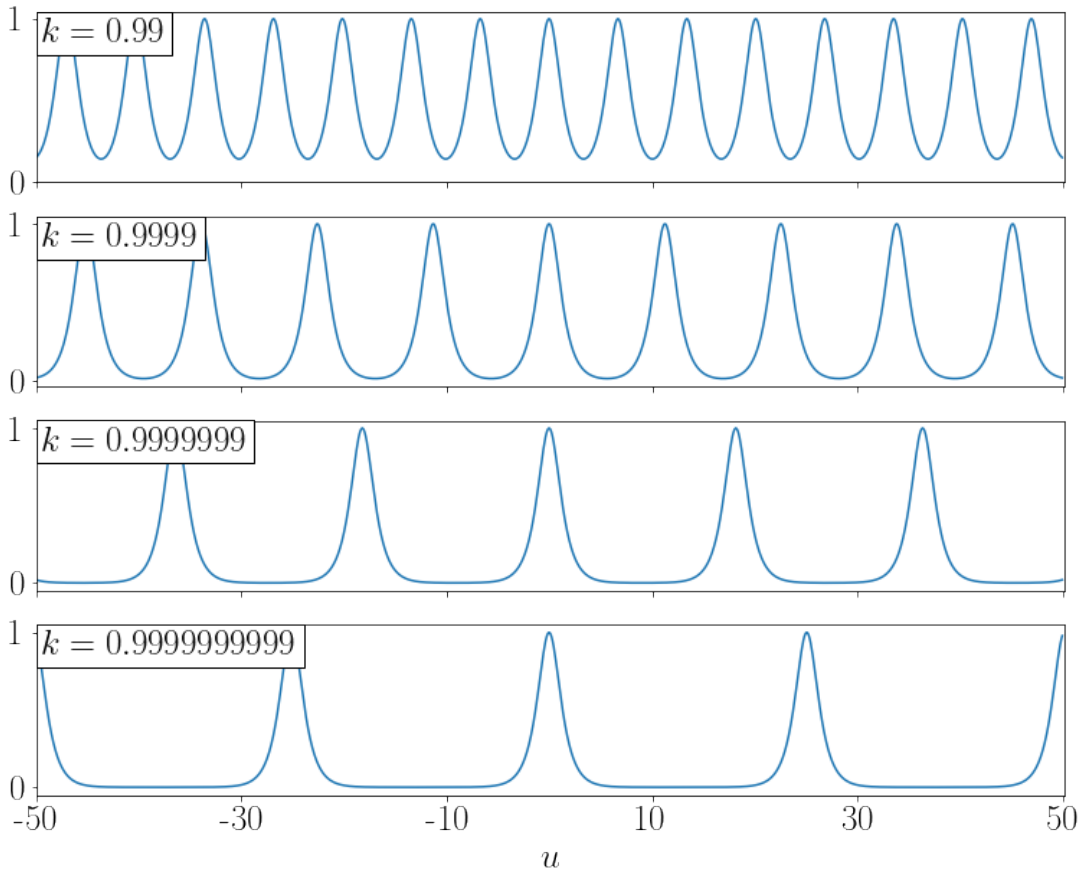

Figure 2.9: The dn function for k values approaching 1.

It was shown by Crisp in 1969 that solutions of the Maxwell-Bloch equations exist that can be defined in terms of these elliptic functions [50]. These solutions, in terms of the Rabi frequency Ω, are given by

$$\Omega(x,t) = \Omega_0 \mathrm{dn}(\eta, k), \tag{2.4.5}$$

$$\Omega(x,t) = \Omega_0 \mathrm{cn}(\eta, k), \tag{2.4.6}$$

where

$$\eta = (t - x/v)/\tau. \tag{2.4.7}$$

v and τ are defined by

$$\frac{1}{v} = \frac{1}{c} + \frac{\mu\tau^2}{2k^2}, \tag{2.4.8}$$

$$\tau = \frac{2}{\Omega_0}, \tag{2.4.9}$$

where c is the speed of light and μ is the propagation coefficient defined by 2.2.77.

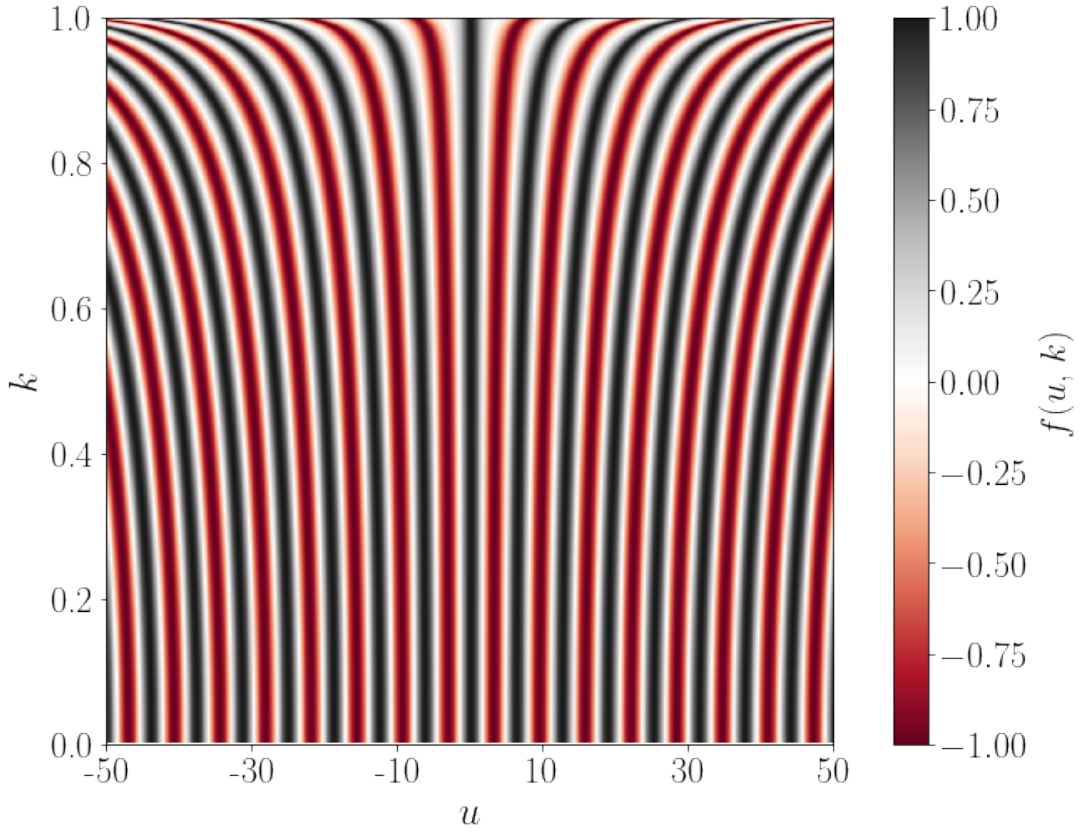

Figure 2.10: The Jacobi cn function for real values of u in the range -50 to 50 and values of k in the range 0 to 1.

(2.4.8) determines the group velocity v of a dnoidal wave with the parameters of τ and k propagating in a medium in which inhomogeneous broadening can be neglected. If inhomogeneous broadening is included, the group velocity is given by [50]

$$\frac{1}{v} = \frac{1}{c} + \frac{\mu\tau^2}{2}\int_{-\infty}^{\infty} \frac{g(\Delta)\mathrm{d}\Delta}{[(k^2 - \Delta^2\tau^2)^2 + 4\Delta^2\tau^2]^{1/2}}, \tag{2.4.10}$$

where c is the speed of light, μ is the propagation constant defined by (2.2.77), τ is defined by (2.4.9), k is the elliptic modulus, Δ is the the detuning of the field and g(Δ) is the Maxwell-Boltzmann distribution in terms of detuning given by

$$g(\Delta) \equiv (c/\omega)f(-c\Delta/\omega), \tag{2.4.11}$$

where ω is the angular frequency of the light and f is the Maxwell-Boltzmann distribution function defined by (2.2.16).

In the limit that $k \to 1$, (2.4.8) and (2.4.9) tend to the hyperbolic secant solution

described in the previous section: i.e.

$$\Omega_0 \mathrm{dn}(\eta, k) \to \Omega_0 \,\mathrm{sech}(\eta), \tag{2.4.12}$$

$$\Omega_0 \mathrm{cn}(\eta, k) \to \Omega_0 \,\mathrm{sech}(\eta), \tag{2.4.13}$$

as

$$k \to 1.$$

Chapter 3

SIT Solitons

In this chapter, we will investigate the propagation of SIT solitons through a medium of two-level resonators. Having explained the key features of SIT in the background theory section, we will now compare the properties of the SIT pulses seen in numerical simulations with analytical predictions. We aim to consolidate and build upon the previous research. In particular, we will compare the speeds and trajectories of the pulses in the numerical results with those of theoretical predictions. We will first consider the case of a system without homogeneous broadening as the analytical theory is well known and this will allow us to check that our program is working properly and the system is well understood. We will then explore SIT in systems in which spontaneous decay (homogeneous broadening) is included and see whether the analytical theory describing SIT in systems without homogeneous broadening can be extended to include it. We will simulate the propagation of a sech-solitons through a medium of ^{85}Rb atoms, resonant with the D1 transition shown in Figure 2.1, at a temperature of 220°C. This system and temperature was chosen since it was the one used for the experiments and simulations on optical quasi-simultons reported in reference [26] and, as previously explained, that research formed the starting point for this work.

3.1 No Homogeneous Broadening

Figure 3.1 shows the propagation of a pulse that is input with a sech-squared intensity profile (i.e. a sech Rabi frequency profile as given by (2.3.6)), a FWHM of 1 ns and a peak intensity of 0.9 kW/cm^2 such that it has a pulse area of 2π. Because the input field has a sech-squared intensity profile with an area of 2π, the pulse maintains a constant shape and intensity throughout the medium as expected from the theory of SIT explained in Chapter 2. It has been known since the initial paper on SIT by McHall and Hahn that a sech-soliton, propagating through a medium in which both homogeneous and inhomogeneous broadening can be neglected, will have a constant velocity of the form [12]

$$v = \frac{2c}{2 + \mu c \tau^2}, \tag{3.1.1}$$

where c is the speed of light, μ is the propagation constant defined by (2.2.77) and τ is defined by (2.4.9). Although it should be noted that McHall and Hahn used a significantly different notation to that shown in (3.1.1). This equation can be obtained from the equation giving the group velocity of a dnoidal wave (2.4.8) if the parameter k is set to unity since a dnoidal wave becomes a sech pulse when $k \to 1$ as previously discussed. The white dotted line in Figure (3.1) shows the theoretical trajectory of the pulse. As can be seen, it appears to agree exactly with the numerical results. Indeed, a detailed comparison between the numerical and theoretical field profiles at each distance reveals that the maximum absolute residual between the analytic and numerical values for the position of the pulse peak is just 0.006 ns. This gives us confidence that our program is working correctly for the simulations which do not include inhomogeneous broadening.

Figure 3.2 shows the propagation of exactly the same sech-soliton as in Figure 3.1 except inhomogeneous broadening (Doppler averaging) is included in the simulation. It has also been known since the initial paper on SIT by McHall and Hahn that a sech-soliton propagating in the presence of inhomogeneous broadening will move at

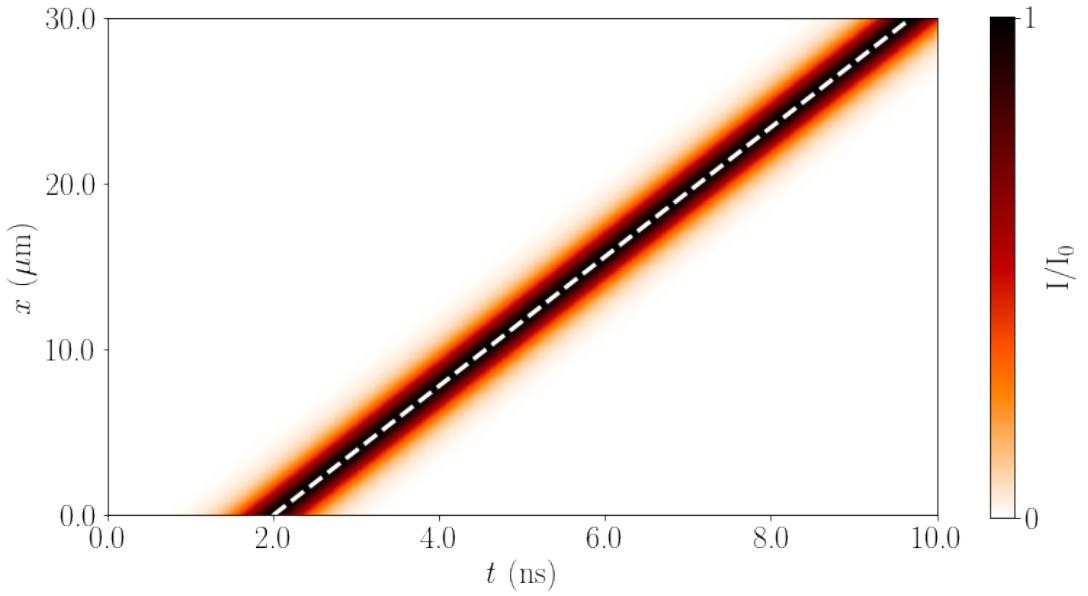

Figure 3.1: Heatmap showing the propagation of a sech-soliton, with a FWHM of 1 ns and a peak intensity of 0.9 kW/cm^2 through a medium of ^{85}Rb atoms at 220°C. The field is resonant with the D1 transition, we neglect the spontaneous decay mechanisms (homogeneous broadening) and there is no Doppler averaging (inhomogeneous broadening). The white dotted line shows the theoretical trajectory of the pulse.

a constant velocity of the form [12]

$$v = 2c\left[2 + \mu\tau^2 c\int_{-\infty}^{\infty}\frac{g(\Delta)d\Delta}{(1+\Delta^2\tau^2)}\right]^{-1}, \tag{3.1.2}$$

where the symbols are defined as previously. Again, this can be obtained from the velocity equation of a dnoidal wave propagating in the presence of inhomogeneous broadening if the parameter k is set to unity (2.4.10). A detailed comparison between the numerical and theoretical field profiles at each distance for the simulation shown in Figure 3.2 reveals that the maximum absolute residual between the analytic and numerical values for the position of the pulse peak is just 0.005 ns. Once again, we have found excellent agreement between the theoretical trajectory and the numerical calculations. This agreement gives us confidence that our program is also working correctly for the case of inhomogeneous broadening.

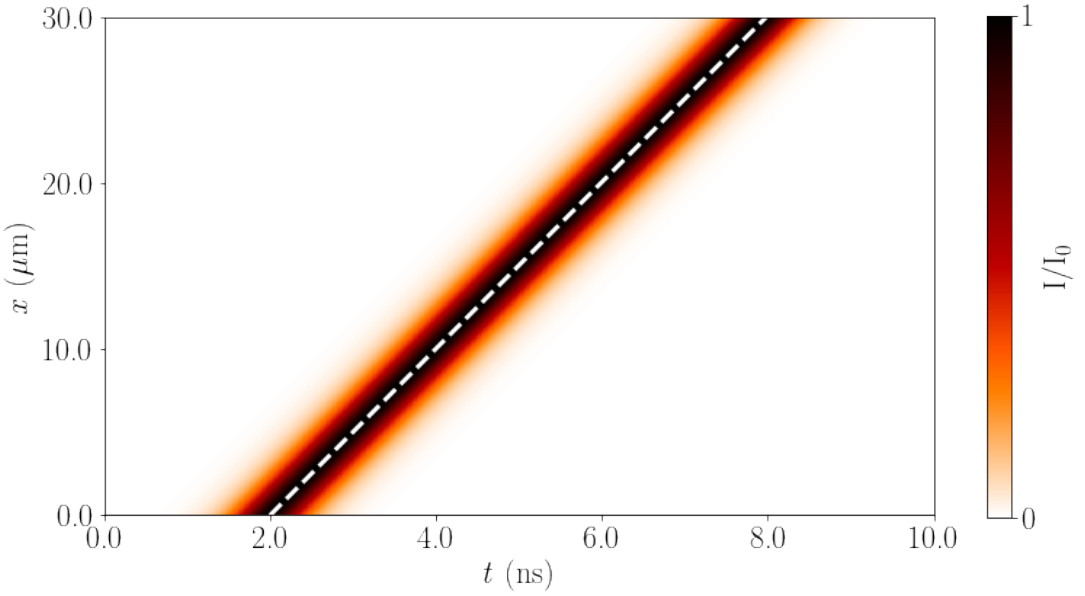

Figure 3.2: Heatmap showing the propagation of a sech-soliton through a medium of ^{85}Rb atoms at 220°C. The field is resonant with the D1 transition, we neglect the spontaneous decay mechanisms (homogeneous broadening) however we do include Doppler averaging (inhomogeneous broadening). The white dotted line shows the theoretical trajectory of the pulse.

3.2 Homogeneous Broadening

We now consider the more realistic case in which we include the spontaneous decay from the excited state to the ground state. In their 1969 paper, McHall and Hahn considered the effect of weak damping (homogeneous broadening) on the propagation of SIT pulses by treating the effect as a small perturbation [12]. They derived an expression for the variation of the total pulse energy with distance valid only in the limit that the pulse was short compared to the homogeneous broadening time (i.e. the reciprocal of the decay constant). A similar first-order perturbation analysis was conducted by Kaup on the complete solution to the Maxwell-Bloch equations for a two-level medium found by the inverse scattering transform and he found that the pulse energy would vary in the same manner as predicted by McHall and Hahn [55]. However, neither of these studies conducted any numerical simulations of SIT solitons propagating in the presence of homogeneous broadening to test these theories (probably in part due to the limited computing resources available at the time). This was done much later by Alhasan, Fiutak and Miklaszewski during the

1990s [64, 65]. In their 1992 paper, Alhasan, Fiutak and Miklaszewski found from their simulations that the pulse area of a short input pulse (i.e. much smaller than the homogeneous broadening time) with an input pulse area in the range π to 3π did indeed still stabilise to an area of 2π (as predicted by the area theorem for the no damping case) and maintained an approximately sech-squared intensity profile for a considerable distance provided the only form of homogeneous broadening was from spontaneous decay and there were no additional broadening mechanisms such as from collisions [64]. Because of the energy loss from the pulse due to homogeneous broadening, its peak intensity would decrease with distance and so the pulse width would increase so that the area remained at a constant value of 2π. However, at some distance the pulse would become too weak and the area would rapidly decrease from 2π to 0π forming a 0-π pulse. 0-π pulses are pulses with an area of zero and therefore they have electric field profiles that oscillate about zero [66]. If collisional broadening was included, the pulse area did not stabilise but it was often seen to oscillate around the 2π value. They also found that pulses with an area larger than 3π would breakup into multiple pulses as is well known to occur for the no damping case. The total pulse area was then seen to stabilise at integer multiples of π but would suddenly decrease by 2π at certain distances due to the collapse of a pulse that had become too weak. This work was then followed up by a paper in 1994 by Miklaszewski and Fiutak in which they investigated the propagation of SIT pulses for pulse widths comparable with the homogeneous broadening time and studied the collapse of the 2π to 0-π pulses in more detail [65]. They performed numerical simulations and also derived some analytic results. We will now perform our own simulations of SIT pulses propagating in the presence of homogeneous broadening and compare our results with those found by Miklaszewski and Fiutak.

Figure 3.3 shows a similar simulation to those presented in reference [65]. It shows the propagation of a pulse with an input sech-squared intensity profile through a medium in which homogeneous broadening is included. It can be seen that the field profile appears to maintain a hyperbolic secant shape for a considerable distance

but that the peak intensity decreases and the pulse width increases with distance as found by Miklaszewski and Fiutak. By 40 μm, the pulse has destabilised and the field has been entirely absorbed. Figure 3.4(a) shows the variation of the pulse area with distance. It can be seen that the area remains constant at 2π until around 33 μm, at which point it rapidly decreases to zero as was first reported by Alhasan et al. [64].

In reference [65], Miklaszewski and Fiutak derive an equation for the variation of the total energy of the field with distance. They claim that the total energy of the field, $E(x)$, varies as [65]

$$\frac{\mathrm{dE}(x)}{\mathrm{d}x} \sim -\Gamma \int_0^\infty \rho_{22}(x,t), \tag{3.2.1}$$

where Γ is the spontaneous decay rate and $\rho_{22}(x,t)$ is the excited state population. This led us to derive an expression for the variation of the pulse energy with distance in our model so as to see whether we also expect the energy to decay in the form of (3.2.1) and to explore whether this is consistent with the numerical results. I must acknowledge my supervisor, Robert Potvliege, for assistance in the following analysis.

We define the quantity, $\varepsilon(x)$, to be

$$\varepsilon(x) = \int_{-\infty}^{\infty} |\Omega|^2 \mathrm{d}t', \tag{3.2.2}$$

where Ω is the Rabi frequency of the field and t' is the shifted time defined by (2.2.67). $\varepsilon(x)$ is proportional to the total energy of the field at the distance x. Differentiating (3.2.2) with respect to x and making use of the propagation equation (and assuming that the single incident field is that of the probe field) (2.2.76) one obtains

$$\frac{\mathrm{d}\varepsilon_\mathrm{p}}{\mathrm{d}x} = \int_{-\infty}^{\infty} (i\mu_\mathrm{p}\Omega_\mathrm{p}^*\rho_{21} - i\mu_\mathrm{p}\Omega\rho_{12})\mathrm{d}t'. \tag{3.2.3}$$

Then, by integrating the optical Bloch equation for $\partial_t\rho_{22}$ (2.2.38) over all time and making the assumption that $\rho_{22} \to 0$ as $t' \to \infty$ (which must be true for a pulsed

input field) it is possible to show that

$$\frac{\mathrm{d}\varepsilon_{\mathrm{p}}}{\mathrm{d}x} = -2\Gamma\mu_{\mathrm{p}}\int_{-\infty}^{\infty}\rho_{22}\mathrm{d}t', \tag{3.2.4}$$

where Γ is the spontaneous decay constant and μ_{p} is the propagation coefficient defined by (2.2.77). This clearly has the same form as the expression found by Miklaszewski and Fiutak (3.2.1). In Figure 3.4(b) we plot ε_p as a function of distance. The solid green line shows the actual value of ε_{p} found by numerically calculating the integral in (3.2.2). The dashed blue line shows the theoretical value based on integrating ρ_{22} over all time at each distance to obtain $\mathrm{d}\varepsilon_p/\mathrm{d}x$ as given by (3.2.4) and then integrating this expression over the propagation distance to obtain the theoretical variation of ε_p with x. It can be seen from Figure 3.4 (b) that the actual and theoretical values of ε_p agree exactly.

It is interesting to explore whether it is possible to go further and calculate the integral in (3.2.4) analytically and therefore to obtain an analytical expression for $\varepsilon(x)$. If we assume that Ω_{p} and ρ_{22} have the same profiles as for the case in which there is no homogeneous broadening (though the values will still change with distance due to the absorption): i.e. $\Omega_{\mathrm{p}} = \Omega_0(x)\,\mathrm{sech}(\eta)$ and $\rho_{22} = \mathrm{sech}^2(\eta)$ where η is defined by (2.4.7), it can be shown that

$$\int_{-\infty}^{\infty}\mathrm{sech}^2(\eta)\mathrm{d}t' = 2\tau(x), \tag{3.2.5}$$

where $\tau(x) = 2/\Omega^0(x)$ and $\Omega^0(x)$ is the peak Rabi frequency at the distance x. Hence we obtain

$$\frac{\mathrm{d}\varepsilon_{\mathrm{p}}}{\mathrm{d}x} = -4\Gamma\mu_{\mathrm{p}}\tau(x). \tag{3.2.6}$$

By differentiating (3.2.2) with respect to x we find that

$$\frac{\mathrm{d}\varepsilon_{\mathrm{p}}}{\mathrm{d}x} = 2\tau(x)\Omega_0(x)\frac{\mathrm{d}\Omega_0(x)}{\mathrm{d}x}. \tag{3.2.7}$$

By equating (3.2.6) and (3.2.7) and integrating we obtain an analytical equation for

the variation of $|\Omega_0(x)|^2$ with distance

$$|\Omega_0(x)|^2 = |\Omega_0(0)|^2 - 4\Gamma\mu x, \tag{3.2.8}$$

where $\Omega_0(0)$ is the peak Rabi frequency of the pulse at $x = 0$ μm and the other symbols are defined as previously. This analytical prediction is shown by the dashed orange line in Figure 3.4(c). It can be clearly seen that it doesn't agree with the actual variation of $|\Omega_0|^2$ with distance shown by the solid green line. The reason for this is that ρ_{22} is actually not that well approximated by a sech function when homogeneous broadening is included. Figure 3.5 shows the profiles of ρ_{22} at the entrance to the medium for the cases of homogeneous broadening and no homogeneous broadening. It can be seen that, somewhat counter-intuitively, including the spontaneous decay actually results in a slower decay of ρ_{22} to zero after the pulse has passed. Indeed, the numerical integration performed to solve (3.2.4) had to be done over a much longer time range (200 ns) in order to satisfy the requirement that $\rho_{22} \to 0$ as $t' \to \infty$. However, it can be seen from Figure 3.4 that (3.2.8) does predict a linear decrease of $|\Omega_0|^2$ with distance as seen in the numerical results. The prediction can in fact be made to agree well by changing the constant of 4 in (3.2.8) to a value of 6.6. This is shown by the dash-dot blue line in Figure 3.4(c). However, the reasoning for this is not clear and would require further investigation to justify.

Finally, we investigate whether the equations that give the pulse velocity when homogeneous broadening is ignored can be extended to include homogeneous broadening. (3.1.1) gives the velocity of an ideal sech soliton when homogeneous broadening is not included. It is interesting to explore whether (3.1.1) also gives the correct instantaneous velocity for a given value of $\tau(x)$ when homogeneous broadening is included. Figure 3.6 is a heatmap of the same simulation as shown in Figure 3.3. We show the theoretical trajectory of the pulse, found by calculating the instantaneous velocity at each time using (3.1.1). It can be seen that this theoretical trajectory agrees very well with the actual trajectory taken by the pulse. Figure 3.7 shows a simulation with the same set of parameters as Figure 3.6 except inhomogeneous

broadening (Doppler averaging) is included. The theoretical trajectory of the pulse shown here is found by calculating the instantaneous velocity at each time using (3.1.2). Once again, it can be seen that the theoretical trajectory agrees very closely with the actual trajectory of the pulse observed in the numerical results. To the best of our knowledge, this is the first time it has been demonstrated that the equations giving the velocity of sech-solitons in the absence of homogeneous broadening can still be used to calculate the instantaneous velocity of a sech-soliton propagating through a medium in which homogeneous broadening is included.

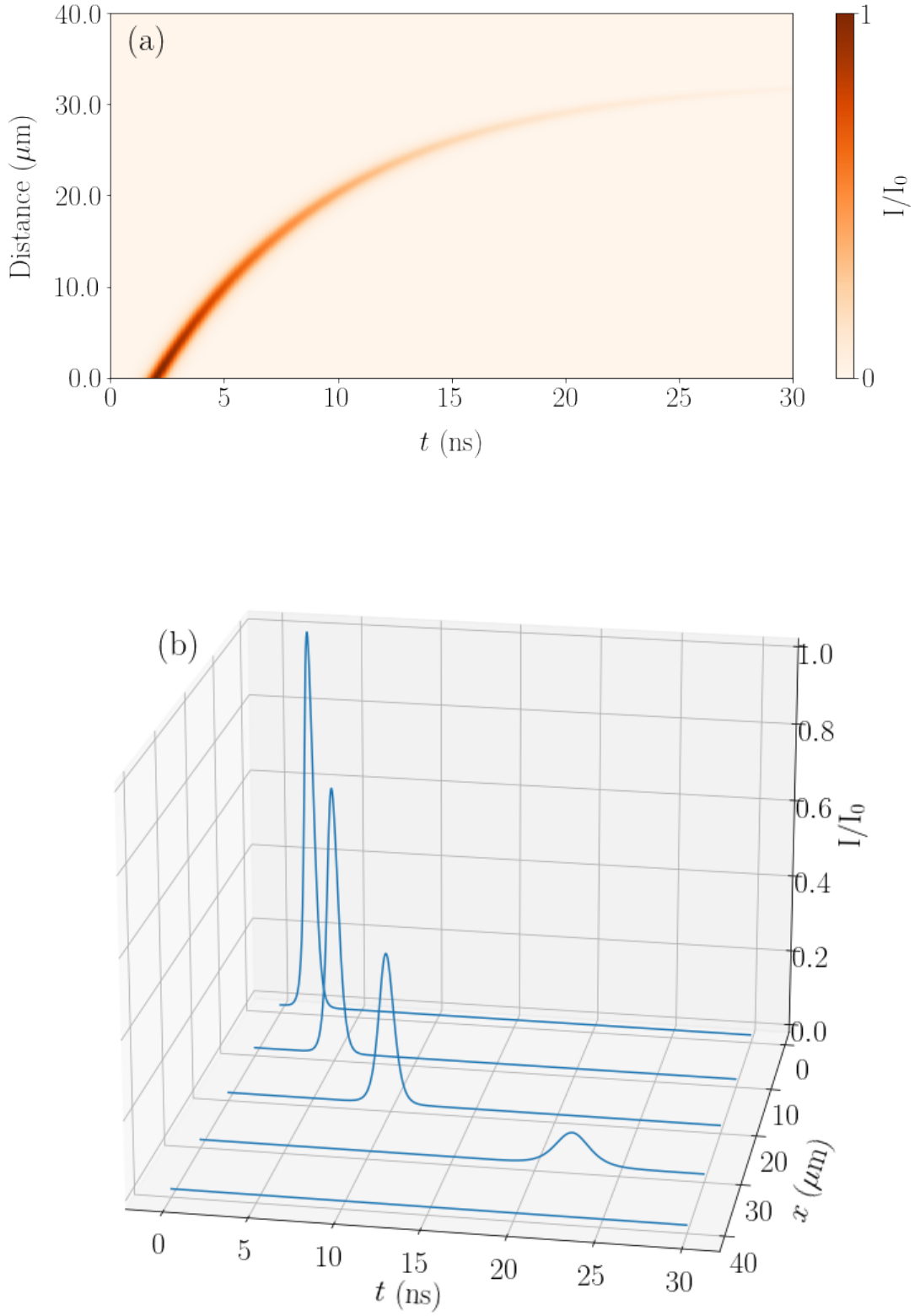

Figure 3.3: The propagation of a pulse with an input sech-squared intensity profile and an area of 2π through a medium of ^{85}Rb atoms at 220°C. The field is resonant with the D1 transition, and we include the spontaneous decay from the excited state. We do not include Doppler averaging (inhomogeneous broadening). I_0 is the input peak intensity. (a) Heatmap plot. (b) Cascade plot.

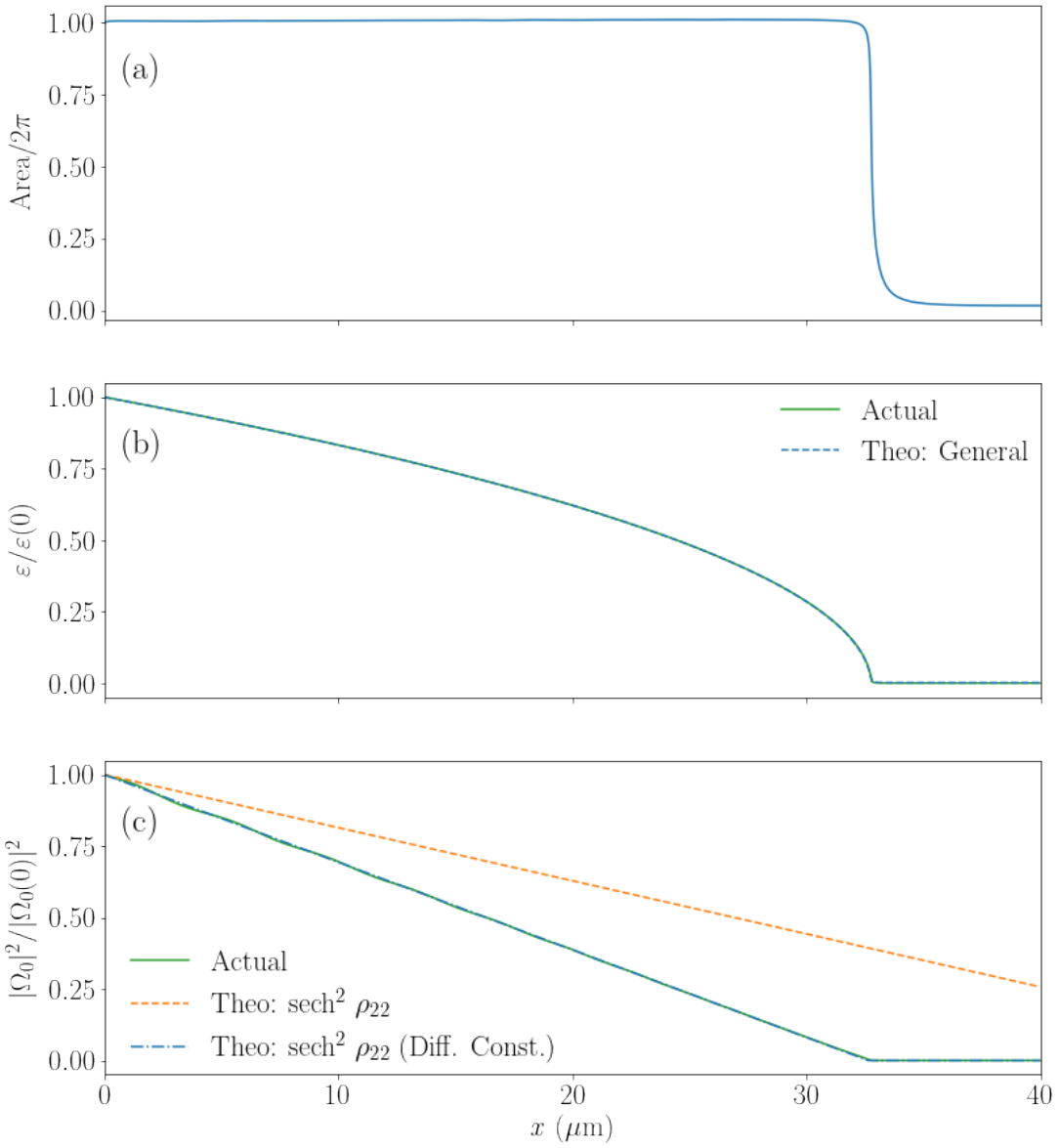

Figure 3.4: The graphs in this figure correspond to the simulation shown in Figure 3.3. (a) The variation of the pulse area with distance. (b) The variation of ε normalised to its value at $x = 0$ as a function of distance . The solid green line is the actual variation seen in the numerical results and the dashed blue line is the theoretical prediction found by numerically integrating ρ_{22} over time at each distance. (c) The variation of $|\Omega_0|^2$ normalised to its value at $x = 0$ as a function of distance. The solid green line is the actual variation seen in the numerical results and the dashed orange line is the analytic prediction with a constant factor of 4. The dash-dot blue line is the analytic prediction with the constant factor adjusted to a value of 6.6 such that the theoretical prediction matches the numerical results.

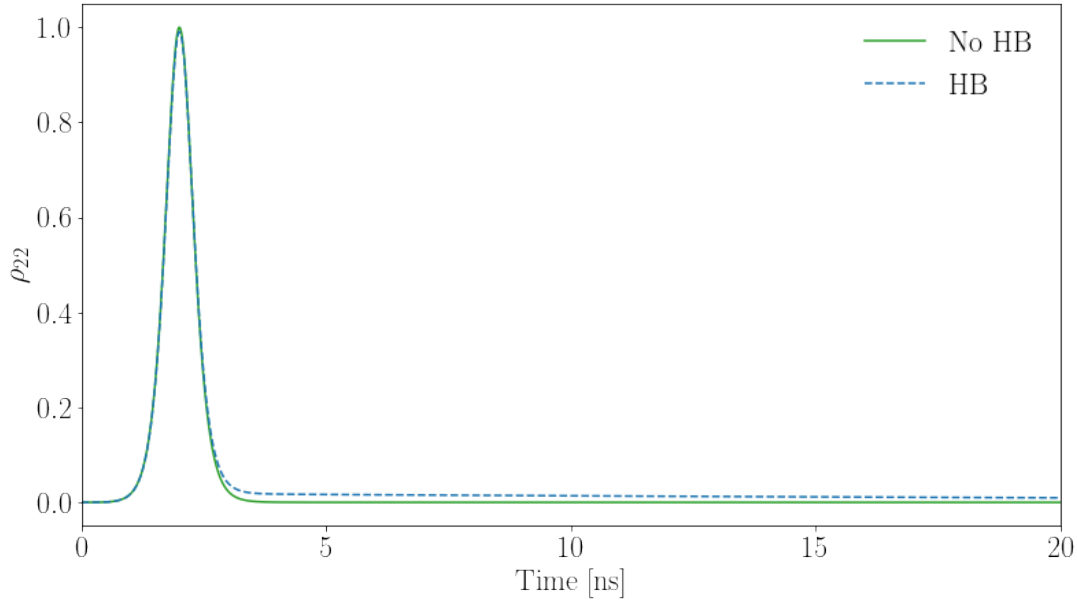

Figure 3.5: ρ_{22} as a function of time at a distance of $x = 0$ μm for the case of no homogeneous broadening (green line) and for the case of homogeneous broadening (dashed blue line).

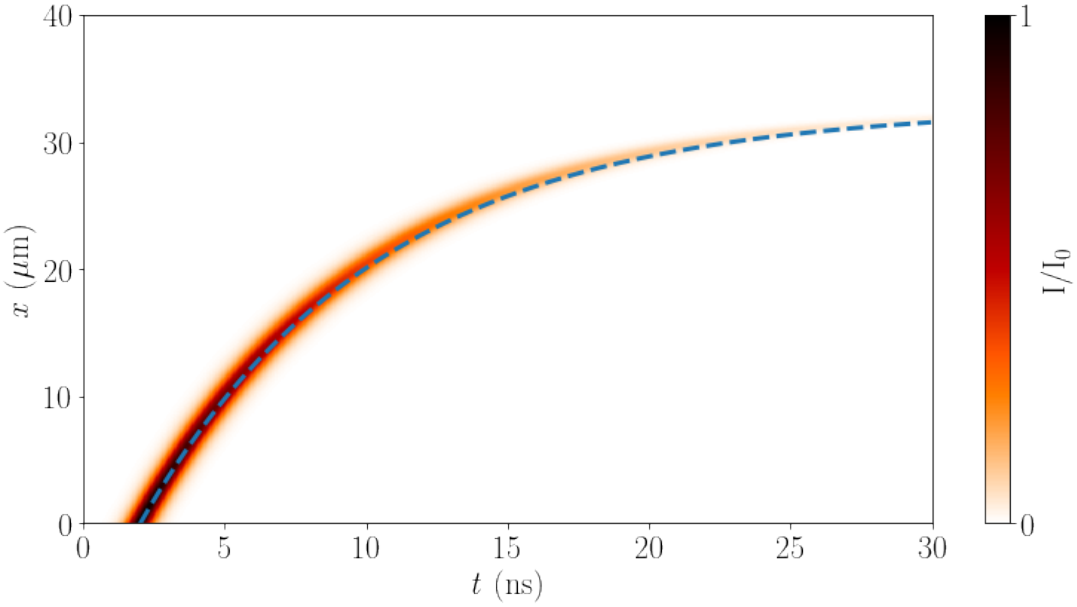

Figure 3.6: Heatmap showing the propagation of a sech-soliton through a medium of ^{85}Rb atoms at 220°C. The field is resonant with the D1 transition, and we include the spontaneous decay from the excited state. We do not include Doppler averaging (inhomogeneous broadening). The blue dotted line shows the theoretical trajectory of the pulse found by calculating the instantaneous velocity of the pulse at each time by using the equation for the velocity of an ideal sech-soliton propagating through a medium in which there is no homogeneous broadening (3.1.1).

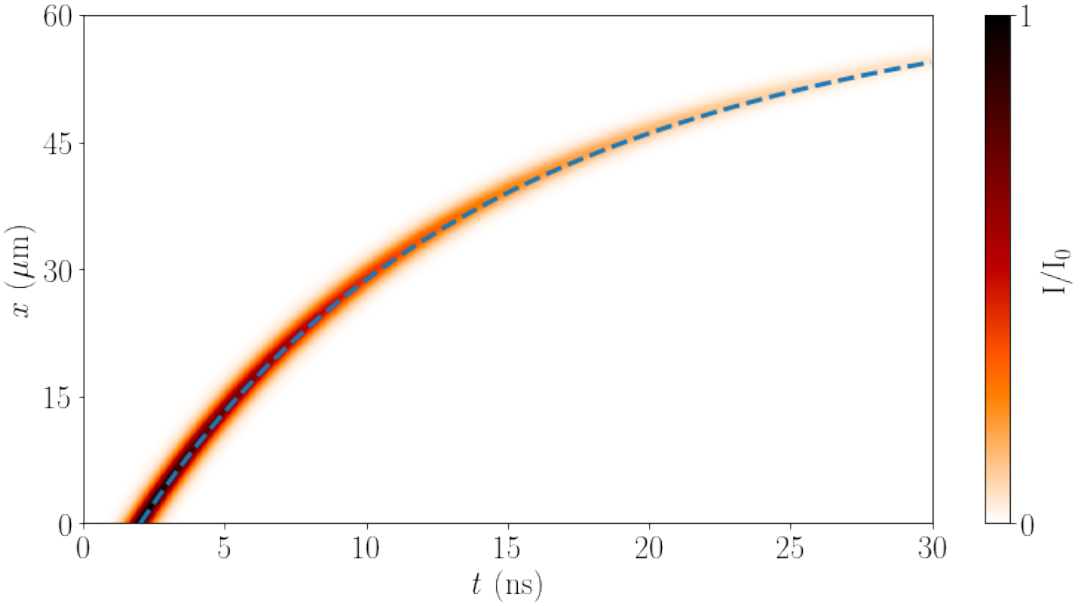

Figure 3.7: Heatmap showing the propagation of a sech-soliton through a medium of ^{85}Rb atoms at 220°C. The field is resonant with the D1 transition, and we include the spontaneous decay from the excited state. Doppler averaging (inhomogeneous broadening) is also included. The blue dotted line shows the theoretical trajectory of the pulse found by calculating the instantaneous velocity of the pulse at each time by using the equation for the velocity of an ideal sech-soliton propagating through an inhomogeneously broadened medium in which there is no homogeneous broadening (3.1.2).

3.3 Summary

In this chapter, we explored the propagation of SIT solitons through a medium of two-level resonators. We used numerical simulations to investigate the dynamics of the soliton propagation in the presence or absence of different broadening mechanisms and compared our results to previous numerical studies as well as to analytical predictions. For the case in which there is no homogeneous broadening, the physics is well known and our simulations were in agreement with the established theory. For the case in which homogeneous broadening is included, we found that the total energy of the field decayed in a manner consistent with the predictions of Miklaszewski and Fiutak, though it was not possible to extend these into a completely analytical model. Most notably, it was found that the equations that describe the velocity of sech-solitons in the absence of homogeneous broadening can still be used to calculate the instantaneous velocity of the pulses when homogeneous broadening is included.

Chapter 4

One-Field Optical Transients

Having looked at the propagation of sech-pulses, we will now investigate a different type of light field propagating through a medium of two-level resonators: that of a continuous wave (CW) input. CW fields are frequently used in vapour cell experiments. They may at first seem to be an uninteresting case since a CW field will quickly reach a steady state with a two-level system due to the balancing out of the effects of optical pumping from the ground to the excited state and spontaneous decay from the excited to the ground state. However, during the time that the field is being turned on and shortly after, the field and atoms will be in a region of transience and interesting dynamics may occur. We will study these optical transients in this chapter.

4.1 No Homogeneous Broadening

Before investigating the transient effects that would occur in any real atomic system with spontaneous decay, it is first useful to explore what the solutions to the Maxwell-Bloch equations for CW input fields are when homogeneous broadening is not included. This will help us to better understand the effects that occur when homogeneous broadening is included and there is also substantial previous literature on this case that we can compare our results to.

The propagation of a CW field resonant with a two-level medium without homogeneous broadening but including inhomogeneous broadening was first analysed by Crisp in 1972 [28]. He performed a numerical analysis that showed that a step-function input pulse (i.e. a pulse that was turned on instantaneously to a constant intensity at some time) got reshaped into a train of pulses as the field progressed further into the medium. Crisp had shown previously that the Jacobi dnoidal and cnoidal functions satisfy the Maxwell-Bloch equations for the propagation of a resonant light field through an inhomogeneously broadened medium of two-level resonators [50]. He then compared the train of pulses formed from the CW field with the dnoidal and cnoidal wave solutions and found that the pulse trains that arose from the CW input could be described quite accurately by a dnoidal wave of the form of (2.4.5) with a parameter of $k = 0.8$. He found that regardless of the input intensity, the dnoidal wave that most closely approximated the pulse train had the parameter of $k = 0.8$ and therefore suggested that this was the asymptotic solution (i.e. that a CW field input into a two-level medium would always reshape into a pulse train described by a dnoidal function with a parameter $k = 0.8$). The problem was later revisited by Horovitz and Rosenberg in 1982, although they did not include inhomogeneous broadening in their study as Crisp had done. They found that, in fact, there was no single asymptotic solution of the form suggested by Crisp [29]. By investigating numerically the propagation of pulses over longer times and further distances than considered by Crisp, they found that the pulses became narrower and gained a larger peak amplitude the further they propagated. They found that at a given distance and over a short region of time the pulse train could indeed be approximated by a dnoidal function with a parameter k but that the value of k needed to approximate the pulse train got closer to 1 as distance increased. However this could not be described by a single dnoidal function of the form of (2.4.5) with a k parameter that tends to 1 as distance goes to infinity since the average time separation of the pulses in the pulse trains seen in their simulations appeared constant at all distances and the pulses of a dnoidal wave get further apart as k increases as was explained in

Chapter 2. Horowitz and Rosenberg explained the effect by introducing an asymptotic area theorem that restricts the time average of the field to be equal to that of the input field. They defined the CW pulse area to be

$$\theta(x) = \int_{-\infty}^{t} \Omega(x, t') \, \mathrm{d}t', \tag{4.1.1}$$

where θ is the area, t is the time at which the area is being calculated and $\Omega(x, t)$ is the Rabi frequency [29]. This extends the pulse area theorem of McHall and Hahn to CW inputs. We will now conduct our own study of these effects. We will compare our results to the findings of Crisp and Horovitz and Rosenberg and look at what happens at further distances and longer times than considered in these studies.

We now present the results of simulations very similar to those performed by Crisp and Horovitz and Rosenberg. However, we choose to study the specific system of a field resonant with the D2 transition in ^{85}Rb since, as previously explained, we are framing our investigation in the context of vapour cell experiments. We consider the D2 transition rather than the D1 transition as this seemed more logical considering we will study a two-field case in the next chapter in which the field resonant with the D2 transition is strong. We also decided to model a vapour at a temperature of 80°C rather than the 220°C temperature considered in the work on optical simultons [26] as doing so lowers the atomic density and allows for propagation lengths on the order of millimetres rather than micrometers which may be more amenable to experiment. However, these choices do not affect the physics we will consider here in any important way.

We first consider the same situation as considered by Horovitz and Rosenberg: a CW input field is switched on instantaneously at $t = 0$ ns and propagates through a medium in which there is no inhomogeneous broadening. This is shown in Figure 4.1. We show the modulus of the electric field amplitude (normalised to the input) rather than the intensity as this makes some of the features clearer to see. The modulus of

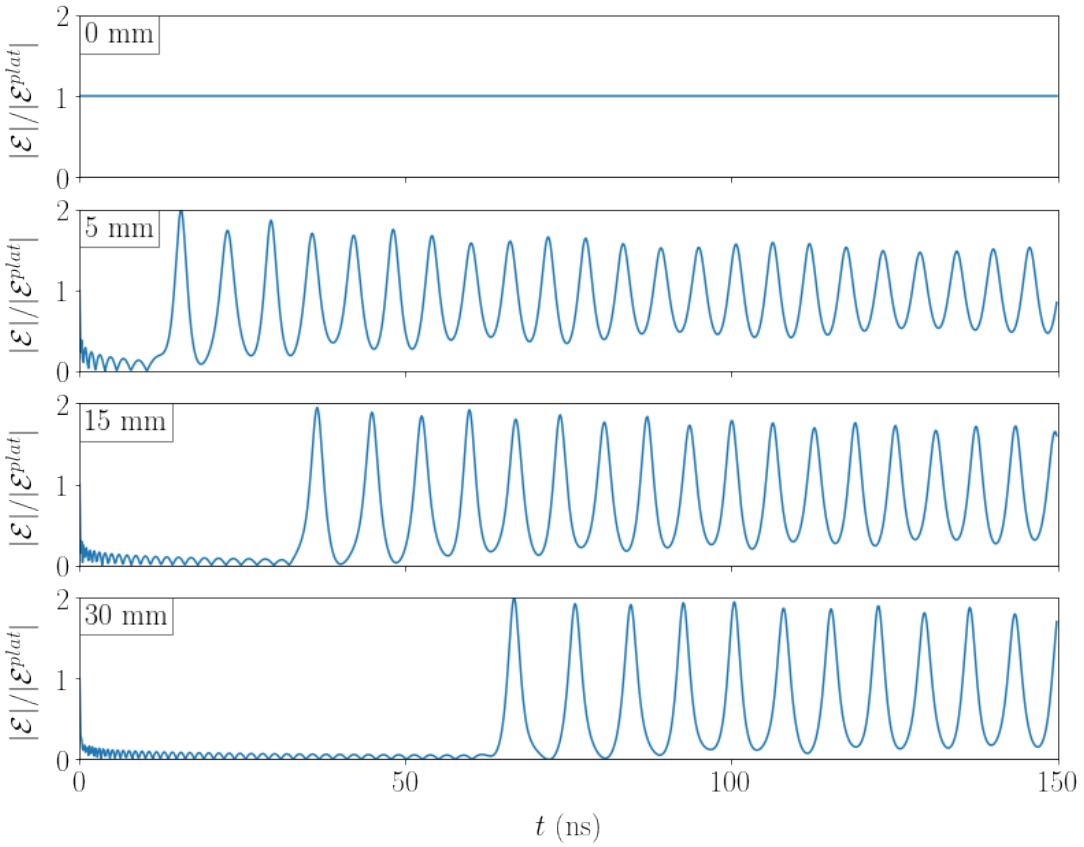

Figure 4.1: Propagation of a CW field which is instantaneously turned on at $t = 0$ ns. $I^{plat} = 5$ W/cm^2 and $|\mathcal{E}|$ is related to I as shown in (4.1.2). Both homogeneous and inhomogeneous broadening are neglected.

the electric field amplitude $|\mathcal{E}|$ is related to the intensity I by

$$|\mathcal{E}| = \sqrt{\frac{2I}{c\epsilon_0}}, \tag{4.1.2}$$

where c is the speed of light and ϵ_0 is the permittivity of free space. It can be seen that the field breaks up into a train of pulses as it travels into the medium as was found by both of the previous studies. It can also be seen that there is an initial spike at $t = 0$ ns. This is known as an optical precursor and represents a pulse propagating at the speed of light [31]. This happens as a result of the instantaneous turn-on of the field since light is initially input into the medium so fast that there is effectively no absorption [29]. There are then small oscillations of $|\mathcal{E}|/|\mathcal{E}^{plat}|$ which correspond to oscillations of the field about zero. These are the 0-π pulses we discussed in the previous chapter [66]. In similarity to the theory of SIT, these 0-π pulses result from the fact that the pulse area of the input field is below π until a certain time (which

will vary depending on the intensity) and so the field in this region will tend towards a state with an area of zero as it propagates further into the medium. At later times it can be seen that a train of pulses have been formed. The troughs of the pulses do not go to zero and the heights of the peaks and troughs are varied as was seen in the results of Crisp and Horovitz [28, 29]. It can also be seen that the pulses become sharper and narrower as they travel further in agreement with the behaviour found by Horovitz and Rosenberg [29].

Both Crisp and Horovitz reported that the mean time separation of the pulses (i.e. the time difference between successive peaks) remained constant. However, it appears that the average time separation of the pulses in Figure 4.1 increases with distance. Indeed, it is found that the mean time separation of the pulses at 5 mm is 5.9 ns, at 15 mm it is 6.7 ns and at 30 mm it is 7.7 ns. To investigate this further we ran a simulation with the same input field as in Figure 4.1 over a longer time range of 300 ns and a distance of 120 mm. This is shown in Figure 4.2. It is immediately apparent from this figure that the time separation between the pulses is not constant. This calls in to question the asymptotic area theorem of Horovitz and Rosenberg. In Figure 4.3, we plot the pulse area (minus its value at 250 ns) over 2π as a function of time for the field profiles shown in Figure 4.2. The pulse area is given by (4.1.1). It can be seen that the number of complete pulses that have formed prior to a given time is equal to the multiple of 2π that the area was last at. For example, at 40 mm and 300 ns the area (relative to its value at 250 ns) is just below $12 \times 2\pi$ and so we would expect there to be 11 complete pulses between 250 ns and 300 ns. It can be seen from Figure 4.2 that this is indeed the case (the 12th pulse is in the process of forming since the area is approaching $12\times2\pi$). It therefore seems that this is the key feature: the pulse area integrated over each pulse (i.e. between the minima either side of each pulse) is always equal to 2π irrespective of the distance into the medium. This does not restrict the time separation of the pulses to be constant as concluded by Horovitz and Rosenberg. It seems that they arrived at that conclusion because they did not go far enough into the medium (quite possibly due to the limitations

of the computing resources available at the time). Unfortunately, there is not time within the present study to look into this in more depth. However, it is certainly an intriguing result and warrants further investigation in the future.

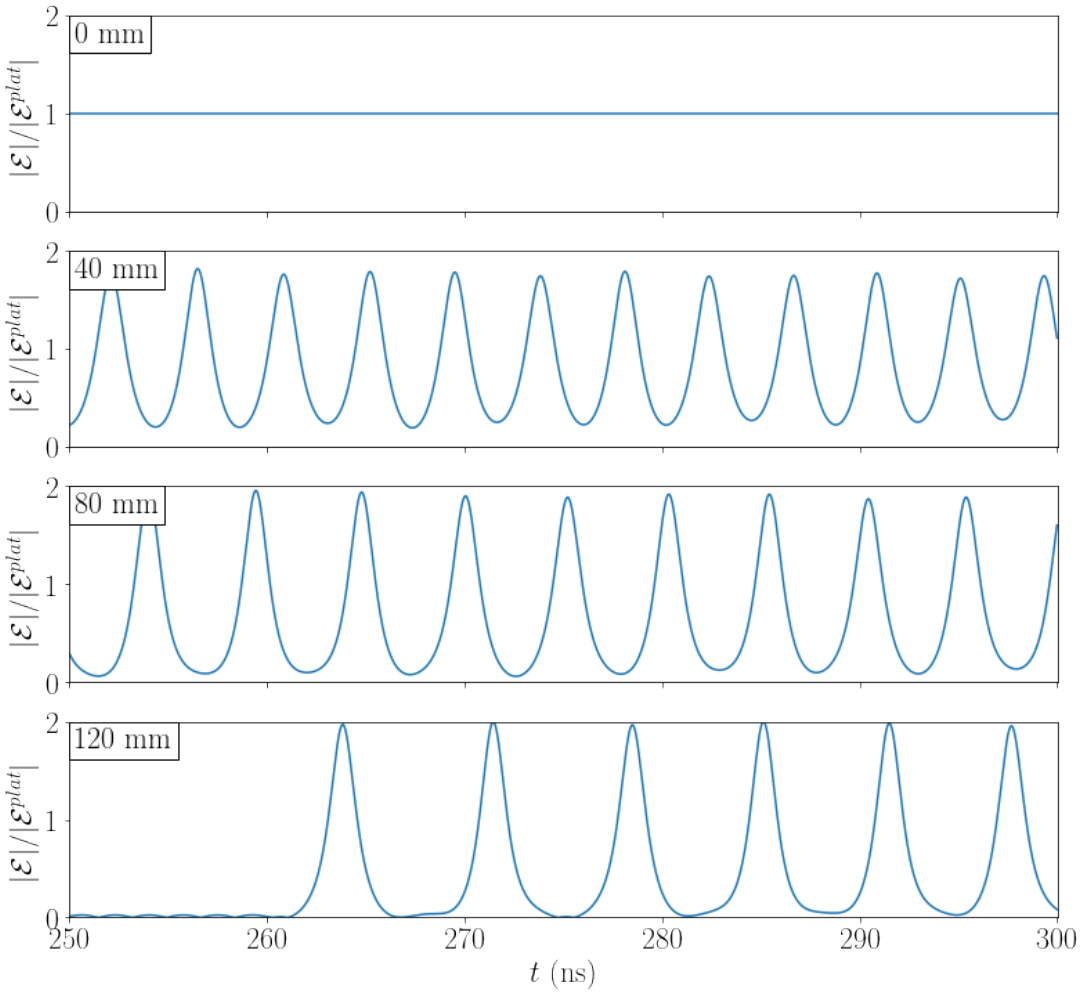

Figure 4.2: Propagation of a CW field which is instantaneously turned on at $t = 0$ ns. $I^{plat} = 5$ W/cm^2 and $|\mathcal{E}|$ is related to I as shown in (4.1.2). Both homogeneous and inhomogeneous broadening are neglected.

In a real experiment, an input CW field would take a non-zero amount of time to reach a constant intensity. A typical CW field, switched on with a Pockels cell, may take ∼2 ns to reach a constant intensity. Figure 4.4 shows a similar set of results to those in Figure 4.1 except the input field is turned on smoothly from 0 ns to 2 ns, plateauing out at a constant intensity of $I^{plat} = 5$ W/cm^2. It can be seen that the field evolves in the same way as for the case of instantaneous turn-on except the optical precursor spike at $t = 0$ is no longer present, as was predicted by Horovitz

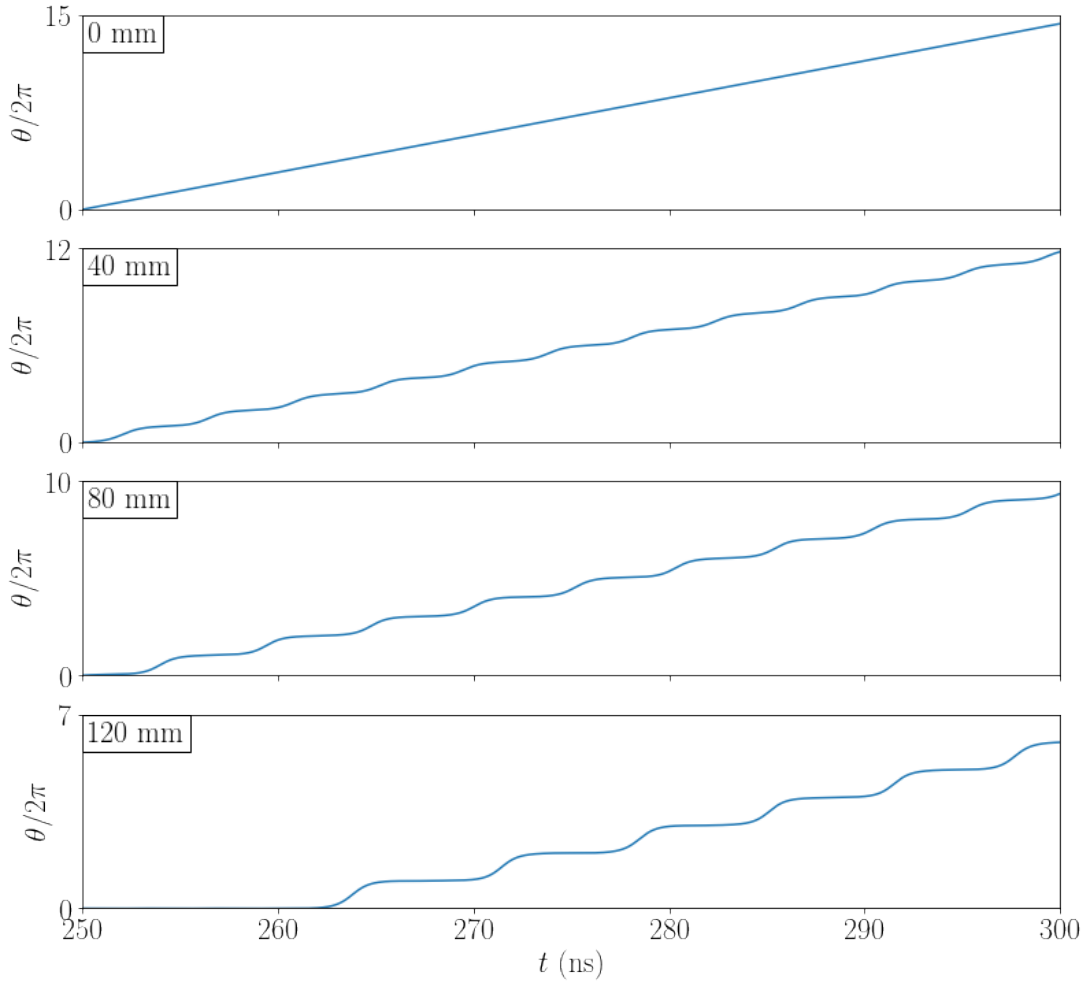

Figure 4.3: The CW pulse area (minus its value at 250 ns) as defined by (4.1.1) as a function of time corresponding to the field profiles shown in Figure 4.2.

and Rosenberg.

Inhomogeneous broadening was included in Crisp's analysis, but not in the work of Horovitz and Rosenberg. They claim that including it was not likely to have an effect on their results, except in terms of re-normalising parameters [29]. We will check that claim now. Figure 4.5 shows a set of results with the same input parameters as in Figure 4.4 except inhomogeneous broadening is included in the simulation. It can be seen that a train of pulses still form in the presence of inhomogeneous broadening but the 0-π pulses are no longer present. This happens because the 0-π pulses produced by different velocity classes do not oscillate in phase with each other and, since the field oscillates about zero, this results in the field having an average value of zero when averaged over all velocity classes. It can also be seen that the group

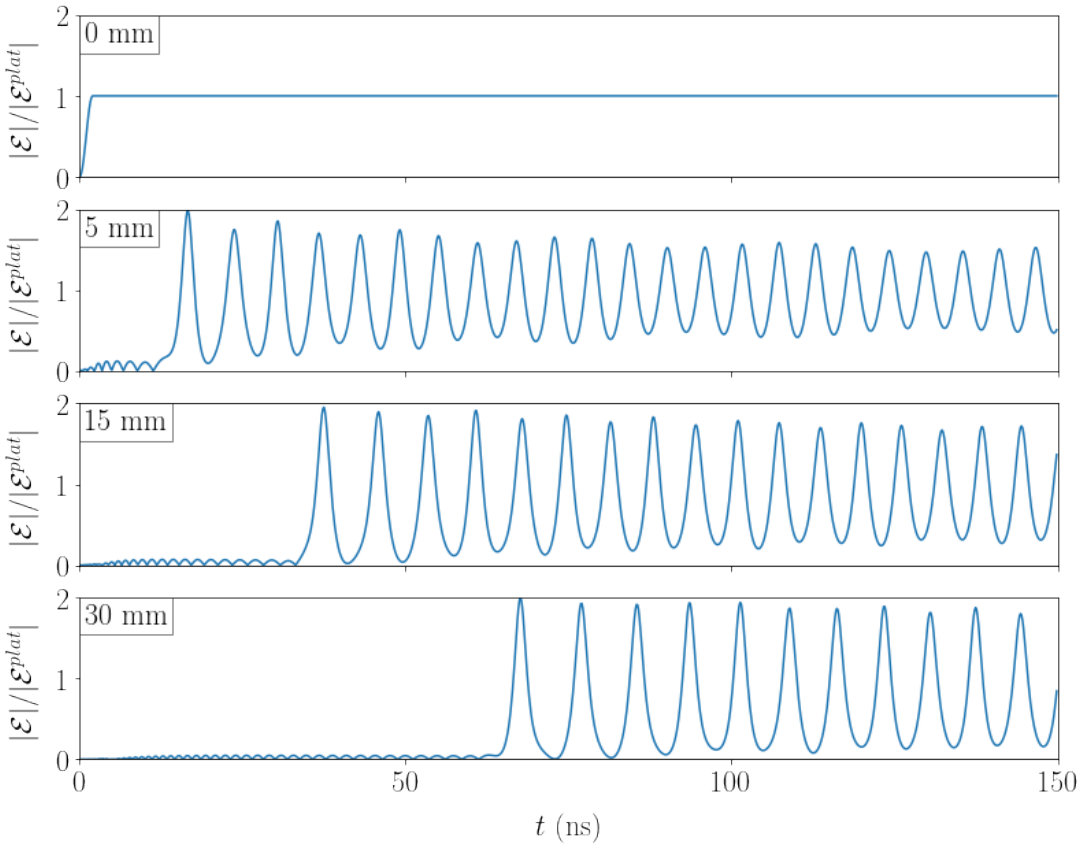

Figure 4.4: Propagation of a CW field which is turned on smoothly between $t = 0$ ns and $t = 2$ ns. $I^{plat} = 5$ W/cm^2 and $|\mathcal{E}|$ is related to I as shown in (4.1.2). Both homogeneous and inhomogeneous broadening are neglected.

velocity of the pulses is faster when inhomogeneous broadening is included since the peaks at a given distance occur earlier than for the case without inhomogeneous broadening. This is due to the fact that most of the light is de-tuned from resonance when inhomogeneous broadening is included due to the Doppler shifts which leads to a higher group velocity as given by (2.4.10).

We now compare the pulse trains formed from the CW field with the dnoidal wave solutions of the inhomogeneously broadened Maxwell-Bloch equations found by Crisp [50]. Figure 4.6(a) shows a heatmap plot of the same simulation as shown in Figure 4.5. Parts (b) to (d) of Figure 4.6 show the normalised intensity of the field at various distances along with the best fitting dnoidal wave. The Rabi frequency of the dnoidal wave is defined by (2.4.5) but we will write it again here for ease:

$$\Omega(x,t) = \Omega_0(x)\mathrm{dn}(\eta,k), \tag{4.1.3}$$

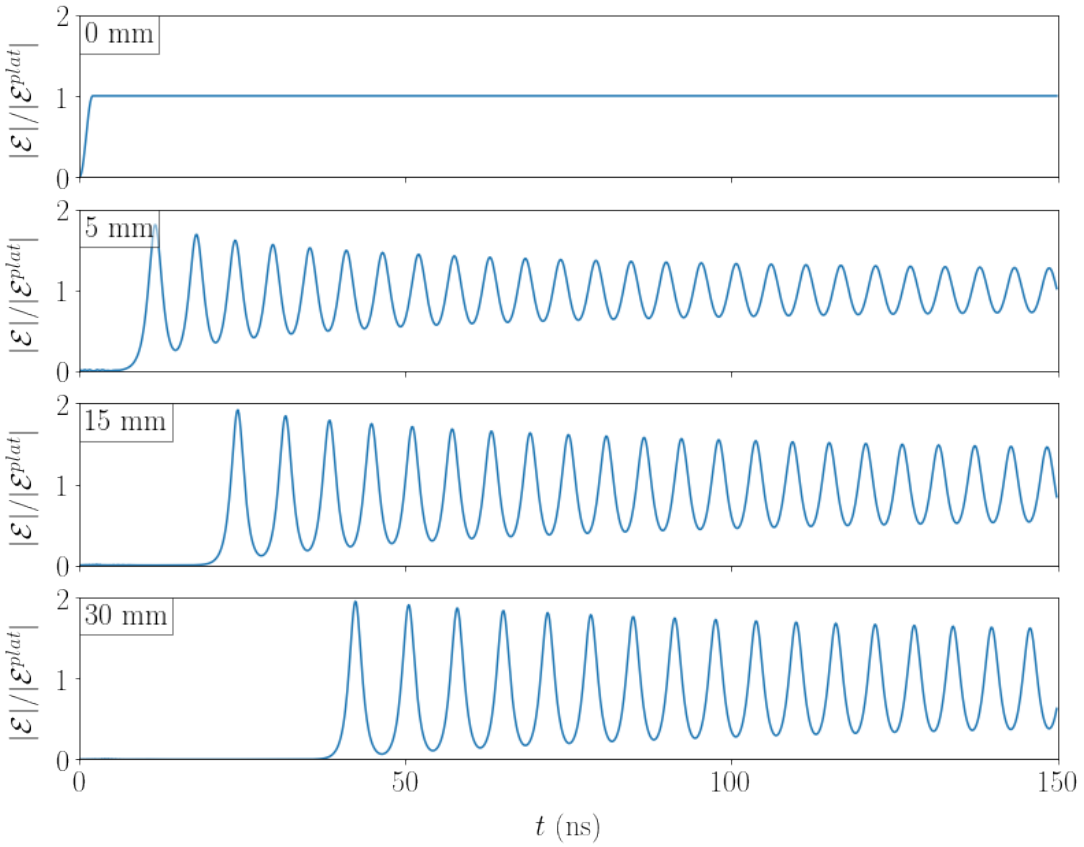

Figure 4.5: Propagation of a CW field which is turned on smoothly between $t = 0$ ns and $t = 2$ ns. $I^{plat} = 5$ W/cm^2 and $|\mathcal{E}|$ is related to I as shown in (4.1.2). Homogeneous broadening is neglected but inhomogeneous broadening is included.

where $\Omega_0(x)$ is the peak Rabi frequency of the wave at distance x, k is a parameter between 0 and 1 and η is given by

$$\eta = (t - x/v)/\tau \ . \tag{4.1.4}$$

v is the velocity given by (2.4.10) and τ is defined as

$$\tau(x) = \frac{2}{\Omega_0(x)}. \tag{4.1.5}$$

It can be seen that the dnoidal wave is a good approximation to the field within a small time range, but that the parameter k of the best fitting function increases with distance as seen by Crisp and Horovitz. The dnoidal wave is only a good approximation over a small time range since the heights of the peaks and troughs of the field change with time and so the amplitude of the best fitting dnoidal function must vary with time. Indeed, it appears that the pulse train is evolving into a train

of sech pulses as it moves deeper into the medium. This is similar to what was observed by Horovitz and Rosenberg. However, without their restriction on the time separation of the field, it seems that the pulses would become infinitely separated sech solitons as $x \to \infty$. This is an interesting possibility, but a further investigation over a greater distance (and possibility some kind of analytical study) would be required to confirm it. The dashed-blue line shows the theoretical prediction for the trajectory of the dnoidal function that most closely matches the field between $t = 120$ ns and $t = 180$ ns at $x = 25$ mm (i.e. the function shown in Figure 4.6(b)). The trajectory is calculated by using the velocity obtained from 2.4.10. It can be seen that in the region close to $x = 25$ mm, the theoretical trajectory agrees well with the actual trajectory taken by the pulses. However, the k parameter varies with distance and so the theoretical trajectory of the pulses based of the k parameter at $x = 25$ mm is clearly not valid for all distances.

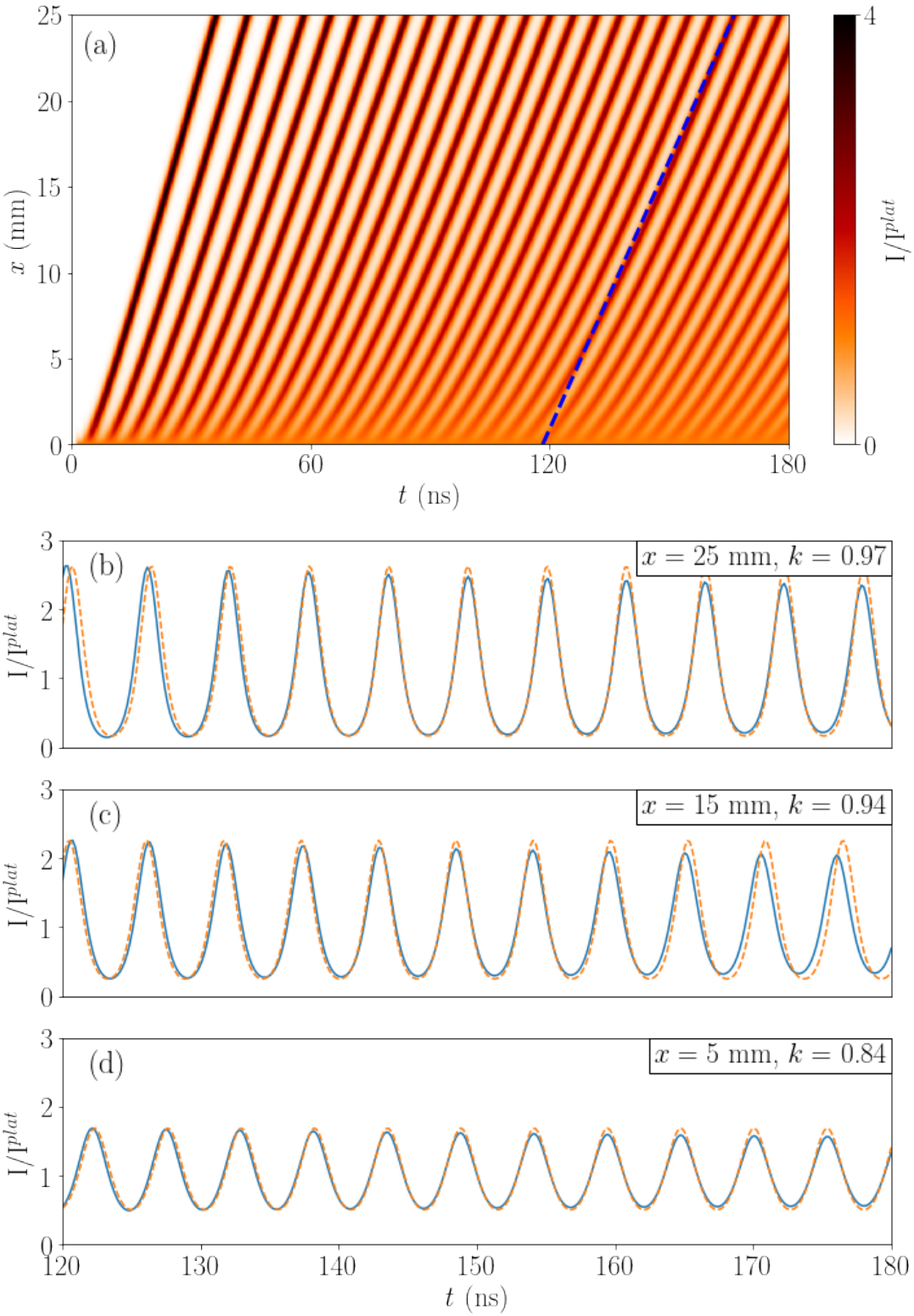

Figure 4.6: (a) Heatmap of a field with $I^{plat} = 5$ W/cm^2, turned on smoothly between $t = 0$ ns and $t = 2$ ns. The dashed-blue line shows the theoretical velocity calculated for the dnoidal wave that most closely matches the field between $t = 120$ ns and $t = 180$ ns at $x = 25$ mm. (b) The normalised intensity between $t = 120$ ns and $t = 180$ ns at $x = 25$ mm (solid blue line) plotted along with the best-fitting dnoidal function (dashed orange line with the parameter k shown on the figure). (c) The same as (b) but at $x = 15$ mm. (d) The same as (b) but at $x = 5$ mm.

4.2 Homogeneous Broadening

We now investigate the much more realistic situation in which a CW input field propagates through a two-level medium in which there is spontaneous decay from the excited state to the ground state (homogeneous broadening). It is well known that the Rabi oscillations that result when a CW field interacts with a two-level system are damped due to spontaneous decay [38]. This causes a two-level system driven by a CW field to reach a steady state (i.e the density matrix and field become constant in time). However, it takes a certain amount of time for such a system to reach the steady state. Before the steady state is reached, a dynamics would occur that is surely similar to the situation we considered in the previous subsection (i.e a breakup of the CW field into a train of pulses as it travels further into the medium). There is little previous research that has focused on this issue. Indeed, in the paper by Horovitz and Rosenberg [29] on the propagation of CW fields in the absence of homogeneous broadening, they simply state that the effect of homogeneous broadening on their results is unclear and that further study is required to address this. A study was conducted by Macke and Segard [31] in 2010 in which they did study the propagation of a CW field through a two-level medium of homogeneously broadened resonators. They presented graphs which showed that transient pulse trains did indeed form from the CW field as it propagated into the medium before the system reached a steady state. However, the focus of their paper was on the optical precursors that occur ahead of the main field (i.e the 0-π pulses that we discussed in the previous section) and they say little about the transient pulse trains that form from the main field. We will therefore conduct our own investigation, aiming to elucidate and clarify the work that has been done previously.

We again consider fields resonant with the D2 transition in ^{85}Rb and set the temperature of the vapour to 80°C. Figure 4.7 shows the propagation of fields with input plateau intensities of $I^{plat} = 5$ W/cm^2 and $I^{plat} = 15$ W/cm^2 which are both turned on smoothly between $t = 0$ ns and $t = 2$ ns. It can be seen that there is a breakup

of the fields into trains of pulses at short times but that the contrast (difference in intensity between maxima and minima) decreases as time progresses until the fields reach a steady state with constant intensity. This is due to the spontaneous decay from the upper state to the lower state. More insight can be found by looking at the variation of the populations and coherences shown in Figure 4.8. It can be seen that the decay term dampens the oscillation in the populations until a steady state is reached when ρ_{11}, ρ_{33} and the imaginary part of the ρ_{13} coherence term are constant. Our results show the same features as found in the simulations of Macke and Segard [31]: i.e. a CW field breaks up into a train of pulses and the oscillations are damped until a steady state is reached after a sufficient time. We will now explore what governs the absorption distance (i.e. the distance the field travels into the medium before it is absorbed) and compare the situation to the case of an SIT soliton propagating in the presence of homogeneous broadening that we examined in Chapter 3.

The variation of the intensity with distance in the steady state region obeys the equation [34]

$$\frac{\mathrm{d}I(\Delta)}{\mathrm{d}x} = -\kappa(\Delta, I)I(\Delta), \tag{4.2.1}$$

where I is the intensity of field (in the steady state region), x is the distance into the medium, κ is the (intensity dependent) absorption coefficient and Δ is the detuning of the field defined by $\Delta = \omega - \omega_0$ where ω is the frequency of the light and ω_0 is the resonance frequency. In the simulations considered here the input light has a frequency that is exactly resonant with the transition (i.e. $\omega = \omega_0$). However, when inhomogeneous broadening is included, different frequencies of light are seen by different atoms due to the Doppler effect and Δ becomes a function of the atomic velocity u_x given by

$$\Delta(u_x) = -\omega_0 u_x/c. \tag{4.2.2}$$

This means that (4.2.1) must be solved separately for each velocity class and an average must be found by weighting the sum of these solutions with the Maxwell-

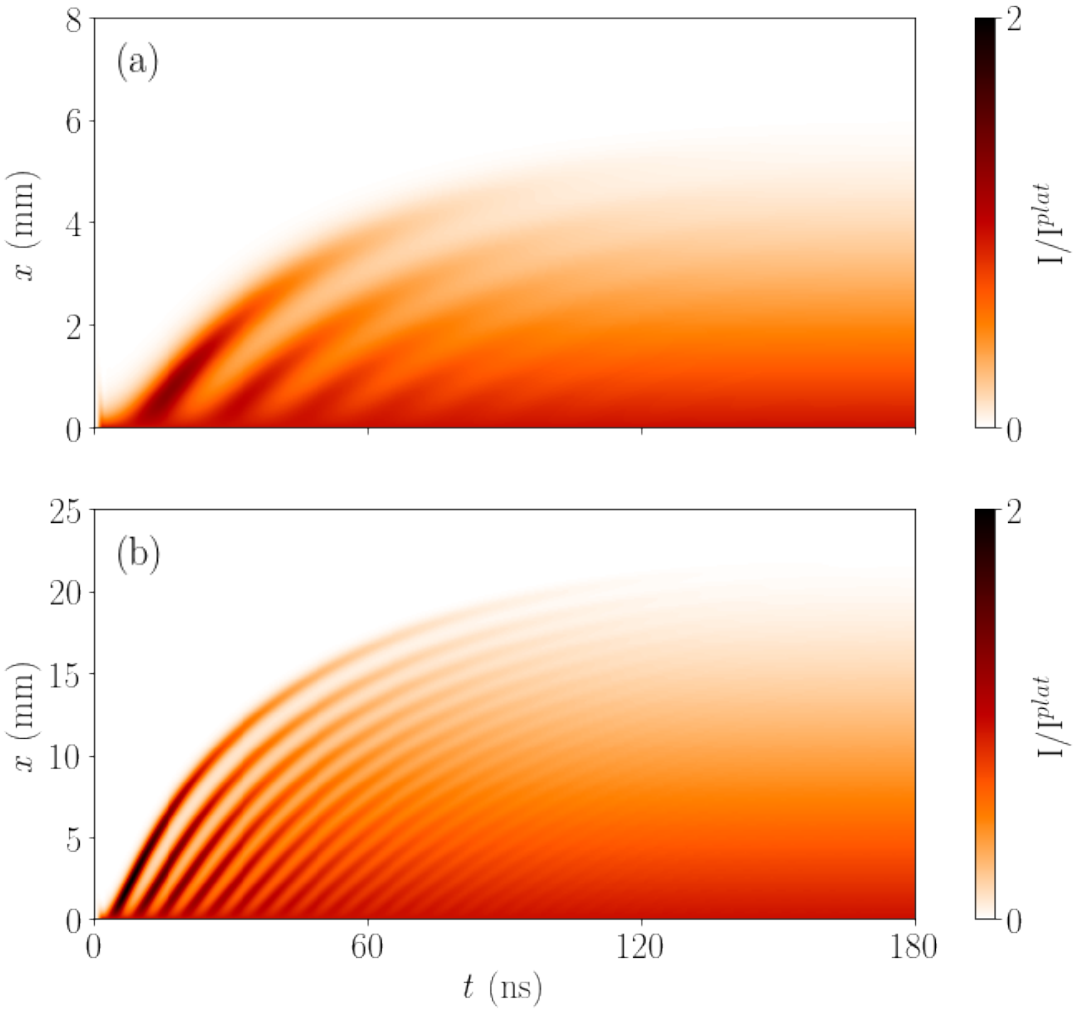

Figure 4.7: (a) Heatmap of a field with $I^{plat} = 50\text{mW/cm}^2$. (b) Heatmap of a field with $I^{plat} = 5\text{W/cm}^2$. Both fields are turned on smoothly between $t = 0$ ns and $t = 2$ ns and the simulations include homogeneous broadening and inhomogeneous broadening.

Boltzmann distribution function defined by (2.2.16). To make a simpler comparison, we will compare (4.2.1) to the numerical results for a case in which inhomogeneous broadening is neglected. In this case, κ is given by [34]

$$\kappa(0, I) = -\frac{\mathcal{N}\sigma(0)}{1 + I/I_{\text{sat}}(0)}, \tag{4.2.3}$$

where $\mathcal{N}$ is the atom density, $\sigma(0)$ is the (on-resonance) absorption cross-section, I is the intensity and $I_{\text{sat}}(0)$ is the (on-resonance) saturation intensity. For a two-level atom, and for linearly polarised light propagating along one axis, $\sigma(0)$ is given by [34]

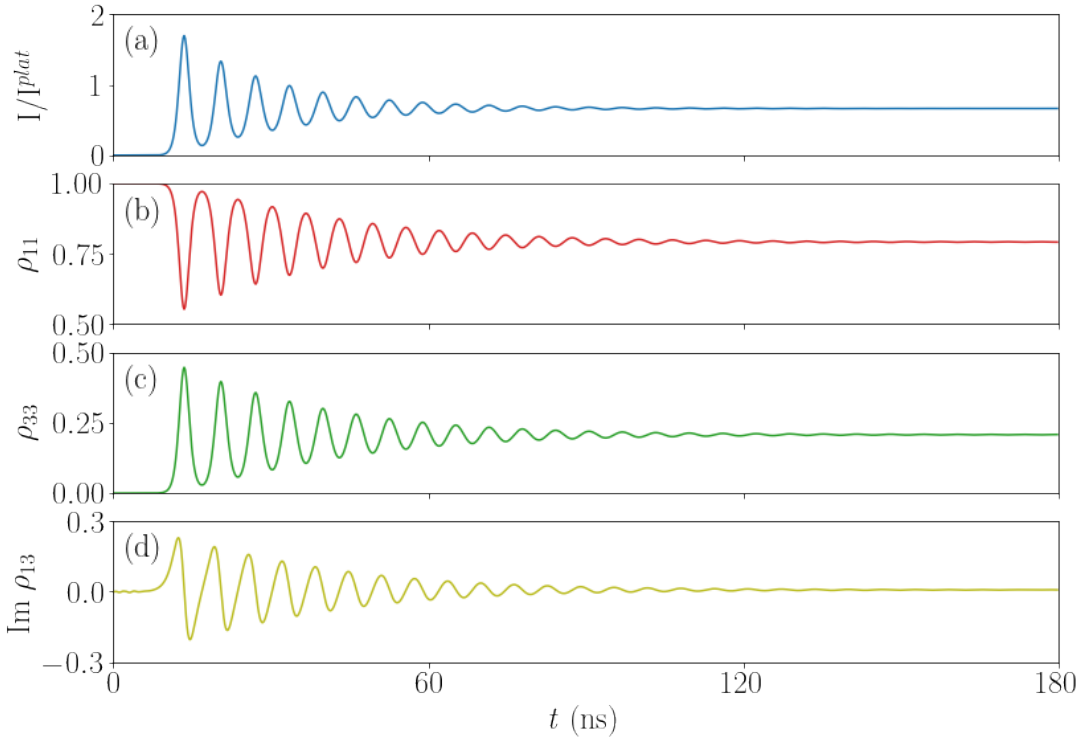

Figure 4.8: The field, populations and coherence's at 5 μm into the medium for an input field with $I^{plat} = 5$ W/cm^2. Both homogeneous broadening and inhomogeneous broadening are included. (a) The intensity normalised to the plateau intensity. (b) the ground state population ρ_{11}. (c) the excited state population ρ_{33}. (d) the imaginary part of the ρ_{13} coherence.

$$\sigma(0) = \frac{\lambda_0^2}{\pi}, \tag{4.2.4}$$

where λ_0 is the resonance wavelength ($\lambda_0 = 2\pi c/\omega_0$). $I_{\text{sat}}(0)$ is given by [34]

$$I_{\text{sat}}(0) = \frac{\pi h c \Gamma}{\lambda_0^3}, \tag{4.2.5}$$

where Γ is the spontaneous decay rate from the excited state to the ground state and the other symbols are defined as previously. Substituting (4.2.3), (4.2.4) and (4.2.5) into (4.2.1) we obtain

$$\frac{\mathrm{d}I}{\mathrm{d}x} = -\frac{\mathcal{N}\sigma(0)I}{1 + I/I_{\text{sat}}(0)}. \tag{4.2.6}$$

It can be seen from (4.2.6) that if $I \gg I_{\text{sat}}(0)$, then $\mathrm{d}I/\mathrm{d}x \approx -\mathcal{N}\sigma(0)I_{\text{sat}}(0)$ and hence $I = -\mathcal{N}\sigma(0)I_{\text{sat}}(0)x + I_0$. However, if $I \ll I_{\text{sat}}(0)$ then $\mathrm{d}I/\mathrm{d}x \approx -\mathcal{N}\sigma(0)I$ and hence $I = I_0 \exp(-\mathcal{N}\sigma_0 x)$ in accordance with Beer's law [57]. (4.2.6) does in

fact have a general solution given by

$$I(0) = I_{\text{sat}}(0) W\left[\frac{I_0}{I_{\text{sat}}(0)} \exp\left(I_0/I_{\text{sat}}(0) - \mathcal{N}\sigma(0)x\right)\right], \tag{4.2.7}$$

where W is the Lambert W function [67]. The Lambert W function is defined as the inverse of the function $y = xe^x$ for $x \geq -1$ (its principal branch) [67]. Figure 4.9 shows the variation of the intensity in the steady state region of a field with a plateau intensity of 5 W/cm^2 turned on smoothly over 2 ns. We have also plotted the theoretical prediction given by (4.2.7). It can be seen that the numerical results are in good agreement with the theory and that the intensity decreases linearly with distance. This is because the saturation intensity for the D2 transition in ^{85}Rb is $I_{\text{sat}} = 5$ mW/cm^2 and we are considering a field which has an input intensity 1000× this value. Once the intensity has reached the saturation intensity, it is then absorbed very rapidly (and nonlinearly) over ∼20 μm as shown in Figure 4.10. For intensities $I \ll I_{\text{sat}}(0)$, (4.2.7) converges to Beer's law and the intensity decays exponentially with distance.

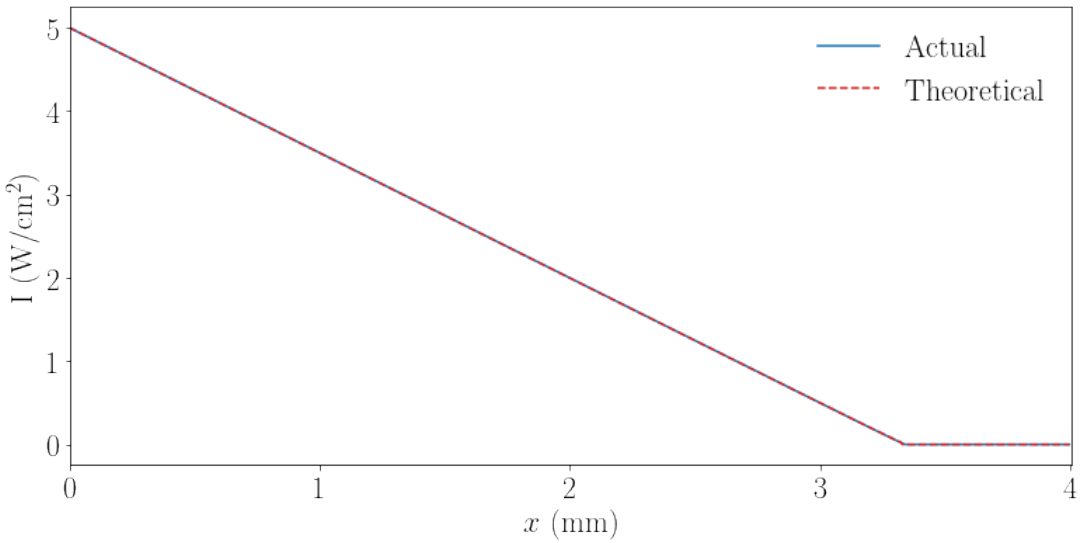

Figure 4.9: The variation of the intensity with distance in the steady state region ($t = 300$ ns) for a field with $I^{plat} = 5$ W/cm^2 that has been turned on smoothly over 2 ns. The solid blue line shows the intensity obtained from the numerical results and the dashed red line shows the theoretical intensity predicted by (4.2.7).

If inhomogeneous broadening is included, the situation is more complicated and the intensity variation with distance in the steady state as found from the numerical

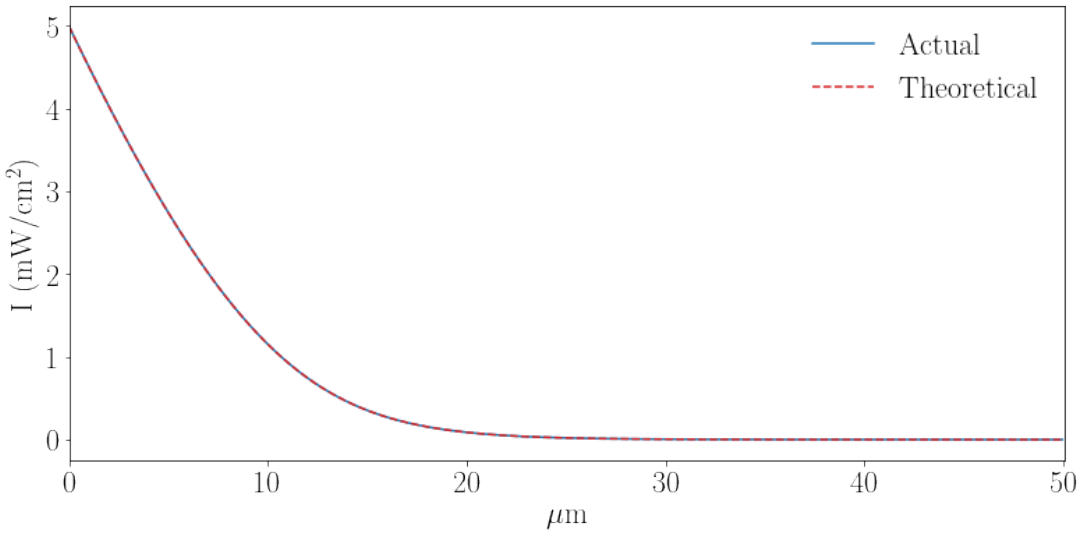

Figure 4.10: The variation of the intensity with distance in the steady state region ($t = 300$ ns) for a field with $I^{plat} = 5$ mW/cm^2 that has been turned on smoothly over 2 ns. The solid blue line shows the intensity obtained from the numerical results and the dashed red line shows the theoretical intensity predicted by (4.2.7).

results is shown in Figure 4.11. It can be seen that the intensity variation is nonlinear at much higher intensities than seen in the case without inhomogeneous broadening. This is because the saturation intensity increases as the light becomes further detuned from the resonance frequency and the intensity of the light for the inhomogeneously broadened case is an average over the Maxwell-Boltzmann distribution of velocity classes (detunings).

The pulses in the pulse trains which exist shortly after the turn-on of the field shown in Figure 4.7 appear to show a similar behaviour to the sech-solitons of SIT explored in the previous chapter. Their peak amplitudes decrease and their widths increase as the pulses travel further into the medium. We will now compare the propagation of a pulse on a pulse train formed from a CW field with a comparable sech-soliton. Figure 4.12(a) is a heatmap of the field formed from a CW input which was turned on smoothly between $t = 0$ ns and $t = 2$ ns and had an plateau intensity of 5 W/cm^2. The field is shown starting from a distance of 1.5 mm into the medium, after the pulse train has already formed. Figure 4.12(b) is a heatmap of a sech pulse which has a peak intensity the same as that of the first pulse of the train in (a) at $x = 1.5$ mm. A comparison of the profiles of the two fields at two distances are shown in parts (c)

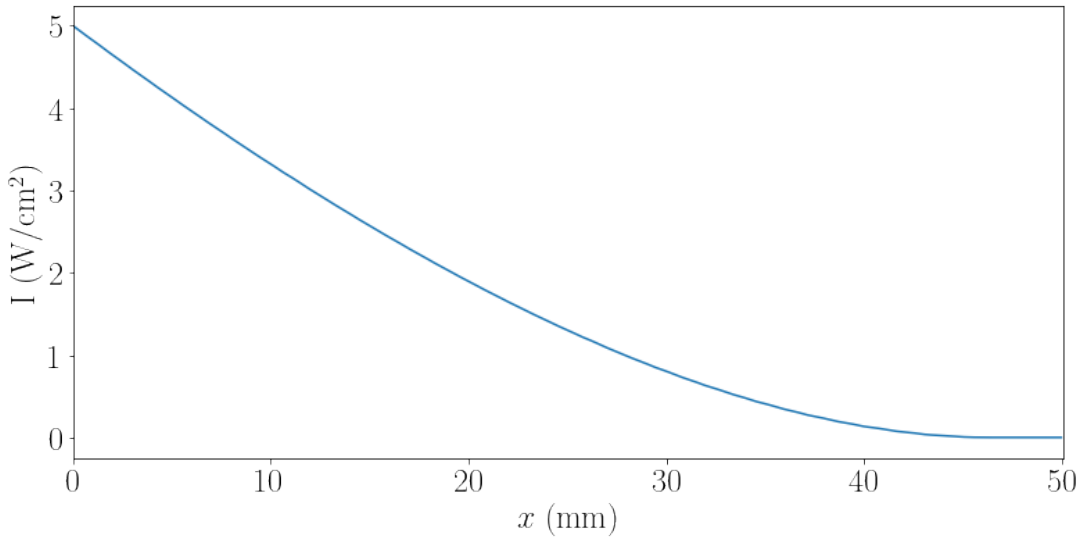

Figure 4.11: The variation of the intensity with distance in the steady state region ($t = 300$ ns) for a field with $I^{plat} = 5$ mW/cm^2 that has been turned on smoothly over 2 ns (this is the intensity variation seen in the numerical results). The simulation includes both homogeneous broadening and inhomogeneous broadening.

and (d) of Figure 4.12. The simulation included homogeneous broadening but not inhomogeneous broadening so as to reduce the computation time. It can be seen that the trajectories are similar, but not identical. The sech-soliton has a smaller peak intensity than that of the first pulse of the pulse train at $x = 2.8$ mm and is absorbed slightly more rapidly. It is clear that the pulses of the pulse trains formed from the CW field are not exact sech pulses since the field does not go to zero either side of these pulses as it does for a pure sech pulse. However, the first pulse of the train is quite closely approximated by a sech pulse (as can be seen from Figure 4.12(c)) and it follows a similar trajectory to one through the medium. It is also the case that the atomic medium is entirely in the ground state prior to the arrival of both the sech-soliton and the first pulse in the pulse train at each time and distance. This is not the case for the pulses further along the train and these are also clearly less well approximated by a sech-function. There is not time within the present investigation to explore the connection between the pulse trains formed from a CW field and sech-solitons in more detail but it appears that the first pulse of the pulse train formed from a CW field propagates similarly to a comparable sech-soliton.

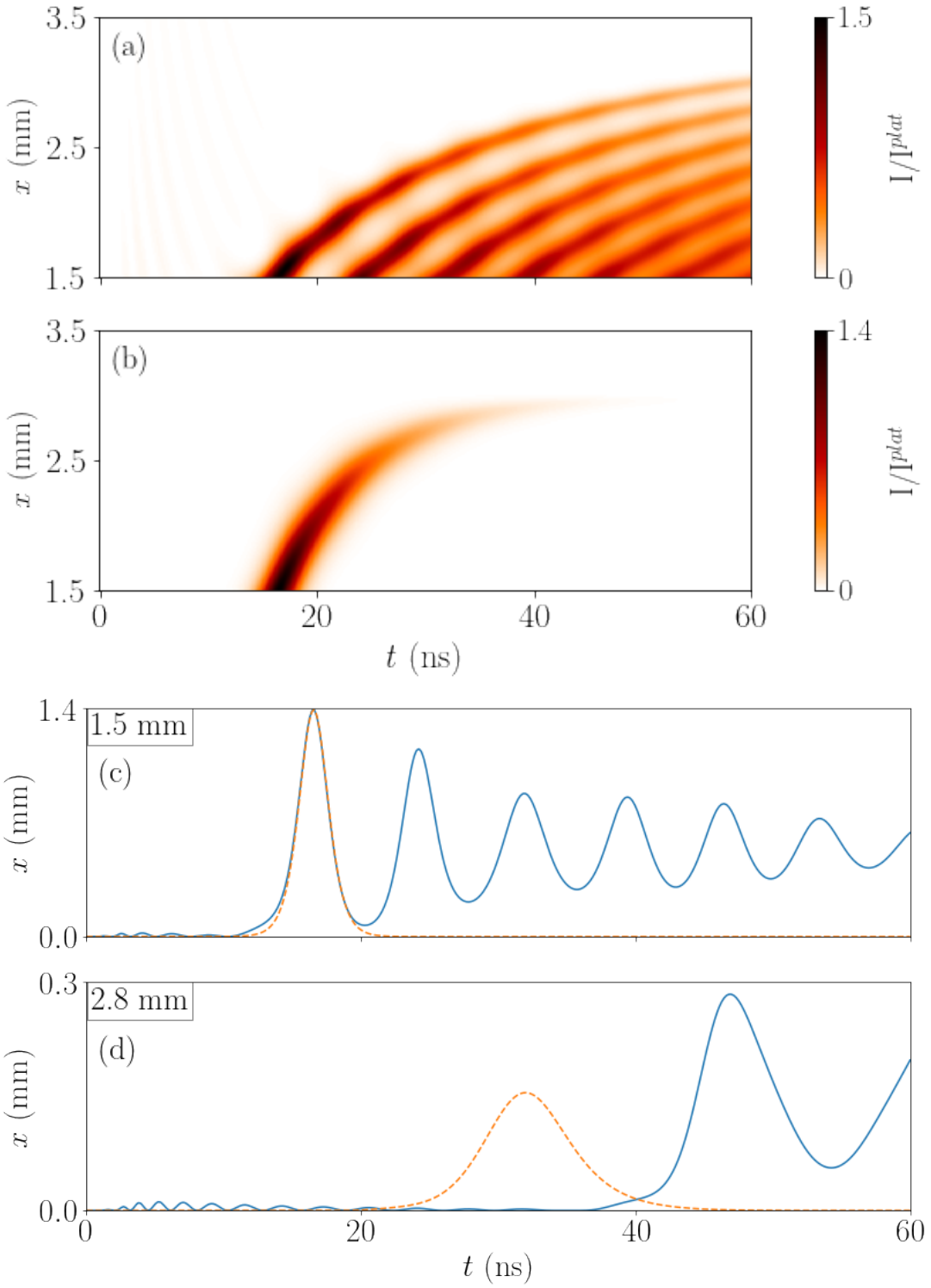

Figure 4.12: Comparison of the transient pulse train formed from a CW field with a sech-soliton. (a) Heatmap of a field with $I^{plat} = 5$ W/cm^2 (which was turned on smoothly between $t = 0$ ns and $t = 2$ ns), but starting from a distance of 1.5 mm into the medium after the pulse train has already formed. (b) A sech-soliton with a peak intensity the same as that of the peak intensity of the first pulse in the train at 1.5 mm. (c) The field profiles of the pulse train (solid blue line) and sech-soliton (dashed orange line) at a distance of 1.5 mm. (d) The same as (c) but at a distance of 2.8 mm. The simulation includes homogeneous broadening but not inhomogeneous broadening.

4.3 Summary

In this chapter, we explored the propagation of CW fields through a medium of two-level resonators, focusing on the dynamics that occur shortly after such fields are turned on. We first looked at the case in which homogeneous broadening was ignored, since there was substantial literature to compare our results to. It was found that a CW field breaks up into a train of pulses as it propagates into the medium, as had been observed previously by Crisp [28] and Horovitz and Rosenberg [29]. Importantly, it was found that our results were not in agreement with one of the key findings of Horovitz and Rosenberg: namely their asymptotic area theorem which required that the average time separation between the pulses is constant for all distances. Instead, by going to greater distances than they had considered, we found that in fact the pulses are seen to separate as distance increases. We also compared the dnoidal wave solutions to the Maxwell-Bloch equations found by Crisp [50] with the pulse trains formed from a CW field and found that a dnoidal wave with a certain parameter k was a good approximation to the field at a particular distance and over small time region. We then considered the more realistic situation in which homogeneous broadening was included. We observed that pulse trains were still seen to form from a CW field shortly after it was turned on, however the oscillations were damped and the system reached a steady state after a period of time, as had been seen previously in the simulations of Macke and Segard [31]. We compared the absorption of the fields in the steady state with the established theory, and found that the theoretical predictions were in agreement with our numerical results. We also compared the propagation of a sech-soliton with the transient pulse train formed from the CW field. It was observed that the first pulse in the train propagates similarly to a comparable sech-soliton.

Chapter 5

Two-Field Optical Transients

Having studied the propagation of CW fields through a medium of two-level resonators in the previous chapter, we now turn our attention to the case in which there are two CW fields, each resonant with a transition of a three-level V-system. In Chapter 2, we discussed in depth the previous work on optical simultons that was conducted here at Durham [26]. In that study, Ogden et al. considered the propagation effects that occur when a weak CW probe field is resonant with the D1 transition in ^{85}Rb and a strong, pulsed coupling field is resonant with the D2 transition. We will now extend that investigation to the case in which the coupling field is a strong CW field instead of a pulse. To the best of our knowledge this is the first time that such a case has been studied. We will compare the physics of this situation with that of the optical simultons of reference [26], to the one-field cases we have studied in the previous chapters and to the EIT phenomenon that we discussed in Chapter 2. As was done in reference [26], we will consider the three-level V-system of ^{85}Rb shown in Figure 2.1. However in contrast to [26], we choose to set the temperature of the vapour to 80°C rather than 220°C which lowers the atomic density and allows for propagation lengths of millimetres rather than micrometers. As explained previously, this choice of temperature should not be regarded as particularly important.

5.1 Weak Probe

5.1.1 No Inhomogeneous Broadening

We first consider the simpler situation in which inhomogeneous broadening is neglected. Figure 5.1 shows a simulation in which a strong CW coupling field and a weak CW probe field are both incident on the medium. Both fields are turned on smoothly over 2 ns reaching plateau intensities of $I_{\mathrm{c}}^{plat} = 5$ W/cm^2 and $I_{\mathrm{p}}^{plat} = 1$ μW/cm^2.

In the absence of the coupling field, the probe field would be absorbed very rap-

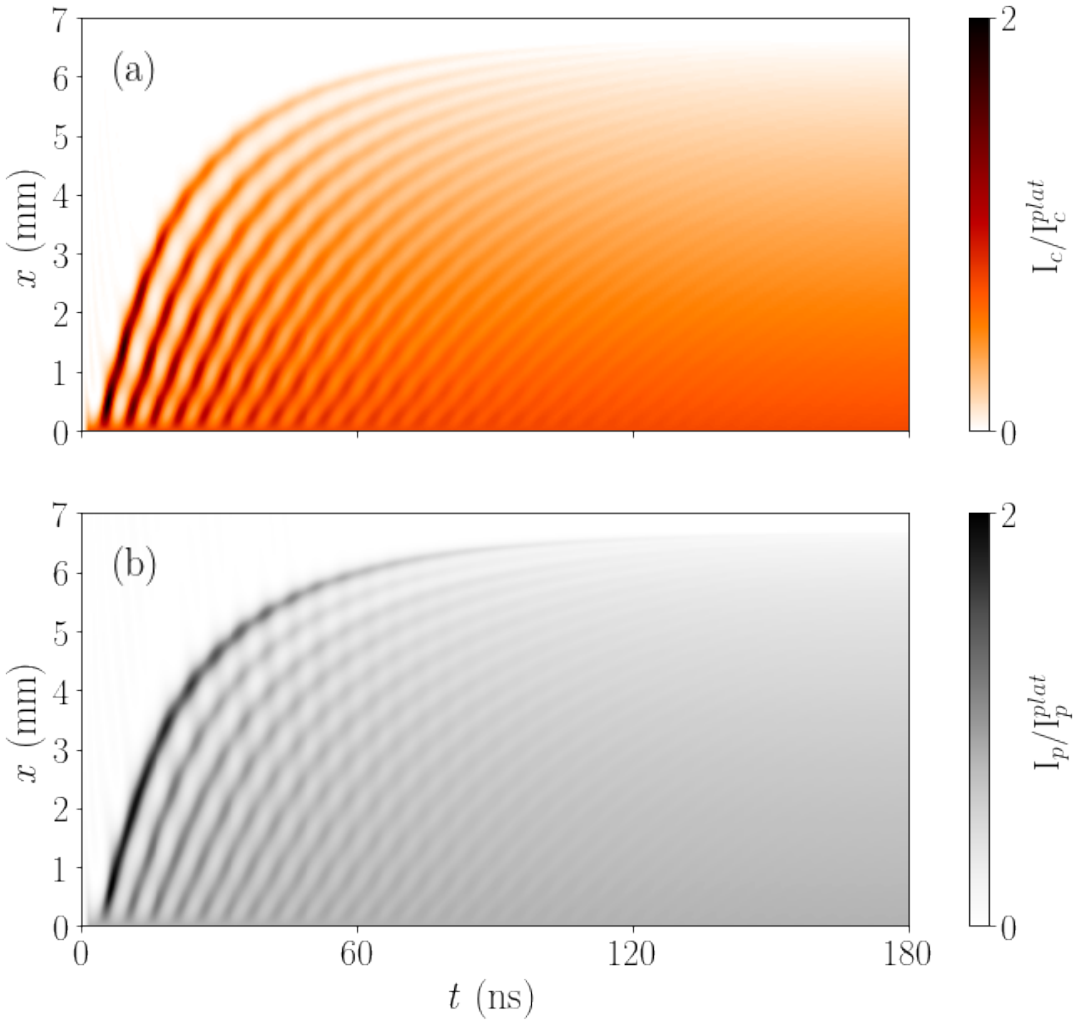

Figure 5.1: Heatmaps showing the co-propagation of a strong CW coupling field and a very weak CW probe field. (a) shows the coupling field with $I_{\mathrm{c}}^{plat} = 5$ W/cm^2. (b) shows the probe field with $I_{\mathrm{p}}^{plat} = 1$ μW/cm^2. Both fields are turned on smoothly between $t = 0$ ns and $t = 2$ ns. The simulation includes homogeneous broadening but not inhomogeneous broadening.

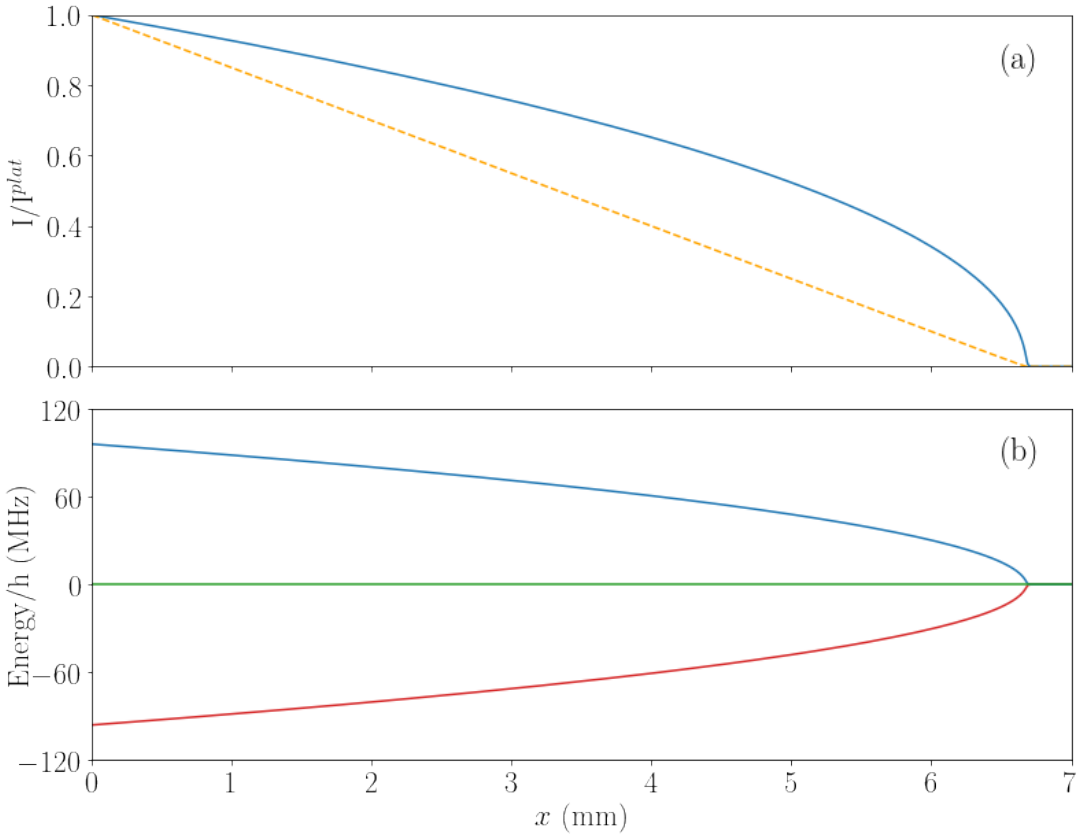

Figure 5.2: This figure corresponds to the heatmaps shown in Figure 5.1 at a time of 180 ns. (a) The dashed (orange) curve is the intensity of the the coupling field normalised to its input plateau intensity, $I_{\mathrm{c}}^{plat} = 5$ W/cm^2. The solid (blue) curve is the intensity of the probe field normalised to its input plateau intensity, $I_{\mathrm{p}}^{plat} = 1$ μW/cm^2. (b) The eigenenergies of the three-level system correrssponding to the fields in (a).

idly (∼10 μm) due to its very low intensity as we showed in the previous chapter. However, when the strong coupling field is also present, the probe field is able to travel much further into the medium as can be seen in Figure 5.1. In fact, the probe field travels the same distance into the medium as the coupling field does. The probe field also breaks up into a train of pulses in accordance with the coupling field. Each pulse of the probe field train is seen to co-propagate with (i.e. follows the same trajectory as) a pulse of the coupling field train. The situation therefore appears to be very similar to that of the optical simultons of reference [26], in which the weak probe field was transmitted through the medium by means of the strong coupling field. There was also a co-propagation effect by which each pulse that formed on one transition followed exactly the same trajectory as a corresponding

pulse on the adjacent transition, as is the case in the results shown in Figure 5.1. As was discussed in Chapter 2, Ogden et al. attributed the mechanism underpinning the optical quasi-simultons phenomenon to that of soliton-induced transparency (SOIT), as explored previously by Kozlov and Kozlova [58, 59]. However, as the name suggests, this relies on the field inducing the transparency to be a sech-soliton (or at least certainly well approximated by one). That is not the case here. Indeed, a transparency is induced on the probe field by the coupling field even after the steady state has been reached and there are no pulses at all. The mechanism that gives rise to the transparency seen in this situation seems therefore to be of a different nature to SOIT.

In Chapter 1, we introduced the concept of electromagnetically-induced transparency (EIT). This is the effect by which the absorption of a weak probe field can be significantly reduced due to the application of a strong coupling field [20]. In a way, such a definition also applies to the SOIT effect in which a strong coupling field (i.e. a soliton) induces a transparency on a weak probe field. However, the term EIT is usually only used to describe such an effect in situations in which the atom-light system is in a steady state (i.e the density matrix and fields have relaxed to constant values). This is exactly the situation shown in Figure 5.1 for large times: by 180 ns the pulse oscillations have all disappeared due to the effect of the spontaneous decay and the fields and density matrix at each distance have become constant with time (though they are of course not constant with distance due to the absorption). It therefore seems likely that the transparency induced on the probe in this region is related to that of V-system EIT. V-EIT has recently by studied experimentally by Higgins and Hughes here at Durham [7] and their study led us to consider the role of EIT in our results. As was explained in Chapter 1, EIT in V-systems is almost entirely due to Autler-Townes splitting [22, 23]. The Autler-Townes effect (or AC Stark effect) is the effect by which an intense coupling field changes the eigenstates of the coupled field plus atom Hamiltonian [22]. These eigenstates (called Dressed states) are split in energy by an amount $\hbar\Omega_c$ (for an on-resonance coupling field

with a Rabi frequency of Ω_c) and this means that the probe field is no longer resonant with the D1 transition and can propagate through the medium as though it were transparent [22]. We will now compare the absorption of the fields with distance in the steady state region of Figure 5.1 (using the largest time available from the simulation of 180 ns since this is closest to the condition of a steady state) with the variation of the eigenenergies of the coupled field plus atom Hamiltonian. Figure 5.2(a) shows the variation of the (normalised) intensities of the probe and coupling fields as a function of distance corresponding to the fields shown in Figure 5.1 at a time of 180 ns. Figure 5.2(b) shows the three eigenenergies of the coupled field plus atom Hamiltonian as a function of distance corresponding to the field intensities shown in (a). These eigenenergies are calculated by diagonalising the interaction Hamiltonian that was derived in Chapter 2 (2.2.32) using the values for the probe and coupling Rabi frequencies at each distance found from the numerical results. It can be seen that the eigenstates are split significantly at $x = 0$ mm. The natural linewidth of the D1 transition is given by the spontaneous decay constant $\Gamma = 5.75$ MHz. This corresponds to an energy splitting of $h \times 5.75$ MHz which is clearly much smaller than the energy splitting of $h \times 192$ MHz seen at $x = 0$ in Figure 5.2(b). Therefore the probe field, which is tuned to the bare state D1 transition frequency, is not on resonance with the medium at $x = 0$. As the coupling field is absorbed, the splitting of the eigenenergies is reduced until it becomes comparable to the linewidth of the state at around 6.7 mm, at which point the probe field gets absorbed very rapidly. From Figure 5.2(a), it can be seen that, although both fields are absorbed over the same distance, the absorption profiles are different for the two fields. The coupling field decreases linearly with distance, as expected from the theory discussed in the previous chapter, but the probe field absorption is nonlinear. This is also a result of the AT splitting. Initially, the splitting of the eigenenergies is large which means that the probe field is far off-resonance and so it is absorbed slowly with distance. However, as distance increases and the coupling field intensity decreases, the size of the AT splitting reduces and so the probe field becomes closer to being on resonance

which causes its rate of absorption to increase. It therefore seems that AT splitting accounts for the transparency that occurs once the fields have reached a steady state. The very first pulse of the train that forms from the strong CW field is fairly well approximated by a sech-soliton (as was explained in the previous chapter) and so the transparency effect that occurs at short times would seem to be similar to that of SOIT. However, it can be seen from Figure 5.1 that the first pulse of the pulse train that forms on the probe field goes no further into the medium than the field does in the steady state. It seems therefore that the phenomena of SOIT and V-EIT (caused by AT splitting) are in some way different aspects of the same underlying effect. More research is clearly required to understand the exact nature of this relation. However, these results certainly suggest that a connection between SOIT and V-EIT must exist and provide a strong motivation for a future study on this issue.

5.1.2 Inhomogeneous Broadening

We now consider the situation in which inhomogeneous broadening is included. Figure 5.3 shows a simulation identical to that of Figure 5.1 except inhomogeneous broadening is included. The features are the same as seen in the case without inhomogeneous broadening except the fields travel further and there are no 0-π pulses for the reasons explained in the previous chapter. Figure 5.4(a) shows the variation of the intensity of the fields shown in Figure 5.3 in the steady state (using the largest time available from the simulation of 180 ns since this is closest to the condition of a steady state). Figure 5.4(b) shows the three eigenenergies of the coupled field plus atom Hamiltonian as a function of distance corresponding to the field intensities shown in part (a). It can be seen that the absorption of the coupling field is nonlinear when inhomogeneous broadening is included, as discussed in the previous chapter, which makes the absorption profile of the probe more difficult to interpret. It can be seen from Figure 5.4(a) that the rate of absorption of the probe field still increases with distance, as was seen in the case without inhomogeneous broadening (the wobbles towards the end are due to the fact that at $t = 180$ ns there

is still some pulse oscillation and the steady state has not been completely obtained). However, the rate of change of the probe intensity with respect to distance is less extreme than in the no-inhomogeneous broadening case. This is because the rate of change of the coupling field intensity with respect to distance actually increases with distance when inhomogeneous broadening is included (whereas it is constant in the no-inhomogeneous broadening case) which means that the rate of change of the AT splitting energy with respect to distance is slower. Apart from the difference in absorption profiles, the underlying physics of the inhomogeneously broadened case appears to be identical to the one without inhomogeneous broadening described previously and our conclusions and questions about the mechanisms giving rise to the transparency effect are the same.

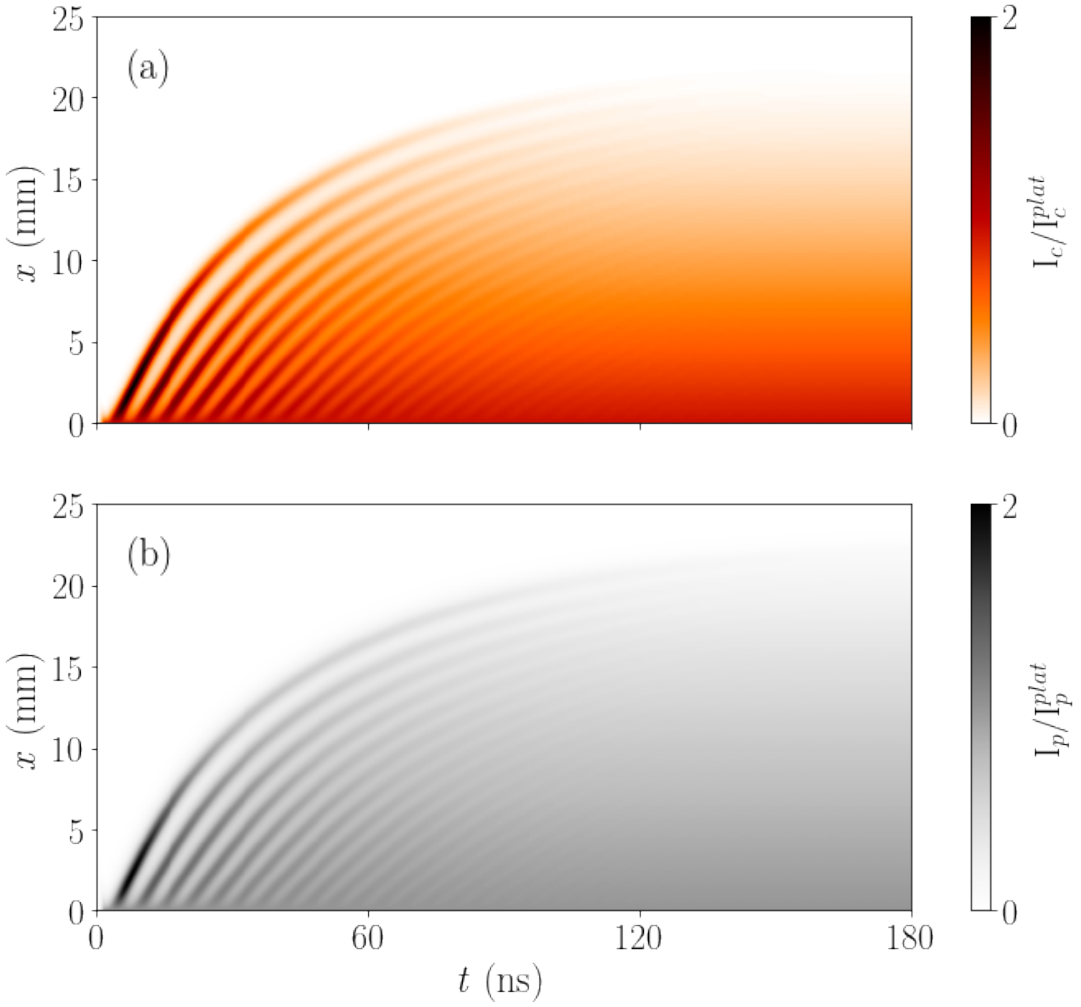

Figure 5.3: Heatmaps showing the co-propagation of a strong CW coupling field and a very weak CW probe field. (a) shows the coupling field with $I_{\mathrm{c}}^{plat} = 5$ W/cm^2. (b) shows the probe field with $I_{\mathrm{p}}^{plat} = 1$ μW/cm^2. Both fields are turned on smoothly between $t = 0$ ns and $t = 2$ ns. The simulation includes both homogeneous broadening and inhomogeneous broadening.

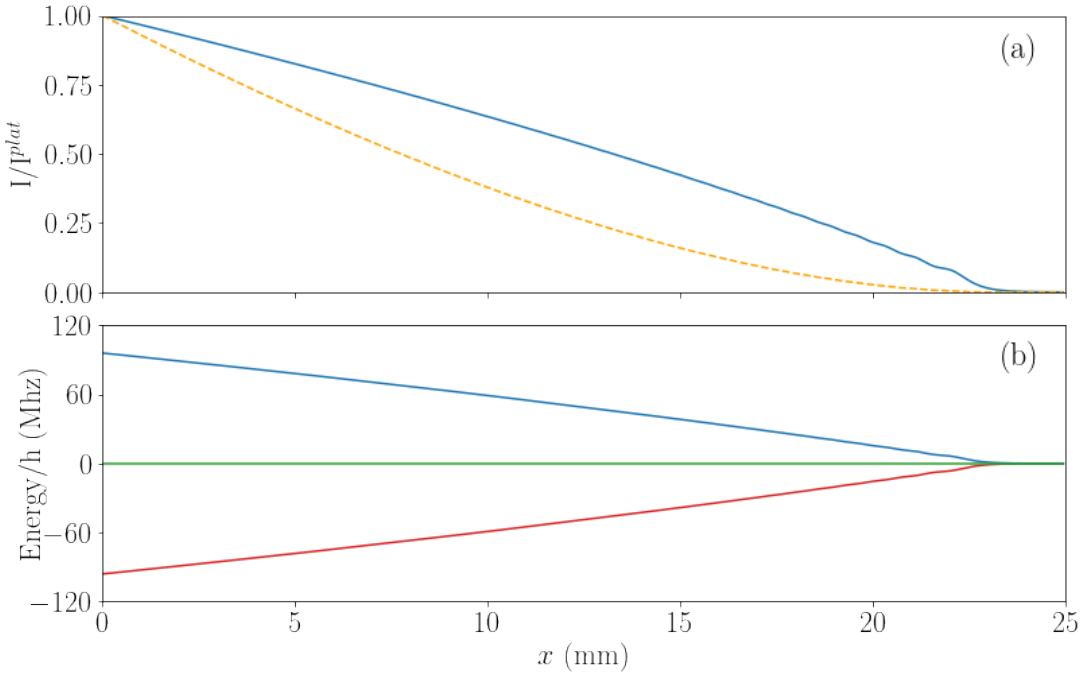

Figure 5.4: This figure corresponds to the heatmaps shown in Figure 5.3 at a time of 180 ns. (a) The dashed (orange) curve is the intensity of the coupling field normalised to its plateau intensity, $I_c^{plat} = 5$ W/cm^2. The solid (blue) curve is the intensity of the probe field normalised to its plateau intensity, $I_p^{plat} = 1$ μW/cm^2. (b) The eigenenergies of the three-level system corresponding to the fields in (a).

5.2 Strong Probe

Finally, we will investigate the situation in which both the incident fields are strong. Figure 5.5 shows a simulation in which both the coupling and probe fields have an input plateau intensity of $I^{plat} = 5$ W/cm^2. Parts (a) and (b) show the coupling and probe fields, respectively, propagating in the absence of the other field and parts (c) and (d) show the coupling and probe fields when they are co-propagating (i.e. when both fields are present). Figure 5.6(a) shows the variation with distance of the normalised intensities of the fields in the steady state (using the largest time available from the simulation of 180 ns since this is closest to the condition of a steady state). It can be seen that both fields travel significantly further into the medium when they co-propagate than when they propagate independent of each other. It can also be seen that they both travel the same distance into the medium when they co-propagate. Figure 5.6(b) shows the three eigenenergies of the coupled field plus atom Hamiltonian as a function of distance corresponding to the field intensities shown in part (a). It can be seen that the energy splitting at $x = 0$ mm is $h \times 234$ MHz. This is larger than the energy splitting at $x = 0$ mm of $h \times 190$ MHz shown in Figure 5.4(b) for the case in which the probe field is weak. Therefore, it appears that when both the coupling and probe fields are strong, they are both contributing to the AT splitting and thus effectively each inducing a transparency on the other field. This is what allows the fields to propagate further into the medium when propagating together than they do when propagating separately. In this situation, the eigenstates of the field plus atom Hamiltonian can be thought of as being doubly dressed by the two fields. Such doubly-dressed states have been explored experimentally in Ladder systems [68, 69], but to our knowledge they have not been considered previously in V-systems. At early times (i.e. prior to the steady state), it can be seen from Figure 5.5 that the pulses that form on each transition when both fields propagate together follow exactly the same trajectories, despite the fact the trajectories of the pulses that form from each field when they propagate

independent of each other is different (e.g. compare the trajectories of the first pulse of the train in each of the graphs of Figure 5.5). This is another intriguing effect but the exact mechanism that gives rise to it is currently unclear. It could possibly be related to the SOIT effects described by Kozlov and Kozlova [58, 59] that we discussed in Chapter 1, though without the requirement that one of the fields must be a sech-soliton. More research is certainly required to fully understand the physics behind these effects.

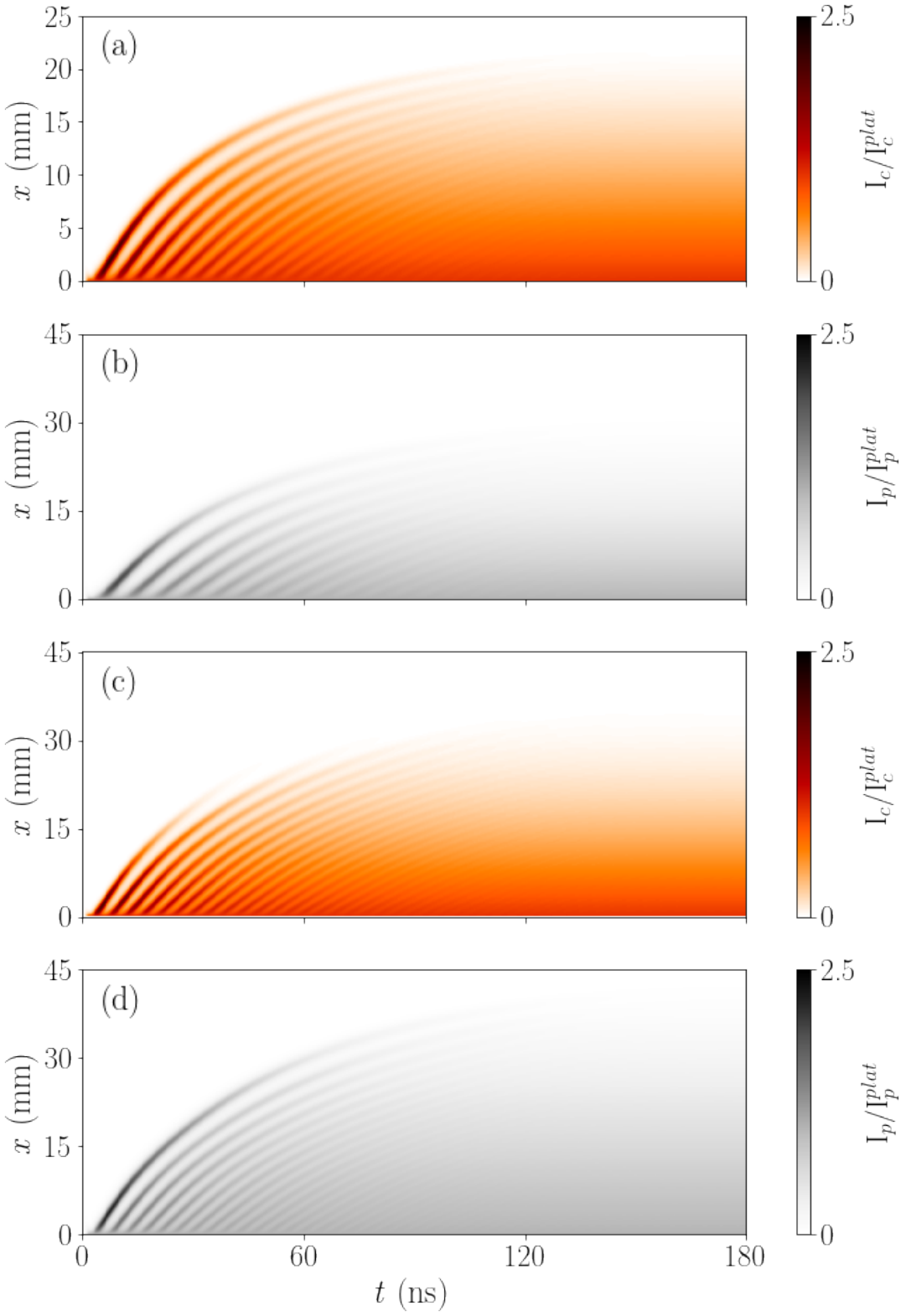

Figure 5.5: Heatmaps showing the propagation of a strong CW coupling field and a strong CW probe field. $I_{\mathrm{c}}^{plat} = I_{\mathrm{p}}^{plat} = 5$ W/cm^2. (a) The coupling field propagating in the absence of the probe field. (b) The probe field propagating in the absence of the coupling field. (c) The coupling field that is co-propagating with the probe field. (d) The probe field that is co-propagating with the coupling field. Both fields are turned on smoothly between $t = 0$ ns and $t = 2$ ns. The simulation includes both homogeneous broadening and inhomogeneous broadening.

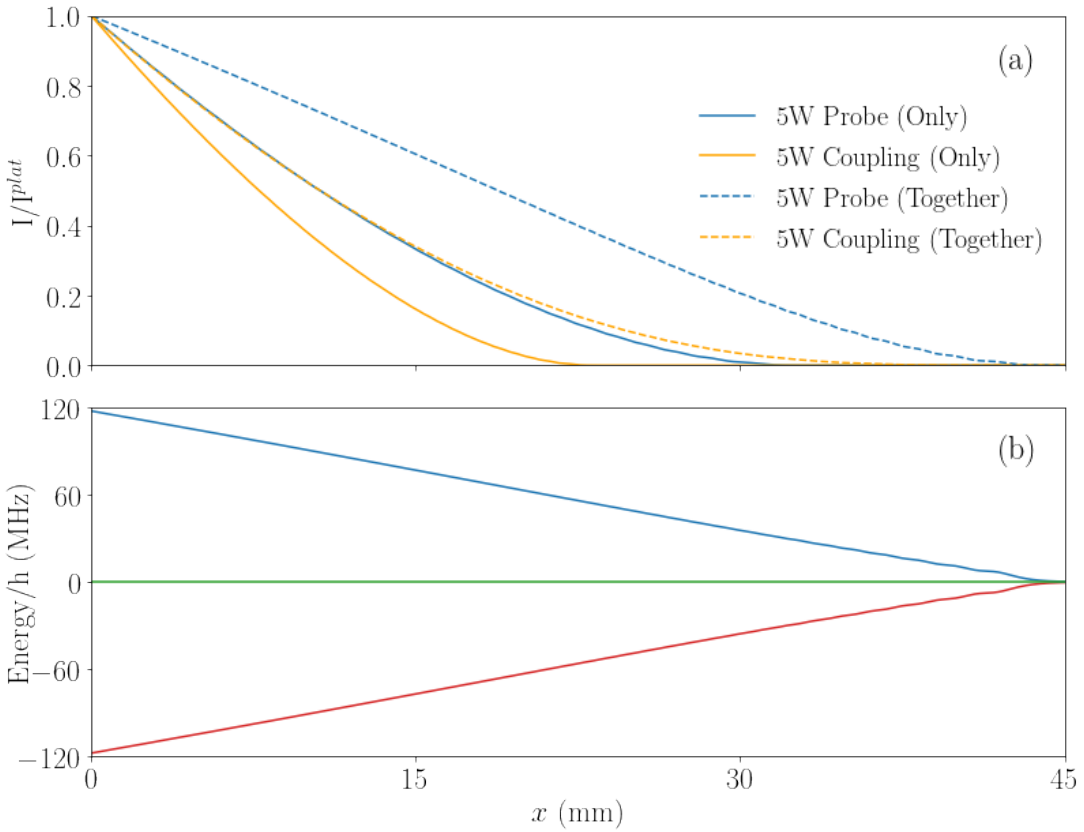

Figure 5.6: This figure corresponds to the heatmaps shown in parts (c) and (d) of Figure 5.5 at a time of 180 ns. (a) The normalised intensities of: the probe field propagating in the absence of the coupling field (solid blue line), the coupling field propagating in the absence of the probe field (solid yellow line), the probe field co-propagating with the coupling field (dashed blue line), the coupling field co-propagating with the probe field (dashed yellow line). (b) The eigenenergies of the three-level system corresponding to the co-propagating fields in (a).

5.3 Summary

In this chapter, we explored the propagation of two CW fields through a medium of homogeneously broadened three-level resonators, focusing on the dynamics that occur shortly after such fields are turned on. It was found that a weak CW probe field is able to travel much further into the medium when coincident with a strong CW coupling field than it can in the absence of the strong coupling field. At early times before the steady state was reached, the CW probe field was reshaped into a transient pulse train, in response to the pulse train formed from the strong CW field. Each pulse of the train on one transition was seen to follow an identical trajectory to that on the other transition, a property also displayed by the quasi-simultons studied by Ogden et al. [26]. To the best of our knowledge it is the first time that such a situation has been studied. It was found that the transparency of the probe induced by the coupling field in the steady state region could be explained by the well known Autler-Townes effect [22], but that further research was required to elucidate the precise nature of the transparency mechanism prior to the steady state being obtained. We then considered the case in which both fields were strong. It was observed that in this case, both fields traveled further into the medium when they were coincident than they did when they propagated independent of each other. In the steady state region, this was again attributable to an Autler-Townes effect, but the mechanism behind the dynamics that occurred before the steady state was reached needed further study to clarify.

Chapter 6

Conclusions

In this thesis, we have used computer simulations and theoretical techniques to explore the physics of light propagation in two and three level media. We have framed our investigation around a specific system in ^{85}Rb, but our results apply more generally to a wide variety of systems. In the first chapter, we introduced the important nonlinear propagation effects of SIT and simultons as well as the more widely known effect of EIT. We explained that whilst many of these effects have been known about for some time, there is much that is unclear about the underlying physics that links them. The aim of our investigation was to study these effects, seeking to compare our results with the existing literature and extend them to cases not considered previously.

In Chapter 2, we outlined the theoretical framework commonly used to study the propagation of light through atomic systems. We derived the optical Bloch equations describing the state of the atoms with time and a propagation equation describing the state of the field with distance collectively referred to as the Maxwell-Bloch equations. We explained that we would solve these equations numerically in order to simulate the propagation of light through atomic media. We then reviewed some important studies that had previously investigated the phenomena of SIT solitons, optical simultons and pulse trains [12, 26, 50].

We then began our investigation by exploring the propagation of SIT solitons through

a medium of two-level resonators. For the case in which there was no homogeneous broadening, it was found that the physics is well understood and our results were in agreement with the established theory. For the case in which homogeneous broadening was included, we observed a behaviour consistent with the work of Miklaszewski and Fiutak [65]. We then showed a interesting result, which we believe has not been shown previously, in which the instantaneous velocity of a sech-soliton propagating in the presence of homogeneous broadening was shown to be the same as that given by the equation describing the velocity of a sech-soliton in the absence of homogeneous broadening.

In Chapter 4, we looked at the propagation of CW fields through a medium of two-level resonators, focusing on the dynamics that occur shortly after such fields are turned on. In the absence of homogeneous broadening, it was found that a CW field breaks up into a train of pulses as it propagates into the medium, as had been observed previously by Crisp [28] and Horovitz and Rosenberg [29]. We then reported an important finding: namely that the average time separation of the pulses seen in our results was not constant with distance as had been claimed by Horovitz and Rosenberg. By going to greater distances than they had considered, we found that in fact the pulses are seen to separate as distance increases. We also found that the dnoidal waves studied by Crisp [50] with a particular parameter k were good approximations to the pulse trains formed from a CW field at a particular distance and over small time region. When we incorporated homogeneous broadening into our simulations, we observed that pulse trains were still seen to form from a CW field shortly after it was turned on, however the oscillations were damped and the system reached a steady state after a period of time. These results were consistent with those of Macke and Segard [31] and the absorption profiles of the fields in the steady state region was in agreement with the established theory. Lastly, we compared the propagation of a sech-soliton with the transient pulse train formed from the CW field and it was found that the first pulse in the train propagated similarly to a comparable sech-soliton.

Finally, we considered the propagation of two CW fields through a medium of homogeneously broadened three-level resonators, once again focusing on the dynamics that occur shortly after such fields are turned on. It was found that a weak CW probe field is able to travel much further into the medium when coincident with a strong CW coupling field than it can in the absence of the strong coupling field. We also observed the formation of transient pulse trains on both fields, similar to those seen in the one-field case, in which each pulse of the train on one transition was seen to follow an identical trajectory to that of one on the other transition. We noted the similarity to the optical quasi-simultons studied previously in the group here at Durham by Ogden et al. [26] but believe that this is the first time such an effect has been seen with CW input fields. We then looked into the mechanism underpinning the effect, and found that the results seen in the steady state region could be explained by the well known Autler-Townes effect [22]. However, it was noted that further research is required to fully understand the dynamics that occur before the steady state is obtained. We then considered the case in which both fields were strong and it was seen that both fields traveled further into the medium when they were coincident than they did when they propagated independent of each other. Once again, the mechanism underlying the effect in the steady state region was shown to be attributable to AT splitting, but further study is needed to fully understand the phenomenon in the transience region before a steady state is reached.

In conclusion, our investigation has gone some way into elucidating the connection between a variety of effects that occur when light propagates through an atomic medium. We have compared our results to previous studies and made several original findings. We have found that there is much that is still unknown or poorly understood about light propagation effects and it is hoped that this study may help stimulate greater interest in these phenomena. One limitation of our work was that we assumed that the light fields were plane waves and therefore considered propagation along only one-dimension. In the future, it would be interesting to explore the validity of this assumption in different regimes by solving the full three-dimensional Maxwell-Bloch

equations as has been done previously. It should also be noted that the ideal two and three level systems we considered in this thesis are not complete descriptions of real atomic systems, though they are often valid approximations. We considered such ideal systems in this work since the emphasis was on understanding the essence of the propagation effects which can generally be seen with simple models. However, in the future it would be interesting to compare the results obtained with the simple models to those found using more complex ones, for example by including the full hyperfine structure of the D1 and D2 transitions of ^{85}Rb as was done in the work on optical simultons by Ogden et al. [26].

Bibliography

[1] P. W. Milonni and J. H. Eberly. *Laser Physics*. Hoboken: John Wiley Sons, Inc., 2010.

[2] B. Du et al. "High-performance optical sensing based on electromagnetically induced transparency-like effect in Tamm plasmon multilayer structures". In: *Appl. Opt.* 58.7 (2019), p. 4569. DOI: 10.1364/AO.58.004569.

[3] T. Fortier and E. Baumann. "20 years of developments in optical frequency comb technology and applications". In: *Commun. Phys* 2.153 (2019). DOI: 10.1038/s42005-019-0249-y.

[4] D. Browne et al. "From quantum optics to quantum technologies". In: *Prog. Quantum. Electron.* 54 (2017). DOI: 10.1016/j.pquantelec.2017.06.002.

[5] T.F. Cutler et al. "Nanostructured Alkali-Metal Vapor Cells". In: *Phys. Rev. Appl.* 14.034054 (2020). DOI: 10.1103/PhysRevApplied.14.034054.

[6] D. E. Jones, J. D. Franson and T. B. Pittman. "Ladder-type electromagnetically induced transparency using nanofiber-guided light in a warm atomic vapor". In: *Phys. Rev. A* 92.4 (2015), p. 043806. DOI: 10.1103/PhysRevA.92.043806.

[7] C. R. Higgins and I. G. Hughes. "Electromagnetically induced transparency in a V-system with 87Rb vapour in the hyperfine Paschen-Back regime". In: *J. Phys. B: At. Mol. Opt. Phys.* 54.16 (2021). 165403. DOI: 10.1088/1361-6455/ac20be.

[8] D. F. Phillips et al. “Storage of Light in Atomic Vapor”. In: *Phys. Rev. Lett.* 86.5 (2001), p. 783. DOI: 10.1103/PhysRevLett.86.783.

[9] A. K. Mohapatra, T. R. Jackson and C. S. Adams. “Coherent Optical Detection of Highly Excited Rydberg States Using Electromagnetically Induced Transparency”. In: *Phys. Rev. Lett.* 98.11 (2007). 113003. DOI: 10.1103/PhysRevLett.98.113003.

[10] D. Kara and A. K. Mohapatra. “Study of the effect of super-atom dephasing on Rydberg blockade in thermal vapor”. In: *J. Phys. B: At. Mol. Opt. Phys.* 53.24 (2020). 245301. DOI: 10.1088/1361-6455/abc229.

[11] D. Kara, A. Bhowmick and A. K. Mohapatra. “Rydberg interaction induced enhanced excitation in thermal atomic vapor”. In: *Sci. Rep.* 8.1 (2018), p. 5256. DOI: 10.1038/s41598-018-23559-0.

[12] S. L. McHall and E. L. Hahn. “Self-Induced Transparency”. In: *Phys. Rev.* 183.2 (1969), p. 457. DOI: 10.1103/PhysRev.183.457.

[13] J. J. Bannister et al. “Self-Induced Transparency and Resonant Self-Focusing in Atomic Iodine Vapor”. In: *Phys. Rev. Lett.* 44.16 (1980), p. 1062. DOI: 10.1103/PhysRevLett.44.1062.

[14] F. Ripka et al. “A room-temperature single-photon source based on strongly interacting Rydberg atoms”. In: *Science* 362.6413 (2018), p. 446. DOI: 10.1126/science.aau1949.

[15] A. Urvoy et al. “Strongly Correlated Growth of Rydberg Aggregates in a Vapor Cell”. In: *Phys. Rev. Lett.* 114.20 (2015). 203002. DOI: 10.1103/PhysRevLett.114.203002.

[16] A. I. Maimistov and A. M. Basharov. *Nonlinear Optical Waves*. Dordrecht: Springer, 1999.

[17] H. Riesen et al. “Ultra-slow light propagation by self-induced transparency in ruby in the superhyperfine limit”. In: *Opt. Lett.* 42.10 (2017), p. 1871. DOI: 10.1364/OL.42.001871.

[18] S. E. Harris, J. E. Field and A. Imamoğlu. "Nonlinear optical processes using electromagnetically induced transparency". In: *Phys. Rev. Lett.* 64.10 (1990), p. 1107. DOI: 10.1103/PhysRevLett.64.1107.

[19] G. Alzetta et al. "An experimental method for the observation of r.f. transitions and laser beat resonances in oriented Na vapour". In: *Nuov. Cim. B* 36 (1976), p. 5. DOI: 10.1007/BF02749417.

[20] M. Fleischhauer, A. Imamoglu and J. P. Marangos. "Electromagnetically induced transparency: Optics in coherent media". In: *Rev. Mod. Phys.* 77.2 (2005), p. 633. DOI: 10.1103/RevModPhys.77.633.

[21] U. Fano. "Effects of Configuration Interaction on Intensities and Phase Shifts". In: *Phys. Rev.* 124.6 (1961), p. 1866. DOI: 10.1103/PhysRev.124.1866.

[22] S. H. Autler and C. H. Townes. "Stark Effect in Rapidly Varying Fields". In: *Phys. Rev.* 100.2 (1955), p. 703. DOI: 10.1103/PhysRev.100.703.

[23] S. Khan, V. Bharti and V. Natarajan. "Role of dressed-state interference in electromagnetically induced transparency". In: *Phys. Lett. A* 380.48 (2016), p. 4100. DOI: 10.1016/j.physleta.2016.10.030.

[24] B. Peng et al. "What is and what is not electromagnetically induced transparency in whispering-gallery microcavities". In: *Nat. Commun.* 5 (2014). 5082. DOI: 10.1038/ncomms6082.

[25] M. J. Konopnicki and J. H. Eberly. "Simultaneous propagation of short different-wavelength optical pulses". In: *Phys. Rev. A* 24.5 (1981), p. 2567. DOI: 10.1103/PhysRevA.24.2567.

[26] T. P. Ogden et al. "Quasisimultons in Thermal Atomic Vapors". In: *Phys. Rev. Lett.* 123.24 (2019). 243604. DOI: 10.1103/PhysRevLett.123.243604.

[27] Z. Bai et al. "Self-Induced Transparency and Resonant Self-Focusing in Atomic Iodine Vapor". In: *Phys. Rev. Lett.* 125.26 (2020). 263605. DOI: 10.1103/PhysRevLett.125.263605.

[28] M. D. Crisp. "Propagation of Step-Function Light Pulses in a Resonant Medium". In: *Phys. Rev.* 5.3 (1972), p. 1365. DOI: 10.1103/PhysRevLett.22.820.

[29] Horovitz B and Rosenberg N. "Self-induced transparency and the soliton lattice". In: *Phys. Rev. A* 26.5 (1982), p. 2799. DOI: 10.1103/PhysRevA.26.2799.

[30] Kaup D J. "Coherent pulse propagation: A comparison of the complete solution with the McCall-Hahn theory and others". In: *Phys. Rev. A* 16.2 (1977), p. 704. DOI: 10.1103/PhysRevA.16.704.

[31] Macke B and Segard B. "Optical precursors with self-induced transparency". In: *Phys. Rev. A* 81.015803 (2010). DOI: 10.1103/PhysRevA.81.015803.

[32] M. A. Newbold and G. J. Salamo. "Effects of Relaxation on Coherent Continuous-Pulse-Train Propagation". In: *Phys. Rev. Lett.* 42.14 (1979), p. 887. DOI: 10.1103/PhysRevLett.42.887.

[33] M. Nakazawa et al. "Self-induced-transparency solitons in an erbium-doped fiber waveguide". In: *Phys. Rev. A* 45.1 (1992), R23(R). DOI: 10.1103/PhysRevA.45.R23.

[34] C. J. Foot. *Atomic physics*. Oxford: Oxford University Press, 2007.

[35] J. Devanathon. *Angular momentum techniques in quantum mechanics*. Dordrecht: Kluwer Academic Publishers, 1999.

[36] E. P. Wigner and J.J. Griffin. *Group Theory and Its Application to the Quantum Mechanics of Atomic Spectra*. New York: Academic Press, 1959.

[37] D. A. Steck. *Rubidium 85 D Line Data*. available online at http://steck.us/alkalidata (revision 2.2.3, 9 July 2021).

[38] R. Loudon. *The Quantum theory of Light*. Oxford: Oxford University Press, 2000.

[39] S. C. Rand. *Lectures on light : nonlinear and quantum optics using the density matrix*. Oxford: Oxford University Press, 2010.

[40] L. Boltzmann. "Über die Beziehung zwischen dem zweiten Hauptsatze der mechanischen Wärmetheorie und der Wahrscheinlichkeitsrechnung respective den Sätzen über das Wärmegleichgewicht". In: *Wiener Berichte* 76 (1877), p. 373.

[41] J. C. Slater. "Atomic Radii in Crystals". In: *J. Chem. Phys.* 41 (1964), p. 3199.

[42] N. H. List et. al. "Beyond the electric-dipole approximation: A formulation and implementation of molecular response theory for the description of absorption of electromagnetic field radiation". In: *J. Chem. Phys.* 142 (2015). 244111.

[43] D. A. Steck. *Quantum and Atom Optics*. available online at http://steck.us/teaching (revision 0.13.10, 22 September 2021).

[44] K. B. Whaley and J. C. Light. "Rotating-frame transformations: A new approximation for multiphoton absorption and dissociation in laser fields". In: *Phys. Rev. A* 29.3 (1984), p. 1188. DOI: 10.1103/PhysRevA.29.1188.

[45] R. Shankar. *Principles of Quantum Mechanics*. New York: Springer, 1994.

[46] G. Lindblad. "On the generators of quantum dynamical semigroups". In: *Commun. Math. Phys.* 48 (1976), p. 119. DOI: 10.1007/BF01608499.

[47] A. Icsevgi and W. E. Lamb. "Propagation of Light Pulses in a Laser Amplifier". In: *Phys. Rev.* 185.2 (1969), p. 517. DOI: 10.1103/PhysRev.185.517.

[48] D. J. Griffiths. *Introduction to Electrodynamics*. Cambridge: Cambridge University Press, 2017.

[49] A. Peres. *Quantum Theory: Concepts and Methods*. Dordrecht: Springer, 1993.

[50] M. D. Crisp. "Distortionless Propagation of Light Through an Optical Medium". In: *Phys. Rev.* 22.16 (1969), p. 820. DOI: 10.1103/PhysRevLett.22.820.

[51] A. C. Scott, F. Y. F. Chu and D. W. McLaughlin. "The soliton: A new concept in applied science". In: *Proc. IEEE* 61.10 (1973), p. 1443. DOI: 10.1109/PROC.1973.9296.

[52] G.L. Lamb. "Analytical Descriptions of Ultrashort Optical Pulse Propagation in a Resonant Medium". In: *Rev. Mod. Phys.* 43.2 (1971), p. 99. DOI: 10.1103/RevModPhys.43.99.

[53] M. J. Ablowitz, D. J. Kaup and A. C. Newell. "Coherent pulse propagation, a dispersive, irreversible phenomenon". In: *J. Math. Phys* 15.11 (1974), p. 1852. DOI: 10.1063/1.1666551.

[54] C. S. Gardner et al. "Method for Solving the Korteweg-deVries Equation". In: *Phys. Rev. Lett.* 19.19 (1967), p. 095. DOI: 10.1103/PhysRevLett.19.1095.

[55] D. J. Kaup. "Coherent pulse propagation: A comparison of the complete solution with the McCall-Hahn theory and others". In: *Phys. Rev. A* 16.2 (1977), p. 704. DOI: 10.1103/PhysRevA.16.704.

[56] E. Fazio et al. "Observation of photorefractive simultons in lithium niobate". In: *Opt. Express* 18.8 (2010), p. 7972. DOI: 10.1364/OE.18.007972.

[57] Beer A. "Bestimmung der Absorption des rothen Lichts in farbigen Flüssigkeiten". In: *Ann. Phys.* 162.4 (1852), p. 78. DOI: 10.1002/andp.18521620505.

[58] V. V. Kozlov and E. B. Kozlova. "Raman amplification of ultrashort light pulses in inhomogeneously broadened three-level systems". In: *Opt. Spectrosc.* 107.1 (2009), p. 129. DOI: 10.1134/S0030400X09070194.

[59] V. V. Kozlov and E. B. Kozlova. "Soliton-induced transparency of inhomogeneously broadened three-level atoms". In: *Opt. Spectrosc.* 108.5 (2010), p. 780. DOI: 10.1134/S0030400X10050176.

[60] V. V. Kozlov and E. E. Fradkin. "Coherent effects in ultrashort pulse propagation through an optically thick three-level medium". In: *Jetp. Lett.* 68.5 (1998), p. 383. DOI: 10.1134/1.567877.

[61] P. F. Byrd and M.D. Friedman. *Handbook of Elliptic Integrals for Engineers and Scientists*. Berlin: Springer, 1971.

[62] H. Alatas and A. Saputra. "Cnoidal, Dnoidal and Snoidal Spatial Waves in a Nonlinear Reflection Grating". In: *AIP Conf. Proc .* 1325 (2010). 186. DOI: 10.1063/1.3537893.

[63] E. A.-B. Abdel-Salam. "Quasi-Periodic, Periodic Waves, and Soliton Solutions for the Combined KdV-mKdV Equation". In: *Z. Naturforsch. A* 64.9 (2009), p. 639. DOI: 10.1515/zna-2009-9-1016.

[64] A M. Alhasan, J. Fiutak and W. Miklaszewski. "The influence of the atomic relaxation on the resonant propagation of short light pulses". In: *Z. Physik B - Condensed Matter* 88 (1992), p. 349. DOI: 10.1007/BF01470924.

[65] Miklaszewski W and Fiutak J. "The effect of the homogeneous broadening on the propagation of the light pulses". In: *Z. Phys. B* 93 (1994), p. 491. DOI: 10.1007/BF01314253.

[66] D. J. Kaup and L. R. Scacca. "Generation of $0 - \pi$ pulses from a zero-area pulse in coherent pulse propagation". In: *J Opt Soc Am* 70.2 (1980), p. 224. DOI: 10.1364/JOSA.70.000224.

[67] T. P. Dence. "A Brief Look into the Lambert W Function". In: *Appl. Math.* 4.6 (2013), p. 887. DOI: 10.4236/am.2013.46122.

[68] R. Y. Chang et al. "Doubly dressed states in a ladder-type system with electromagnetically induced transparency". In: *Phys. Rev. A* 76.5 (2007). 053420. DOI: 10.1103/PhysRevA.76.053420.

[69] C. Wei and N. B. Manson. *AC Stark splitting of a three-level system driven by two strong fields*. Summaries of Papers Presented at the International Quantum Electronics Conference: IEEE, 1998.